

Atomically Precise Water-Soluble Gold Nanoclusters: Straightforward Synthesis and Tuning of Physicochemical Properties

Thesis

Submitted for the degree of

Doctor of Philosophy

in

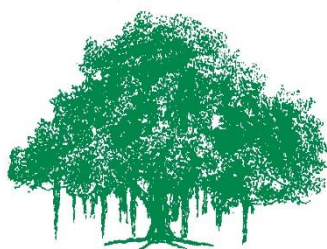
Computational Natural Sciences

Submitted by

Ramakrishna Itteboina

Roll No. 201066006

ramakrishna.i@research.iiit.ac.in



IIIT HYDERABAD

International Institute of Information Technology, Hyderabad (IIIT-H)

Hyderabad – 500032, INDIA.

May, 2018

DECLARATION OF AUTHORSHIP

I, Ramakrishna Itteboina, declare that this Ph.D. thesis titled “Atomically Precise Water-Soluble Gold Nanoclusters: Straightforward Synthesis and Tuning of Properties” is based on my own work.

I confirm that:

- This work was done wholly while in candidature for a research degree at the International Institute of Information Technology-Hyderabad.
- Wherever I have consulted the published work of others, I have documented/acknowledged all work/sources of information.

Ramakrishna Itteboina

Date: 11-05-2018

CERTIFICATE

I hereby certify that the matter embodied in this thesis entitled “Atomically Precise Water-Soluble Gold Nanoclusters: Straightforward Synthesis and Tuning of Properties” has been carried out by Ramakrishna Itteboina at the Center for Computational Natural Sciences and Bioinformatics (CCNSB), International Institute of Information Technology (IIIT), Hyderabad, India, under my supervision and that it will not be submitted elsewhere for the award of any degree or diploma.

Date: 11-05-2018

(Dr. Tapan Kumar Sau)
Supervisor

Acknowledgements

I express my deep gratitude to my professor, Dr. Tapan Kumar Sau, whose continuous encouragement and valuable advice helped me to acquire necessary research skills and complete this research work successfully. Apart from research, thought-provoking discussions with him on various topics helped me to grow personally.

I thank my lab mates Shweta, Parijat, and Arunganshu for their support in the lab. I acknowledge and thank Dr. NV Suresh Kumar for helping me by carrying out computational work for some of my experimental findings. I would also like to acknowledge and extend my sincere gratitude to my collaborators, Dr. Partha Ghosal (Defence Metallurgical Research Lab, Hyderabad), Prof. Tatsuya Tsukuda (The University of Tokyo), Monica Kannan (University of Hyderabad) and U. Divya Madhuri (University of Hyderabad) for their kind help and fruitful discussions. I would like to acknowledge Dr. T. Pradeep, Dr. T. Udayabhaskararao, Dr. Rongchao Jin and Dr. Amala Dass for their advice and suggestions. I would like to thank all the faculty members of CCNSB for providing a healthy research ambiance and for well-organized courses.

I would like to thank Mr. Girish, Mr. Balsantosh, and Mrs. Sirisha Salaka for kind supports with administrative works. I appreciate Mr. Umesh for helping us in keeping our laboratory clean and neat. I would like to acknowledge and thank CSIR, India, for providing me the fellowship that helped me to achieve my goal.

The warmth and love of people around us give us enormous enthusiasm and confidence which motivate us to achieve higher goals. I have always cherished the company of my friends Mohan Maruthi Sena, Bipin Singh, Kartheek Pitta, Preethi SP, Navneet, Ramesh Cheerla, Rajitha, Broto, Prashanthi Dharanipragada, Antarip Halder, Sandhya Rai, Sohini Bhattacharya, Prathyusha, Suresh Gorle, Shruti, Manasri, Siladitya, Ramya, Nishtha, Tanashree, and Sanchari.

Finally, I express my heartfelt gratitude and huge thanks to my parents, brother, sister, and my wife whose continuous encouragement has motivated me on this long journey. I would like to dedicate my thesis to my parents.

ABSTRACT

Metal clusters with ultra-small size offer many novel properties such as molecule-like optical transitions, photoluminescence, quantized charging, chirality, and so on. Ligand-protected metal nanoclusters with precise compositions appear to be promising building units of various functional materials. Novel properties and promising applications make metal clusters a prolific target of fundamental and applied research. The major challenges of the nanocluster research are developing synthesis protocols for precise control of cluster size, achieving tunability of nanocluster properties, and imparting stability and desired functionality to the clusters particularly in aqueous and biological media. Cluster synthesis often involves multi-step, two-phase methods and results in mixed-sized products that require time-consuming post-synthesis size-separation and surface-modification steps. Therefore, we need to develop straightforward synthesis protocols that can directly produce stable, atomically precise metal nanoclusters in high yields. Further, we need to develop guiding principles for the rational design of desired nanoclusters and tailoring the properties of the nanoclusters. The thesis work attempts to address some of these challenges by taking the cases of two representative nanoclusters, $\text{Au}_{18}(\text{SCH}_2\text{CH}_2\text{COOH})_{14}$ and $\text{Au}_{25}(\text{SCH}_2\text{CH}_2\text{COOH})_{18}$ as examples.

We have developed straightforward direct synthesis methods capable of producing atomically precise gold nanoclusters in high yield in an aqueous medium. We have synthesized two representative nanoclusters, $\text{Au}_{18}(\text{SCH}_2\text{CH}_2\text{COOH})_{14}$ and $\text{Au}_{25}(\text{SCH}_2\text{CH}_2\text{COOH})_{18}$. Among various gold nanoclusters, $\text{Au}_{25}\text{L}_{18}$ (where L= ligand) is a ubiquitous nanocluster because of its extraordinarily high stability, unlike $\text{Au}_{18}\text{L}_{14}$. Our synthesis of atomically-precise water-soluble gold nanoclusters involved a common reducing agent, NaBH_4 , and a short carbon chain bifunctional ligand, $\text{HSCH}_2\text{CH}_2\text{COOH}$ (3-mercaptopropionic acid, MPA) under ambient conditions. We have explored the essential factors that influence the size focusing and stability of water-soluble gold clusters. The synthesis methods do not require maintenance of any special reaction conditions, such as pH, temperatures (such as high or low temperatures), special reagent, etc. By our choice of the bifunctional capping ligand, MPA, we were able to impart water solubility to the gold clusters. Further, we have demonstrated that this kind of

capping ligand allows tailoring of nanocluster stability and properties such as photoluminescence, Raman scattering, catalytic properties, etc. over a wide range in aqueous media simply via the variation of the pH of the media. It also allows transfer of the clusters into an organic solvent such as toluene by using a phase transfer reagent such as tetraoctylammonium bromide (TOAB). We have demonstrated that relative quantities of capping agent to gold precursor ratio ($[\text{thiol}/\text{Au}]$) and the gold precursor to reducing agent ($[\text{Au}]/[\text{NaBH}_4]$) ratios play decisive roles in obtaining size-focused atomically-precise gold nanoclusters. The work will open up new avenues for the rational synthesis of definite sized clusters and tuning of their properties in aqueous media.

Contents

| | |
|------------------------|-----------|
| Contents | VI |
| List of figures | X |
| List of tables | IX |

Chapter 1 General Introduction

| | |
|--|---|
| 1.1 Background: Ultra-small metal nanoclusters | 1 |
| 1.2 Background: Gold Nanoclusters | 2 |
| 1.3 Water-soluble gold nanoclusters: Synthesis and applications | 4 |
| 1.3.1 Obtaining atomically precise water-soluble gold nanoclusters | 6 |
| 1.3.1.1 Post-synthesis separation of nanoclusters | 6 |
| 1.3.1.2 Size focusing | 7 |
| 1.3.1.2.1 Core-etching (thermal and ligand etching) based size focusing methods | 7 |
| 1.4 Aim and theme of the thesis work | 8 |

Chapter 2 Instrumentations for Characterizations of Nanoclusters

| | |
|--|----|
| 2.1 UV-Visible Spectroscopy | 10 |
| 2.2 Infrared (IR) spectroscopic analysis | 11 |
| 2.3 Photoluminescence (PL) | 11 |
| 2.4 Transmission electron microscopy (TEM) | 12 |
| 2.5 Energy Dispersive X-ray Analysis (EDAX) | 12 |
| 2.6 Thermogravimetric analysis (TGA) | 12 |
| 2.7 MALDI-MS (Matrix-Assisted Laser Desorption Ionization mass spectrometry) | 13 |

| | |
|---|----|
| 2.8 X-ray photoelectron spectroscopy (XPS) | 14 |
| 2.9 Polyacrylamide Gel Electrophoresis (PAGE) | 15 |
| 2.10 Electrochemistry | 16 |

Chapter 3 An Efficient One-Pot Synthesis of Stable Au₁₈(MPA)₁₄ Nanocluster in Aqueous Medium

| | |
|--|----|
| 3.1 Introduction | 17 |
| 3.2 Materials and Methods | |
| 3.2.1 Materials | 19 |
| 3.2.2 Synthesis | 19 |
| 3.2.3 Polyacrylamide gel electrophoresis (PAGE) separation | 20 |
| 3.2.4 Other Characterizations | 20 |
| 3.3 Results and Discussion | 21 |
| 3.3.1 MALDI-MS analysis | 28 |
| 3.4 Conclusions | 29 |

CHAPTER 4 Synthesis of Ubiquitous Nanocluster, Au₂₅(MPA)₁₈, in Aqueous Media

| | |
|---|----|
| 4.1 Introduction | 30 |
| 4.2 Materials and Methods | |
| 4.2.1 Materials | 32 |
| 4.2.2 Synthesis | 32 |
| 4.2.3 Polyacrylamide gel electrophoresis (PAGE) | 33 |

| | |
|-------------------------------------|----|
| 4.2.4 Other Characterizations | 33 |
| 4.3 Results and Discussion | 34 |
| 4.4 Conclusions | 39 |

CHAPTER 5 Tailoring the Stability and Photoluminescence Properties of Nanoclusters in Aqueous Media

| | |
|--|----|
| 5.1 Introduction | 41 |
| 5.2 Methods and Characterizations | 42 |
| 5.3 Results and Discussions | 43 |
| 5.3.1 Stability of the Au ₁₈ (MPA) ₁₄ Clusters | 43 |
| 5.3.2 Stability of Au ₂₅ (MPA) ₁₈ clusters | 45 |
| 5.3.3 Photoluminescence of Au ₁₈ (MPA) ₁₄ | 47 |
| 5.3.4 Photoluminescence of Au ₂₅ (MPA) ₁₈ | 50 |
| 5.4 Conclusions | 52 |

CHAPTER 6 Catalytic Properties of Au₁₈(MPA)₁₄ and Au₂₅(MPA)₁₈ Nanoclusters: Reductions of Ortho- and Para-Nitroanilines by NaBH₄ in Water

| | |
|--|----|
| 6.1 Introduction | 53 |
| 6.2 Materials and Methods | |
| 6.2.1 Materials | 56 |
| 6.2.2 Characterizations | 56 |
| 6.2.3 Reduction of Nitroanilines | 56 |
| 6.3 Results and Discussion | 56 |

| | |
|---|--------|
| 6.4 Conclusions | 62 |
| CHAPTER 7 Au₁₈(MPA)₁₄ and Au₂₅(MPA)₁₈ Nanoclusters as Raman Substrates: pH-Mediated Tuning of Raman Scattering Properties of MPA | |
| 7.1 Introduction | 63 |
| 7.2 Materials and Methods | 64 |
| 7.3 Results and Discussion | 65 |
| 7.4 Conclusions | 77 |
| Chapter 8 Summary and General Conclusions | 78 |

List of Figures

| | |
|--|----|
| Figure 1.1 Size comparisons of nanoclusters with nanoparticles and atoms | 1 |
| Figure 1.2 Evolution of band gaps and density of states (DOS) in bulk material, nanoparticles, and nanoclusters. (Ef: Fermi level) | 2 |
| Figure 1.3 Pictorial representation of thiol-protected gold nanocluster | 3 |
| Figure 2.1 Different kinds of matrices used in MALDI-MS analysis | 14 |
| Figure 3.1 Temporal development of UV-Visible absorption spectra during the formation of $\text{Au}_{18}(\text{SC}_2\text{H}_4\text{CO}_2\text{H})_{14}$ | 21 |
| Figure 3.2 Effect of MPA/Gold molar ratio on size selected $\text{Au}_{18}(\text{SC}_2\text{H}_4\text{CO}_2\text{H})_{14}$ clusters synthesis | 22 |
| Figure 3.3 UV-Visible spectrum of $\text{Au}_{18}(\text{SC}_2\text{H}_4\text{CO}_2\text{H})_{14}$ after PAGE separation. The inset shows a photo-image of the gel after PAGE | 23 |
| Figure 3.4 A representative TEM image of $\text{Au}_{18}(\text{SC}_2\text{H}_4\text{CO}_2\text{H})_{14}$ clusters | 23 |
| Figure 3.5 Transmission electron microscope (TEM) images of $\text{Au}_{18}(\text{SC}_2\text{H}_4\text{CO}_2\text{H})_{14}$ nanoclusters showing electron beam induced aggregation | 24 |
| Figure 3.6 FT-IR spectra of MPA (bottom) and $\text{Au}_{18}(\text{SC}_2\text{H}_4\text{CO}_2\text{H})_{14}$ (top) (offset for clarity). The dotted line shows the position of the (S–H) vibrational frequency peak | 24 |
| Figure 3.7 The S (sulfur) $2p$ core level X-ray photoemission spectra (XPS) of Au-MPA nanocluster sample. The spectra were fit by using Gaussian line functions for two S $2p$ doublets with the same full width at half-maximum (fwhm), the standard spin-orbit splitting of 1.2 eV, and a 2:1 (S $2p_{3/2}$)/(S $2p_{1/2}$) area ratio | 25 |

| | |
|---|----|
| Figure 3.8 The Au (gold) 4 <i>f</i> core level X-ray photoemission spectra (XPS) (along with multi-peak curve fitting) of Au-MPA nanocluster sample. Three 4 <i>f</i> doublets (peaks 1, 2 and 3's) with the Gaussian line functions of the same fwhm, 4:3 area ratios and splittings of 3.7 eV were fit for the major two peaks of the experimental spectrum | 26 |
| Figure 3.9 TGA graph of Au ₁₈ (MPA) ₁₄ nanocluster | 27 |
| Figure 3.10 A representative SEM-EDAX spectrum of Au ₁₈ (MPA) ₁₄ nanocluster | 28 |
| Figure 3.11 MALDI-TOF MS of Au ₁₈ (SC ₂ H ₄ CO ₂ H) ₁₄ nanocluster sample | 28 |
| Figure 4.1. UV-Visible spectra of the cluster: direct reduction and stepwise reduction | 34 |
| Figure 4.2. Corresponding UV-vis spectra of the formation of Au ₂₅ (MPA) ₁₈ cluster solution ... | 35 |
| Figure 4.3. PAGE separated Au ₂₅ (MPA) ₁₈ NCs | 36 |
| Figure 4.4 Representative TEM image of Au ₂₅ NCs | 36 |
| Figure 4.5 SEM-EDAX image of Au ₂₅ (MPA) ₁₈ cluster | 37 |
| Figure 4.6 TGA graph of Au ₂₅ (MPA) ₁₈ nanocluster sample | 37 |
| Figure 4.7 Differential Pulse Voltammetry (DPV) data of Au ₂₅ (MPA) ₁₈ in 0.1M KCl solution (to find the HOMO-LUMO band gap of the cluster) | 38 |
| Figure 4.8 The Au 4 <i>f</i> core level x-ray photoemission spectra (XPS) of Au ₂₅ (MPA) ₁₈ | 39 |
| Figure 5.1 Time-dependent UV-Visible absorption spectra of the Au ₁₈ (MPA) ₁₄ cluster solution (pH ~8.6). | 43 |
| Figure 5.2 Time-dependent UV-Visible absorption spectra of the Au ₁₈ (MPA) ₁₄ cluster in toluene solvent medium. | 44 |
| Figure 5.3 UV-vis spectra of the aqueous solutions of Au ₁₈ (MPA) ₁₄ under different pH values: (a) decreasing and (b) increasing pH | 45 |

| | |
|---|----|
| Figure 5.4 Stability of Au ₂₅ (MPA) ₁₈ clusters with pH; Au ₂₅ original cluster (pH 9.4) (a), Au ₂₅ pH 10 (b), Au ₂₅ pH 11 (c), Au ₂₅ pH 12 (d) | 46 |
| Figure 5.5 Au ₂₅ (MPA) ₁₈ cluster stability in acidic pH (at pH 5) | 47 |
| Figure 5.6 pH-Dependent photoluminescence spectra of Au ₁₈ (SC ₂ H ₄ CO ₂ H) ₁₄ at λ _{ex} = 560 (a) and 350 (b) nm | 48 |
| Figure 5.7 pH-Dependent photoluminescence spectra of Au-MPA complex at λ _{ex} =350 nm | 49 |
| Figure 5.8 (a) UV-vis absorption and (b) PL spectra of Au ₁₈ (SC ₂ H ₄ CO ₂ H) ₁₄ before and after the water to organic phase transfer | 50 |
| Figure 5.9 Au ₂₅ (MPA) ₁₈ clusters in acidic and basic medium & their photoluminescence spectra | 51 |
| Figure 6.1 Au ₂₅ catalyzed reduction of ortho-nitroaniline (a,b) and, para-nitroaniline (c,d) by using NaBH ₄ as the reducing agent in water solvent | 58 |
| Figure 6.2 Control experiments: reduction of 2-NA (a), 4-NA (b) by using NaBH ₄ reducing agent in the absence of Au NC catalyst | 58 |
| Figure 6.3 2-NA catalysis with 100, 200 μL Au NC | 60 |
| Figure 6.4 4-NA catalysis with 100, 200 uL Au NC | 61 |
| Figure 7.1 SERS spectra of Au ₂₅ (MPA) ₁₈ nanocluster in basic media | 67 |
| Figure 7.2 SERS spectra of Au ₂₅ (MPA) ₁₈ NCs in acidic media | 67 |
| Figure 7.3 Raman spectra of Au ₁₈ (MPA) ₁₄ under acidic and basic pH conditions | 68 |
| Figure 7.4 Geometries of mercaptopropionic acid (MPA), Au ₃ tagged MPA (Au ₃ -MPA), and dimers of Au ₃ -MPA (Dimer Au ₃ -MPA) optimized at B3LYP/6-31++G U LANL2DZ level of theory in | |

the gas phase. Here, Con1 and con2 stand for the conformation 1 and conformation 2 respectively 73

Figure 7.5 Geometries of Au₃ tagged MPA (acidic-Au₃-MPA), and dimers of Au₃-MPA (Acidic - Dimer Au₃-MPA) optimized at B3LYP/6-31++G U LANL2DZ level of theory in the gas phase. Here, Con1 and con2 stands for conformation 1 and conformation 2 respectively 74

Figure 7.6 Geometries of Au₃ tagged MPA (basic-Au₃-MPA), and dimers of Au₃-MPA (Basic-dimer Au₃-MPA) optimized at B3LYP/6-31++G U LANL2DZ level of theory in the gas phase. Here, Con1 and con2 stand for conformation 1 and conformation 2 respectively 75

Figure 7.7 Depolarization ratios and corresponding Raman spectrum of acidic (below) and basic (above) dimers of Au₃-MPA 76

List of Tables

Table 7.1 SERS signal assignment of MPA bound $\text{Au}_{25}(\text{MPA})_{18}$ clusters 66

Table 7.2 Modes of vibrations, wavenumbers, Raman intensities and depolarization ratios of dimer $\text{Au}_3\text{-MPA}$, con1 optimized at B3LYP/6-31++G U LANL2DZ level of theory in the gas phase. Here, ω : wavenumber, R.I.: Raman Intensity, ρ : Depolarization ratio 72

List of Abbreviations

- HAuCl₄ - Tetrachloroauric(III) acid
- MPA - Mercaptopropionic acid
- TOABr - Tetraoctylammonium bromide
- NaBH₄ - Sodium borohydride
- PAGE - Polyacrylamide gel electrophoresis (PAGE)
- UV - Ultra violet
- FTIR - Fourier-transform infrared spectroscopy
- TEM - Transmission electron microscopy
- EDAX - Energy dispersive X-ray analysis
- TGA - Thermogravimetric analysis
- XPS - X-ray photoelectron spectroscopy
- MALDI - Matrix-assisted laser desorption ionization
- MS - Mass spectrometry
- TOF - Time-of-flight
- DPV - Differential pulse voltammetry
- DFT - Density functional theory
- QY - Quantum yield
- PL - Photoluminescence

LIST OF PUBLICATIONS

1. Shweta Bhardwaj, Ramakrishna Itteboina, and Tapan K. Sau: Observing Ultra-Small Gold Cluster to Plasmonic Nanoparticle Evolution in a One-Pot Aqueous Synthesis. *ChemistrySelect*, 2016, 1, 3091–3096.
2. Ramakrishna Itteboina, U. Divya Madhuri, Partha Ghosal, Monica Kannan, Tapan Kumar Sau, Tatsuya Tsukuda, and Shweta Bhardwaj: Efficient Single-Step Synthesis of Atomically Precise $\text{Au}_{18}(\text{MPA})_{14}$ Clusters: pH-Dependent Stability and Photoluminescence. *J. Phys. Chem. A* 2018, 122, 1228–1234.
3. Ramakrishna Itteboina, and Tapan K. Sau: Sol-Gel Synthesis and Characterizations of Morphology-Controlled Co_3O_4 Particles; *Materials Today: proceedings* (Just accepted)
4. Ramakrishna Itteboina¹, Tapan Kumar Sau, Parijat Ray, Partha Ghosal Synthesis of $\text{Au}_{25}(\text{MPA})_{18}$ Nanoclusters in Aqueous Medium: Catalytic Activity in Reduction of Ortho, Para nitroanilines. (Manuscript to be submitted)
5. Ramakrishna Itteboina, N.V. Suresh, and Tapan Kumar Sau: Aggregation Induced Surface-Enhanced Raman Scattering of $\text{Au}_{25}(\text{MPA})_{18}$ Nanoclusters. (Manuscript To Be Submitted)

CONFERENCES & WORKSHOPS

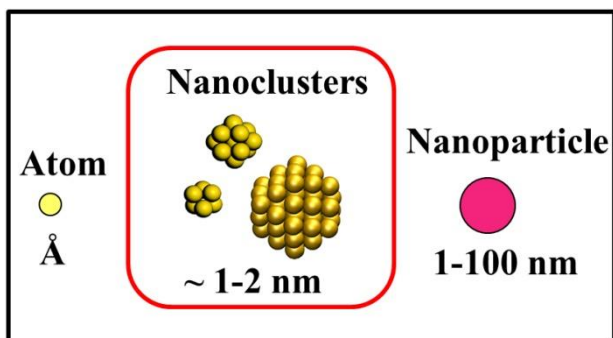
1. 4TH Bangalore nano International conference, Bangalore, December 9-10, 2011.
2. National workshop on “Advances in X-ray powder Diffractometry & Scanning electron microscopy”, Rajiv Gandhi University of Knowledge Technologies (RGUKT), IIIT-Hyderabad, July 15-17, 2013.
3. Ramakrishna Itteboina, Tapan Kumar Sau, Sol-Gel Synthesis of Octahedron-Shaped Cobalt Oxide Particles. 6TH Bangalore India nano International conference, Bangalore, December 4-6, 2013.
4. Ramakrishna Itteboina, Tapan Kumar Sau, Sol-Gel Synthesis of Octahedron-Shaped Cobalt Oxide Particles. ICONSEA-2014, JNTU-Hyderabad, June 26-28, 2014.
5. MCBR Winter School, 2014, DST - SERB Winter School on Modelling chemical and Biological (Re) activity, in association with Indian Institute of Chemical Technology (IICT) and International Institute of Informational Technology (IIIT), Hyderabad, January 2-22, 2014.
6. Attended and presented a poster at “International Conference on Nanoscience and Nanotechnology (ICNAN’16), 19th to 21st October 2016 Vellore, Tamilnadu, India.

General Introduction

1.1 Background: Ultra-small metal nanoclusters

In recent years, nanoscale materials, particularly metal nanoparticles (NPs) and nanoclusters (NCs), have attracted substantial research interest due to their intriguing size and shape dependent physicochemical properties and promising applications. Metal nanoclusters are ultra-small (<2 nm) nanoparticles or nano molecules, typically composed of few tens to hundreds of metal atoms protected by ligand molecules such as thiols, phosphines, amines, selenates, etc. Nanoclusters generally denoted as $M_n(L)_m$ (where n and m represent the number of metal atoms and capping ligands respectively). Because of the ultra-small size, the physicochemical properties of metal NCs substantially differ from their bulk and nanoparticle counterparts.

Figure 1.1 Size comparisons of nanoclusters with nanoparticles and atoms.



In the case of nanoclusters that have a size <2 nm, continuous/semi-continuous density of states breaks down into discrete energy levels (**Figure 1.2**) which results in the unique molecule-like properties, such as HOMO–LUMO (highest occupied and lowest unoccupied molecular orbital) electronic transitions, photoluminescence, quantized charging, intrinsic magnetism, optical activity, and so on. Because of having dimensions in between metal atoms and nanoparticles, clusters can provide a missing link between atoms and nanoparticles. Thus,

the study of the structure and properties of nanoclusters is very important in order to understand the gradual emergence of various properties and crystal structures in solids.

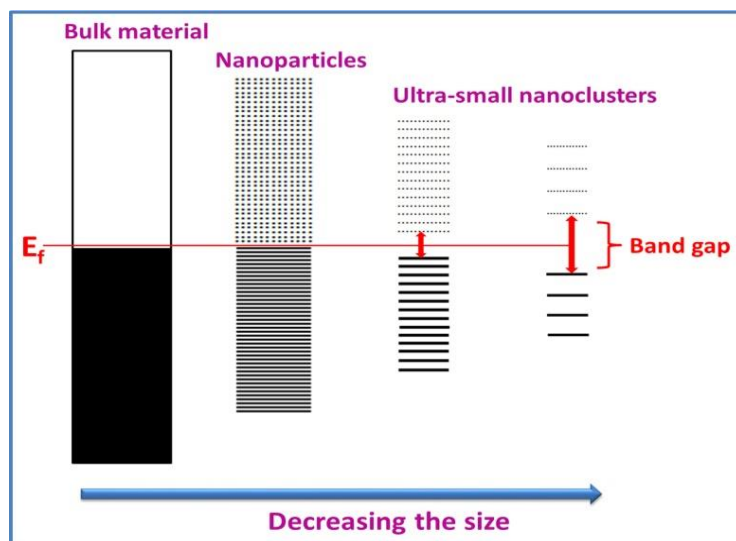


Figure 1.2 Evolution of band gaps and density of states (DOS) in bulk material, nanoparticles, and nanoclusters.^[1] (E_f : Fermi level)

Among various metal nanosystems, gold nanoparticles and nanoclusters have gained a tremendous attention because of their attractive optoelectronic properties, stability, ease of surface modifications, and biocompatibility. The novel properties coupled with an ultra-small size made gold nanoclusters promising candidates for various applications such as catalysis, bio-sensing, fluorescent labeling, cellular imaging, heavy metal ion detection, and so on.^[2-6] Features and properties like the ultra-small size, bio-compatibility, less toxicity, and tunable photo-luminescence of gold NCs are particularly useful for various biological applications.^[7-9]

1.2 Background: Gold Nanoclusters

Research on monolayer protected clusters picked up momentum after the reports of two-phase gold nanoclusters synthesis by Brust and Schiffrin in 1994^[10]. Since then gold

nanoclusters have been prepared by using a number of methods. A majority of them involves two or more steps as in the classic “B Brust two-phase organic-water solvent” method that uses a variety of organic thiols (long chain or aromatic thiols as binding ligands). The thiol-capped ultra-small nanoclusters show high stability in solution as well as solid form. Later, various noble metal nanoclusters (mainly Au, Ag) had been synthesized by using other protecting ligands such as sulfides, phosphines, amines, selenides etc.^[11–15]

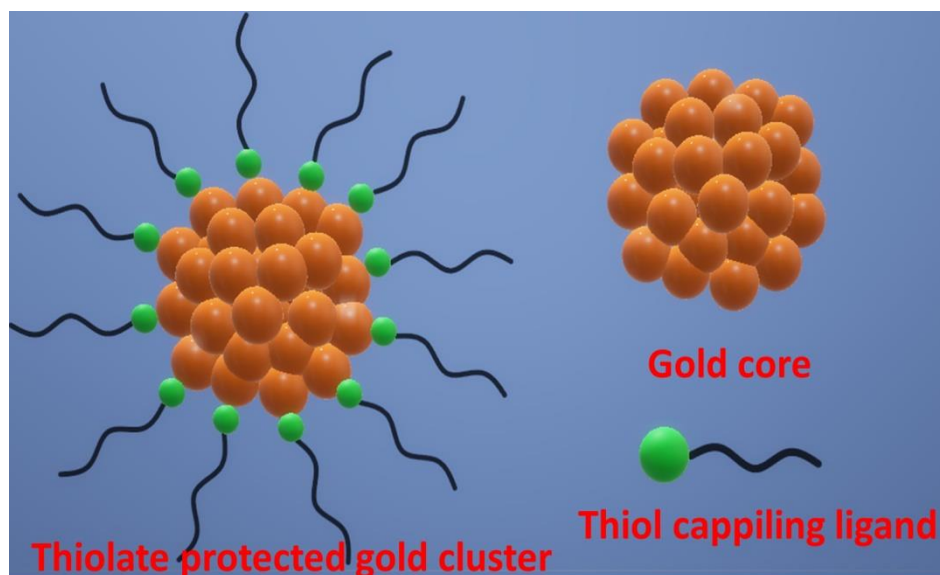


Figure 1.3 pictorial representation of thiol-protected gold nanocluster

B Brust’s two-phase method for the synthesis of monolayer-protected gold nanoclusters motivated many scientists to prepare the gold nanoclusters protected by a variety of organic capping ligands such as alkanethiols and aryl thiols ($R-SH$, $R=$ alkyl, aryl groups). Among various capping ligands, thiol capping ligands were widely used as suitable candidates for the synthesis of gold nanoclusters, because sulfur (S) forms a strong covalent bond ($Au-S$) with gold. Murray and co-workers employed various alkanethiols such as hexane thiol (C_6-SH), octanethiol (C_8-SH), dodecanethiol ($C_{12}-SH$) and arenethiols as capping ligands to prepare the ultra-small monolayer-protected gold nanoparticles of $\sim 1-2$ nm dimensions. They had extensively studied

various electronic properties of the monolayer-protected gold nanoclusters.^[16–18] Kornberg et al. successfully synthesized the ultra-small gold nanoparticles of 1.5- 4 nm sizes by using various carboxylic acid substituted thiol capping ligands.^[19] Similarly, many other synthetic protocols and protecting ligands were reported for the synthesis of ultra-small gold and other metal nanoclusters. Whetten and co-workers reported the synthesis of ultra-small gold nanoclusters by using organic thiol capping ligands (alkanethiol and aryl thiols) of different chain lengths. The same group successfully synthesized and isolated the gold clusters of 38, 75, 101 and 146 atoms and determined cluster sizes by using laser desorption ionization mass spectrometry technique (LDI-MS).^[20,21]

One of the important issues in the nanocluster synthesis is the use of mainly organic solvents (toluene, hexane, etc). In order to impart the strong sulfur-gold ‘soft-soft’ interactions and required inter-cluster steric repulsions, most of the effective capping ligands appear to be long alkyl chain or aryl substituted thiols that are soluble in organic solvents.^[22–24] Thus, a substantial body of work has been done in the synthesis, isolation, and characterization of ‘organic solvent soluble’ gold nanoclusters. Several potential applications of such nanoclusters have also been demonstrated. On the contrary, the synthesis, characterization, and applications of ‘water-soluble’ gold nanoclusters appear to be highly lagging.

1.3 Water soluble gold nanoclusters: Synthesis and applications

In recent times, ligand protected ultra-small gold nanoclusters have drawn the interest of researchers because of their interesting physicochemical properties that are sometimes not observed in their nanoparticle counterparts. Water-soluble or hydrophilic nanoclusters, particularly of gold, can be very useful for various biological applications such as biological labeling, bio-catalysis, and nano-bioconjugates because of their hydrophilic nature and better bio-compatibility compared to organic soluble clusters.^[7,25] Organic solvent-soluble, hazardous hydrophobic capping ligands restrict their usage in many biological applications. Recent studies demonstrated the potential of applications of gold nanoclusters with hydrophilic capping

ligands in various biological fields such as fluorescent biological labeling, sensing, imaging^[6], antimicrobial agents,^[9] drug delivery.^[26] etc.

Recently Xie and co-workers studied how the capping ligand on cluster surface influences the biological processes such as generation of intracellular reactive oxygen species (ROS), cytotoxicity, and genotoxicity. They have employed mercaptopropionic acid (MPA) and glutathione (GSH) protected Au NCs to study the role of capping ligands. According to their studies, MPA-capped Au NCs yield higher intracellular reactive oxygen species (ROS) compared to the glutathione-capped Au NCs, which could be attributed to the higher cellular internalization of MPA-capped Au NCs over glutathione capped ones.^[7] The same group demonstrated that Au-25 nanoclusters showed the superior antimicrobial activity towards both Gram-positive and Gram-negative bacteria compared their larger nanoparticle counterparts.^[9] Zhang and co-workers studied the effect of Au NC charge on their stability in blood plasma, biodistribution, excretion, toxicity and therapeutic potential. They have reported that charge of nanocluster significantly influences the tumor uptake and renal clearance of nanoclusters in vivo studies.^[27] Water-soluble Au NCs display interesting fluorescence properties in the visible spectrum. Bio-compatibility coupled with high photo-stability makes water-soluble Au NCs as suitable candidates in cellular imaging and labeling applications in biology.^[6,28]

Thus, it is evident that the nanocluster surface chemistry plays important roles in various catalytic and biological applications. Therefore, the selection of suitable capping ligands is crucial in the gold nanocluster synthesis in order to make the clusters suitable for various applications. Researchers have employed post-preparation ligand exchange to change the organic solvent-water solubility and other properties of the nanoclusters.^[29–32] Attempts have also been made to synthesize water-soluble gold, silver, and their alloy nanoclusters by using a variety of water-soluble ligands.^[33–36] Often mixed sized clusters were observed as products. Researchers employed mild reducing agents such as carbon monoxide (CO) and sodium cyanoborohydride (NaBH_3CN) to synthesize size selected water-soluble gold nanoclusters.^[37,38] A weak reducing agent provides a mild and controllable reduction kinetics which favors the controlled growth of nanoclusters. However, these reducing agents are poisonous in nature and

require special handling conditions. On the other hand, strong reducing agents often result in the faster reaction kinetics that leads to the formation mixed-sized clusters. In some cases, a strong reducing agent such as NaBH_4 was employed with systematic pH control, in order to regulate the reducing strength of NaBH_4 which depends on the pH of the reaction medium.^[39,40]

1.3.1 Obtaining atomically precise water-soluble gold nanoclusters

As it was mentioned above, one of the major challenges faced in the aqueous metal nanocluster synthesis is the formation of poly-dispersed clusters, that is, the formation of a mixture of different sized clusters. However, the physicochemical properties of the nanoclusters are highly dependent on their size, geometry, and capping ligand. It is, therefore, highly desirable to develop new synthesis protocols that can produce gold nanoclusters with atomic precision in order to explore the properties as well various applications of the nanoclusters. In the following sections, a few strategies that had been employed to obtain the atomically precise gold nanoclusters are mentioned briefly.^[41]

1.3.1.1 Post-synthesis separation of nanoclusters

Researchers had employed various post-synthesis analytical and chemical separation techniques such as polyacrylamide gel electrophoresis (PAGE),^[42,43] size exclusion chromatography (SEC),^[44] high-performance liquid chromatography (HPLC),^[45] thin-layer chromatography (TLC),^[46] fractional precipitation,^[47] and so on to separate the nanoclusters of definite size and composition. First, Tsukuda and coworkers successfully isolated a series of atomically precise glutathione protected gold nanoclusters by employing the polyacrylamide gel electrophoresis (PAGE) separation technique.^[42] They employed electrospray ionization mass spectrometry (ESI-MS) to determine the molecular formula of the synthesized clusters. The isolated clusters were identified as $\text{Au}_{18}(\text{SG})_{11}$, $\text{Au}_{21}(\text{SG})_{12}$, $\text{Au}_{25\pm 1}(\text{SG})_{14\pm 1}$, $\text{Au}_{28}(\text{SG})_{16}$, $\text{Au}_{32}(\text{SG})_{18}$, $\text{Au}_{39}(\text{SG})_{23}$ (SG= Glutathione). This is the first report on the successful mass determination of atomically precise gold nanoclusters using ESI-MS.^[48] Currently, PAGE is a convenient separating technique used to isolate the clusters of a given size. Other chromatographic techniques such as size-exclusion chromatography (SEC), high-performance liquid

chromatography (HPLC), and thin-layer chromatography were also employed to separate a number of nanoclusters such as $\text{Au}_{38}(\text{SR})_{24}$ and $\text{Au}_{40}(\text{SR})_{24}$, and $\text{Au}_{55}(\text{SR})_{31}$.^[46,49–51] However, the post-synthesis separation techniques are always time-consuming, cumbersome, and economically less viable. Therefore, researchers have been exploring various kinetic and thermodynamic control-based size focusing strategies in order to produce the atomically precise gold nanoclusters in high yields.

1.3.1.2 Size focusing

“Size focusing” approach is a synthetic strategy, which allows producing the single sized nanoclusters instead of polydispersed ones in the synthesis. Size focusing approach is a two-step process. First, polydispersed gold clusters are formed and then the pre-synthesized polydispersed nanoclusters are converted into a nearly single sized/monodispersed clusters by the ligand or thermal etching processes.^[52,53] The origin of size focusing lies in the inherent stability difference of different-sized nanoclusters. Therefore, in size focusing process, the more stable clusters form whereas at the expense of the less stable ones. Researchers reported the synthesis of a number of atomically precise gold nanoclusters, e.g., $\text{Au}_{25}(\text{SR})_{18}$, $\text{Au}_{38}(\text{SR})_{24}$, $\text{Au}_{144}(\text{SR})_{60}$ and $\text{Au}_{333}(\text{SR})_{79}$ by using the size focusing approaches.^[54–57]

1.3.1.2.1 Core-etching (thermal and ligand etching) based size focusing methods

Core-etching is also a two-step size focusing method. This involves the conversion of an initially synthesized polydispersed gold nanoclusters into nearly monodispersed (single-sized) gold nanoclusters either by employing the higher temperatures (thermal induced etching) and/or by using the excess thiol ligands (ligand-induced etching).^[53,58–60] For example, Jin’s group and co-workers reported the synthesis of $\text{Au}_{130}(\text{p-MBT})_{50}$, $\text{Au}_{104}(\text{m-MBT})_{41}$ and $\text{Au}_{40}(\text{o-MBT})_{24}$ by using ligand-induced etching at 80-90°C in the presence of excess para-, meta-, ortho-methylbenzenethiols.^[61] Recently, Dass and coworkers reported the synthesis of three distinct Au NCs namely, $\text{Au}_{38}(\text{SCH}_2\text{CH}_2\text{Ph})_{24}$ ($\text{SCH}_2\text{CH}_2\text{Ph}$ = Phenylethanethiol), $\text{Au}_{36}(\text{SPh-tBu})_{24}$, and $\text{Au}_{30}(\text{StBu})_{18}$ (SPh-tBu = 4-tert-butylbenzenethiol) by using the ligand etching protocol. They first synthesized polydispersed glutathione protected Au NCs followed by the ligand etching in

the presence of excess phenylethanethiol (PET) and 4-tert-butylbenzenethiol (SPh-tBu) capping ligands at 80°C.^[62] Similarly, Au₃₈(PET)₂₄ (PET = phenylethanethiol) Au₂₅(SR)₁₈, Au₃₈(SC₁₂H₂₅)₂₄, Au₄₀(SR)₂₄, Au₅₅(SR)₃₁ and several other definite sized Au NCs were prepared in high yields with high purity by using the thermal and ligand-induced etching-based size focusing methods. [55,63][58,64–66]

1.4 Aim and theme of the thesis work

We have noted above that the physicochemical properties of nanoclusters are strongly dependent on the cluster size, composition, structure, solvent medium, and so on. Therefore, the major goals of the nanocluster research remain to be the size-selective synthesis, achieving control of nanocluster properties, and imparting stability and desired functionality to the clusters, particularly in aqueous and biological media. In order to avoid the cost and time-consuming post-synthesis size-separation and surface-modification steps, we need to develop straightforward synthesis protocols that can directly produce stable, atomically-precise metal nanoclusters in high yields. Further, one needs to develop general guiding principles for the rational design of desired nanoclusters and tailoring the properties of the nanoclusters. This requires a detailed understanding of the factors that govern the formation of atomically-precise nanoclusters. This kind of knowledge will open up new avenues for the preparation of various definite sized clusters with different protecting ligands in different solvent media.

The thesis work focuses on the development of straightforward direct synthesis method capable of producing atomically-precise gold nanoclusters in high yield in an aqueous medium. We have taken the cases of two representative nanoclusters, Au₁₈(MPA)₁₄ and Au₂₅(MPA)₁₈. Among various gold nanoclusters, Au₂₅L₁₈ (where L= ligand) is a ubiquitous nanocluster because of its extraordinarily high stability, unlike Au₁₈L₁₄. We report the successful synthesis of atomically-precise water-soluble gold nanoclusters by using the common reducing agent, NaBH₄, and a short carbon chain bifunctional ligand, MPA under ambient conditions. The essential factors that influence the size focusing and stability of water-soluble gold clusters were explored. The synthesis methods do not require maintenance of any special reaction

conditions, such as pH, temperatures (such as high or low temperatures), special reagent, etc. We have chosen a very short carbon chain bifunctional capping ligand, 3-mercaptopropionic acid (MPA), to impart water solubility to the gold clusters. Further, we have demonstrated that this kind of capping ligand allows tailoring of nanocluster stability and properties such as photoluminescence, Raman scattering, etc. over a wide range in aqueous media simply via the variation of pH of the media. It also allows transfer of the clusters into an organic solvent like toluene by using a phase transfer reagent like tetraoctylammonium bromide (TOAB). We have used the common strong reducing agent, NaBH_4 , without any pH control. We have demonstrated that irrespective of the strength of the reducing agent, relative quantities of capping agent to gold precursor ratio ($[\text{thiol}/\text{Au}]$) and the gold precursor to reducing agent ($[\text{Au}]/[\text{NaBH}_4]$) ratios play decisive roles in obtaining size-focused atomically-precise gold nanoclusters. We have employed a number of techniques such as the polyacrylamide gel electrophoresis (PAGE), UV-Visible and FTIR spectroscopies, transmission electron microscopy (TEM), energy dispersive X-ray analysis (EDAX), thermogravimetric analysis (TGA), X-ray photoelectron spectroscopy (XPS) and matrix-assisted laser desorption ionization-time of flight mass spectrometry (MALDI-TOF MS) to characterize the formation, composition, and purity of the clusters. Further, we have studied the photoluminescence, Raman scattering, electrochemical, and catalytic properties of the synthesized water-soluble nanoclusters systems. The work reveals some important principles that can be useful in the development of a general toolbox for the rational design of size-selective synthesis and tailoring the properties of many metal nanoclusters.

Instrumentations for Characterizations of Nanoclusters

The studies of syntheses, characterizations, and properties of ultra-small systems such as nanoclusters are heavily dependent on various apparatus and analytical instruments. For examples, ultraviolet-visible spectroscopy (UV-vis) and photoluminescence spectroscopy (PL) were employed to study the optical absorption and excitation/emission properties of the nanoclusters. Fourier transform infrared spectroscopy (FTIR) was used to study the gold-thiol binding interactions in addition to the functional group's information of the capping ligands. Transmission electron microscopy (TEM) was used to study the cluster size (and cluster aggregation). Energy dispersive X-ray analysis (EDAX) and thermogravimetric analysis (TGA) were used to determine the gold to thiol ratios in the cluster. Electrochemical band gaps (HOMO-LUMO) of the cluster was measured by using differential pulse voltammetry (DPV) technique by using an electrochemical apparatus. X-ray photoelectron spectroscopy (XPS) was used to find the binding energy of Au and S. The molecular weight and molecular formula of the gold clusters were determined by the matrix-assisted laser desorption ionization-time of flight mass spectrometry (MALDI-TOF MS). Synthesized clusters were isolated by using polyacrylamide gel electrophoresis (PAGE) separation technique. In this chapter, we briefly discuss a few such instrumental techniques in the context of nanoclusters.

2.1 UV-Visible Spectroscopy

UV-Visible spectroscopy deals with the electronic transitions associated with the molecules upon absorbing the ultraviolet (200-400nm) and/or visible (400-800nm) electromagnetic radiations. Electronic transitions occur from ground state electronic energy level to the higher electronic energy levels. The spectral peaks observed in the UV-Visible absorption of nanoclusters correspond to different HOMO-LUMO transitions associated with the gold nanoclusters. UV-Visible spectral features strongly vary with the cluster size, geometry

and capping ligands. Atomically precise gold nanoclusters give rise to distinct spectral peaks in UV-Visible spectra. Therefore, UV-Visible spectroscopy acts as a powerful tool in the studies of the cluster formation and size estimation.

2.2 Infrared (IR) spectroscopic analysis

Infrared spectroscopy (IR) is a well-established spectroscopic method for the structural and functional group identification of a molecule. Infrared spectroscopy utilizes the electromagnetic radiation of 2.5 μm to 25 μm (2500 nm to 25000 nm) wavelength. When IR radiation is passed through a sample, some portion of the radiation is absorbed by the sample due to the vibrations of a set of bonds and the rest of it is passed through (transmitted). The resulting IR spectrum creates a molecular fingerprint of the sample. For a molecule to show infrared absorptions, there must be a non-zero change in the electric dipole moment of the molecule during the molecular vibrations. Infra-red analysis elucidates the structural properties of the ligands connected to the metal nanoclusters. By comparing the IR absorption spectra of pure ligands with that of the protected metal nanoclusters, the disappearance of the S-H vibrational band (2535–2564 cm^{-1}) in the nanoclusters confirms the formation of metal-thiol bonding through the sulfur atom. Infrared spectroscopy can also be used to identify the C-S bonding, aggregation, and dimerization of the capping ligands, etc.

2.3 Photoluminescence (PL)

Photoluminescence (PL) spectroscopy is a very efficient, contactless, and nondestructive technique, widely used to study the optoelectronic properties of molecules and semiconducting nanosystems. Photoluminescence involves the spontaneous/instantaneous emission of light from a material upon optical excitation (electromagnetic radiation). As photoluminescence involves de-excitation of electrons from a higher energy level to a lower energy level, every photoluminescent substance displays its own characteristic excitation and emission spectra upon irradiation. Thiolate protected ultra-small metal nanoclusters act as promising candidates for photoluminescence applications. Recent developments proved that water-soluble ultra-small gold nanoclusters act as excellent PL alternatives in biomedical field due to their inherent

biocompatibility and good photoluminescence (PL) properties. PL properties of Au NCs depend on cluster core size and the nature of the protecting ligand.

2.4 Transmission electron microscopy (TEM)

In TEM, a beam of electrons is transmitted through a specimen to form highly magnified images of specimens. Transmission electron microscope has the ability to display ultra-high resolution images compared to traditional optical microscope where the optical lens is used to magnify the image. Normal optical microscope gives the resolution in the order of millimeters whereas TEM gives the nanometer scale resolution. Therefore, TEM is an indispensable tool in the studies of the size and morphological features of ultra-small nanosystems with highly magnified images. High-resolution transmission electron microscope (HRTEM) is used to determine the ultra-small particle size and size distribution. However, during HRTEM measurements of metal nanoclusters, it is advisable to use lower operating voltages (120-160 kV) in order to reduce the nanocluster damage/aggregation by the electron beam illumination.

2.5 Energy Dispersive X-ray Analysis (EDAX)

Energy Dispersive X-ray Analysis (EDAX, EDX or EDS) is a sophisticated analytical technique that is used for the elemental analysis or chemical characterization of a material. Energy dispersive x-ray systems are often attached to scanning electron microscope (SEM) instrument where the SEM captures/selects the region of analysis in the sample and EDAX provides the elemental analysis. SEM-EDAX is a powerful tool to examine the surface morphology, the elemental composition and elemental mapping of a sample.

2.6 Thermogravimetric analysis (TGA)

TGA is a well-established thermal analytical technique where thermal changes of the sample with time as a function of temperature can be measured to estimate the composition of various components presented in the sample. The constant heating rate is essential to understand the minute mass changes in the sample during the heating. SEM-EDAX and TGA

both can provide the valuable information regarding the composition of the gold (Au), sulfur (S) and organic content present in the gold nanocluster sample. Au/S ratio leads to find the molecular formula of the synthesized cluster.

2.7 MALDI-MS (Matrix-Assisted Laser Desorption Ionization mass spectrometry)

It is always a big challenge to determine the exact cluster size by employing only the microscopic methods such as SEM and TEM because of the ultra-small size. Gold clusters had been observed to undergo electron beam induced aggregation upon TEM measurements.^[38] Within this regard, MALDI-MS (matrix-assisted laser desorption ionization mass spectrometry) has emerged as an efficient and effective alternative analytical technique. MALDI-MS is widely used for determining the molecular formula or mass of ligand-protected nanoclusters.

MALDI-MS contains three major components which are **1. High energy laser beam:** which converts the solid analyte molecules into gas phase charged ions. **2. Matrix:** The matrix transfers the laser energy from laser light source to the sample. **3. Detector:** Which detects and separates the ions based on their mass(m)-to-charge(z) ratios. Compared to the other conventional mass spectrometric techniques MALDI-MS allows measuring the mass of high molecular weight compounds such as biomolecules (such as DNA, proteins, peptides, and sugars) and large organic molecules (such as polymers, dendrimers, etc). Because of ultra-small size and less stability, nanoclusters usually have a propensity to undergo fragmentation or aggregation during MALDI analysis. These difficulties make the MALDI- MS analysis quite challenging.

In order to get the intact molecular ion peak in MALDI-MS, it is highly desirable to choose the suitable matrix and tuning the intensity of laser beam during MALDI analysis. Dass and co-workers demonstrated the roles of laser beam intensity and choice of the matrix in getting the fine MALDI of $\text{Au}_{25}(\text{SCH}_2\text{CH}_2\text{Ph})_{18}$ cluster.^[22] Matrices are low molecular weight organic compounds (weak organic acids) having low vapor pressure with volatile nature. The most commonly used matrices in MALDI-MS in cluster research are 3,5-dimethoxy-4-

hydroxycinnamic acid (sinapinic acid), α -cyano-4-hydroxycinnamic acid, 2,5-dihydroxybenzoic acid (DHB), and *trans*-2-[3-(4-*tert*-butylphenyl)-2-methyl-2-propenylidene]malononitrile (DCTB). Different matrices are required for the organic solvent soluble and water-soluble nanoclusters in order to get the proper ionization during MALDI analysis. For example, matrices like sinapinic acid, cinnamic acid, DHB and CHCA usually gives intact molecular ion peaks for water-soluble clusters whereas matrix like DCTB is commonly used for the formation of molecular ion peaks of organic soluble clusters. These matrices are dissolved in highly pure solvents like water or organic solvents (e.g., acetonitrile or ethanol).

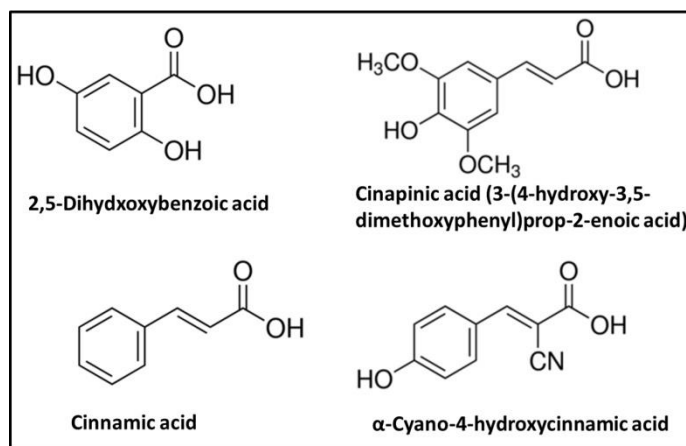


Figure 2.1 Different kinds of matrices used in MALDI-MS analysis

2.8 X-ray photoelectron spectroscopy (XPS):

X-ray photoelectron spectroscopy (XPS) (also known as Electron Spectroscopy for Chemical Analysis, ESCA) is a widely used analytical technique to investigate the chemical composition of surfaces, oxidation states, and relative composition of the constituents. XPS characterization was used to identify the oxidation state and binding energy of the gold clusters. Gold in gold nanoclusters shows their characteristic binding energy in XPS. XPS works on the principles of the photoelectric effect. When an X-ray beam falls on the sample surface, the energy of the X-ray photon is absorbed by the core electron of an atom. If the photon

energy is more than the binding energy of the core electron, the core electron will then escape from the atom and emit out of the surface. The binding energy of solids can be determined by using the below equation.

$$BE = hv - KE - (\phi)$$

Here BE is the binding energy of atom from where electron has ejected, KE is the kinetic energy of electron and Φ is the work function

2.9 Polyacrylamide Gel Electrophoresis (PAGE)

PAGE is a well-established analytical technique for the isolation and purification of biomolecules such as proteins, nucleic acids, and enzymes etc. in biological research. Electrophoresis is the migration of charged molecules in buffered solution in response to an electric field created between a cathode and an anode. PAGE is a simple, rapid and highly sensitive analytical technique for the separation of biomolecules with high accuracy. In PAGE, migration of compounds depends on various factors such as the strength of the applied electric field, net charge and size (molecular weight) of the molecules, ionic strength, viscosity and temperature of the medium.

The typical polyacrylamide gels consist of acrylamide, N,N'-methylenebisacrylamide and a buffer with an adjusted pH. Ammonium persulfate (APS) can be used as a suitable free radical generator as well as stabilizer and N,N',N'-tetramethylethylenediamine (TEMED) is added to initiate polymerization of acrylamide gels. The bisacrylamide forms cross-link in between polyacrylamide molecules during the polymerization. The pore size of the gels can be determined by the following two factors: (i) The total concentration of acrylamide and bisacrylamide (%T) and (ii) the amount of crosslinker (%C). With the increasing %T, the pore size inside the gel decreases. Thus, the higher percentage of gels (with smaller the pore sizes) are required to separate smaller nanoclusters and vice versa. Decreasing %C results in a more open pore structure because of the availability of few cross-linker molecules. When the %C increases, the pore size decreases. Increasing %C beyond 5% also increases the pore size. In addition to

the bisacrylamide, different varieties of crosslinkers such as piperazine diacrylate (PDA), N,N'-bisacrylylcystamine (BAC), and N,N'-diallyltartardiamide (DATD) available.

PAGE separation principles were successfully employed to separate the ultra-small nanoclusters based on their size and charge basis. First, Whetten's group isolated the small-sized glutathione capped gold nanoclusters by using the PAGE separation technique.^[67] Later, Tsukuda and co-workers made significant uses of PAGE in the isolation of atomically precise water-soluble gold nanoclusters.^[48] Recently, Dass et al. demonstrated the PAGE separation of glutathione-capped gold clusters and plasmonic particles from the mixture. They have successfully isolated the 26 unique gold nanocluster and plasmonic particle constituents by using different gel concentrations.^[36]

2.10 Electrochemistry

Electrochemical measurements such as differential pulse voltammetry (DPV) and square wave voltammetry (SWV) were used to measure the electrochemical redox band gap (HOMO-LUMO) of the size selected clusters. Nanoclusters are too small to exhibit the continuum charging behavior of bulk gold. The electrochemical band gap is the voltage difference between first oxidation (O_1) current peak and first reduction current peak (R_1). The electrochemical band gaps are comparable with the optical band gaps measured by the UV-Visible spectral studies. Quantized double-layer charging (QDL) is observed for the cluster size (diameter) range = 1.6 – 2.2 nm, Au_{140} – Au_{314} whereas molecule-like voltammetric behavior has been observed in the case of ultra-small thiol-protected gold nanoclusters such as Au_{75} , Au_{55} , Au_{38} , Au_{25} , Au_{13} , etc. DPV and SWV can be employed as effective tools to understand the redox behavior and band gaps of size-selected cluster species.

An Efficient One-Pot Synthesis of Stable Au₁₈(MPA)₁₄ Nanocluster in Aqueous Medium

3.1 Introduction

Ligand-protected metal clusters with precise compositions appear to be promising building units of various functional materials.^[68–72] Quantum size effects and unique geometrical structures of the ligand-protected metal clusters offer many novel properties such as molecule-like optical transitions,^[67] photoluminescence (PL),^[10,42,73] quantized charging,^[72] and so on. Novel properties along with ultra-small size and promising applications make metal clusters a prolific target of fundamental and applied research.^[5,6,8,9,74–79] Among various metal clusters, thiolated gold clusters have drawn special attention because of their many additional attractive features such as high chemical stability, facile surface chemistry, excellent photostability, interesting photoluminescence properties, less toxicity, and so on.^[28,80–82] Thiolated gold clusters have shown huge potentials for various applications.^[4,71,72,83] Characteristics such as the small size, less toxicity, interesting photoluminescence along with the absence of photo-bleaching make gold nanoclusters suitable as alternative biological labels.^[25,84,85] However, for various fundamental studies and specific applications, one requires atomically-precise, stable nanoclusters of desired size, solubility, and functionality in high yield.

It has been quite challenging to synthesize atomically precise metal clusters in high yield. Often the synthesis methods produce clusters of varied sizes, as a result, the yield is low and they require post-synthesis size-fractionations.^[45,48,86] Further, a majority of the gold nanocluster syntheses involve two or more steps.^[42,73,86] The most common nanocluster synthesis is the classic ‘two-phase organic-water solvent’-based methods that use a variety of organic thiols (long chain or aromatic thiols as binding ligands).^[10] Organic thiols due to their long alkyl chains and thiol groups act as good binding and protecting ligands for gold

nanoclusters in organic solvents.^[22–24,87] The stability of the gold nanoclusters increases with increasing chain length of the thiolate ligand.^[17,88] The other approach that has been employed to prepare nanoclusters is the ‘core-etching’ of relatively large/polydispersed clusters or nanoparticles by the actions of excess binding ligands, suitable ions, and/or thermal effects.^[64,87,89–91]

Dass and co-workers reported the preparation of glutathione protected gold nanoclusters of different sizes and used the PAGE (polyacrylamide gel electrophoresis technique) separation technique for the size separation.^[36] Bürgi et al. synthesized N-isobutyryl-L-cysteine and N-isobutyryl-D-cysteine bound gold nanoclusters of different sizes (Au₁₀₋₁₂, Au-15 and Au-18 gold atoms) and similarly employed the PAGE technique to separate nanoclusters of different sizes.^[92] Yang et al. prepared water-soluble penicillamine-bound gold nanoclusters and used a sequential size-selective precipitation technique for the size-separation.^[93] Jin and co-workers reported a one-pot synthesis method that produced glutathione(SG)-protected Au₂₅(SG)₁₈ nanoclusters along with 2 nm and 4 nm gold nanoparticles. They employed a controlled methanol-induced precipitation method to separate Au₂₅(SG)₁₈ nanoclusters and the gold nanoparticles.^[94]

In addition to the size-control, the stability and desired functionality of the metal clusters particularly in aqueous and biological media are the other important aspects of the cluster synthesis.^[95] Biological applications such as labeling, sensing, and catalysis require stable, aqueous, non-toxic clusters with small hydrodynamic sizes and tailorable properties such as optical absorptions, photoluminescence, etc. An appropriate choice of surface ligands is crucial in improving the stability of the metal clusters as well as imparting desired properties. For example, a few recent studies showed that the aggregations of Au(I)-thiolate based systems led to exhibitions of intense fluorescence.^[37,96–98] Some studies employed post-preparation ligand exchange to change the organic solvent-water solubility and other properties of the nanoclusters.^[13,91]

Here we report a facile, single step synthesis method that produces MPA-bound pure Au₁₈ nanoclusters in an aqueous medium at room temperature by using the typical reducing agent, sodium borohydride (NaBH₄). This synthesis method does not require any purification step or pH control. The clusters can be produced in relatively large quantities and can be obtained in a dry state which can be redispersed in water or methanol for further studies.

3.2 Materials and Methods

3.2.1 Materials

Hydrogen tetrachloroaurate (III) hydrate (HAuCl₄·3H₂O), 3-mercaptopropionic acid (MPA), sodium borohydride (NaBH₄) were purchased from Sigma-Aldrich. Toluene, methanol, and tetraoctylammonium bromide (TOAB) were received from SRL Chemicals Pvt. Ltd., India. The chemicals were used as received. All the glassware were cleaned with aqua-regia. Millipore water with a specific resistance of 18.2 MΩ·cm was used throughout the experiment.

3.2.2 Synthesis

In a typical synthesis, an aqueous solution of HAuCl₄·3H₂O (10 mM, 2.5 mL) was added to that of MPA (5 mM, 12 mL) in a 250 mL round-bottomed flask. The molar ratio of MPA: Au was 2.4:1 (with the final molar ratio of NaBH₄ to Au was [NaBH₄]:[Au] = 10:1). After the addition, the color of the solution changed from yellowish to colorless indicating the formation of Au(I)-MPA complex. The solution was kept stirring continuously by using a magnetic stirrer (~1000 rpm) at room temperature. Ice-cold NaBH₄ (0.1 M, 2.5 mL) with the molar ratio of NaBH₄: Au =10:1 was added to the reaction solution in 5 min after the addition of Au precursor. Then the reaction solution changed its color from colorless to light brown. The stirring continued for 3 hrs. The color of the reaction solution slowly changed from brown to light green during this period.

3.2.3 Polyacrylamide gel electrophoresis (PAGE) separation

Polyacrylamide gel electrophoresis (PAGE) was carried out by using GeNei-Vertical mini Dual Gel System with a 1 mm spacer. After surveying gel compositions suitable for PAGE, we chose 3% (acrylamide/Bis, 94:6) and 30% (acrylamide/Bis, 93:7) acrylamide monomers for the stacking and separation gels, respectively. The eluting buffer consisted of 192 mM glycine and 25 mM tris(hydroxymethylamine). The solid MPA-bound Au nanoclusters were dissolved in 10% (v/v) glycerol-water solution at a concentration of 20 mg/mL for loading. The sample solution was loaded in 1 mm gel lanes and was run for 5 hrs continuously at a constant voltage of 120 V. After the run, the band portion of the gel was cut, crushed and added to ultrapure water and stored in the refrigerator overnight. UV-vis spectrum of the hydrosol was taken after removing the gel lumps by centrifugation.

3.2.4 Other Characterizations

UV-Visible spectra were recorded on a PerkinElmer Lambda 35 UV-Visible spectrometer. FT-IR spectra were measured by using Bruker Tensor 27 instrument in transmittance mode. Thermogravimetric analysis (TGA) was done by using Shimadzu differential thermal analyzer (DTG-60H, Japan) from 25-800°C with 20°C/min heating rate under nitrogen flow. X-ray photoelectron spectroscopy (XPS) measurements of the clusters were performed by using Kratos Axis Ultra DLD spectrometer with an X-ray source for monochromatic Al K α radiation. The binding energy of carbon (C_{1s}) peak (284.8 eV) was used as a reference. SEM-EDAX studies were done using HITACHI SU-1500 variable pressure scanning electron microscope (VP-SEM). Transmission electron microscope (TEM) images were obtained on FEI-Tecnai 20G2 microscope. Mass spectrometric studies were carried out by using matrix-assisted laser desorption ionization time of flight MS (Autoflex III MALDI TOF/TOF, Bruker Dalotnik GmbH, Germany) equipped with smart beam laser (335nm; 1000Hz) in linear positive mode.

3.3 Results and Discussion

Figure 3.1 shows the time evolution of the optical spectra after the addition of NaBH₄ to the solution of MPA and AuCl₄⁻. A light brown color appeared immediately after the addition of NaBH₄ to the reaction mixture and the UV-vis absorption spectrum exhibits small humps at

wavelengths ~ 450 and ~ 560 nm. The humps developed further and then the brown color slowly faded with the progress of the reaction. A new shoulder peak at ~ 620 nm in the UV-vis spectrum developed in ~ 1.5 hours and the reaction solution showed greenish color in ~ 3 hours. The distinct spectral features are indicative of the formation of highly pure Au_{18} nanoclusters. The spectral features of the final product are in nanoclusters good agreement with those of $\text{Au}_{18}(\text{SG})_{14}$ prepared by the groups of Tsukuda^[83] and Xie^[39,99] and $\text{Au}_{18}(\text{SC}_6\text{H}_{11})_{14}$ by Jin^[100] and Zhu^[101].

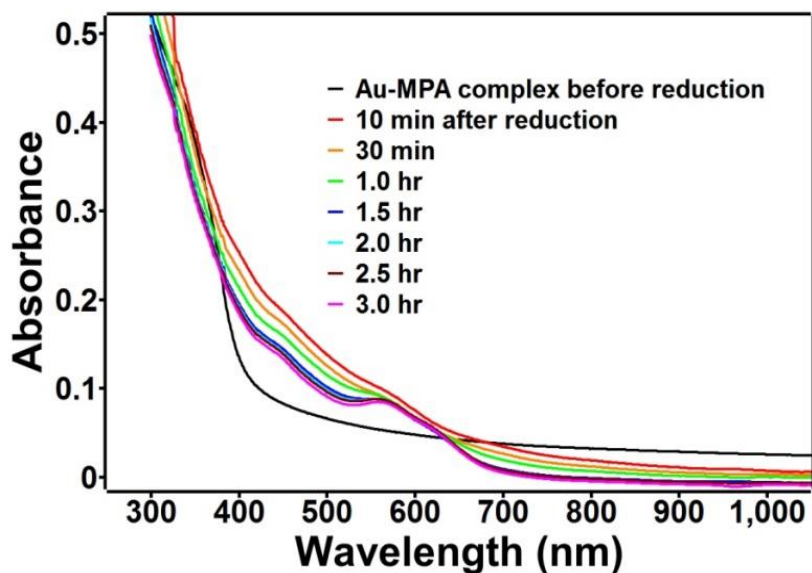


Figure 3.1 Temporal development of UV-Visible absorption spectra during the formation of $\text{Au}_{18}(\text{SC}_2\text{H}_4\text{CO}_2\text{H})_{14}$

Based on the comparison of the optical spectra, we conclude that $\text{Au}_{18}(\text{MPA})_{14}$ was formed selectively by the one-pot reaction, which will be further corroborated below by other studies. We observed that an $[\text{MPA}]:[\text{Au}]$ ratio of 2.4 (with $[\text{NaBH}_4]:[\text{Au}] = 10$) was necessary for the synthesis of an atomically precise cluster, $\text{Au}_{18}(\text{MPA})_{14}$. Other $[\text{MPA}]/[\text{Au}]$ molar ratios produced clusters of mixed sizes (**Figure 3.2**). Xie and co-workers reported the synthesis of BSA-protected gold nanoclusters by maintaining the gold precursor to BSA (bovine serum albumin) ratios.^[102] These results suggest that appropriate kinetic and thermodynamic conditions must be met for the facile high yield synthesis of size-selective clusters. As discussed earlier, an

excess amount of MPA ligand could be involved in converting the initially formed small Au-MPA clusters of various sizes selectively to $\text{Au}_{18}(\text{MPA})_{14}$ by chemical etching. It is interesting to note that ubiquitous magic clusters $\text{Au}_{25}(\text{MPA})_{18}$ were not produced under our synthetic conditions.

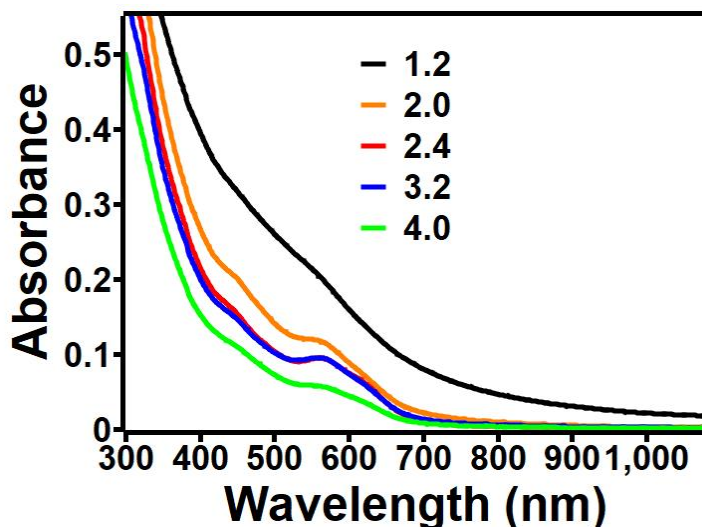


Figure 3.2 UV-Visible absorption spectra showing the effects of MPA to gold molar ratio on the size selected synthesis of $\text{Au}_{18}(\text{SC}_2\text{H}_4\text{CO}_2\text{H})_{14}$ cluster

High monodispersity of the clusters was confirmed by the PAGE and TEM studies. A single band on the PAGE^[43] suggests the formation of a single sized nanocluster (**inset, Figure 3.3**). The absorption spectrum of the PAGE separated nanocluster solution (**Figure 3.3**) matched perfectly with that of the as-prepared nanocluster solution. **Figure 3.4** shows a representative TEM image of the $\text{Au}_{18}(\text{MPA})_{14}$ sample recorded by minimizing the electron beam exposure in order to suppress the electron-beam-induced aggregation (Figure 3.5).^[38] The TEM images show monodisperse particles having sizes in the range of ~ 1.0 to 1.5 nm.

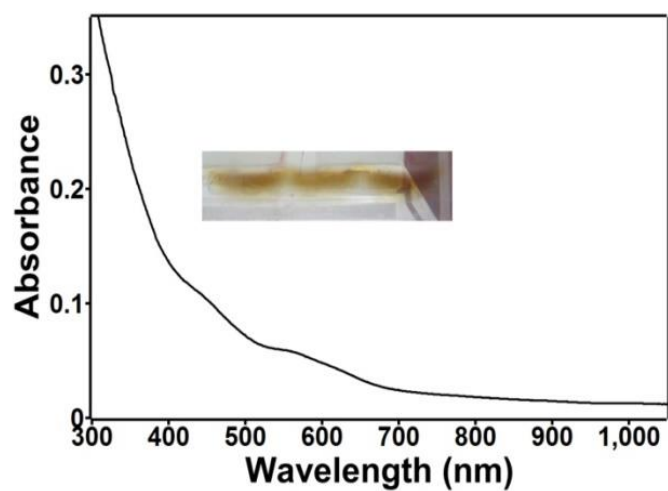


Figure 3.3 UV-Visible spectrum of $\text{Au}_{18}(\text{SC}_2\text{H}_4\text{CO}_2\text{H})_{14}$ after PAGE separation. The inset shows a photo-image of the gel after PAGE

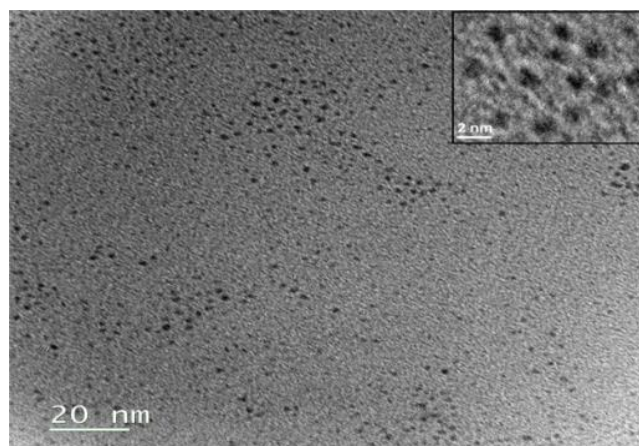


Figure 3.4 A representative TEM image of $\text{Au}_{18}(\text{SC}_2\text{H}_4\text{CO}_2\text{H})_{14}$ clusters

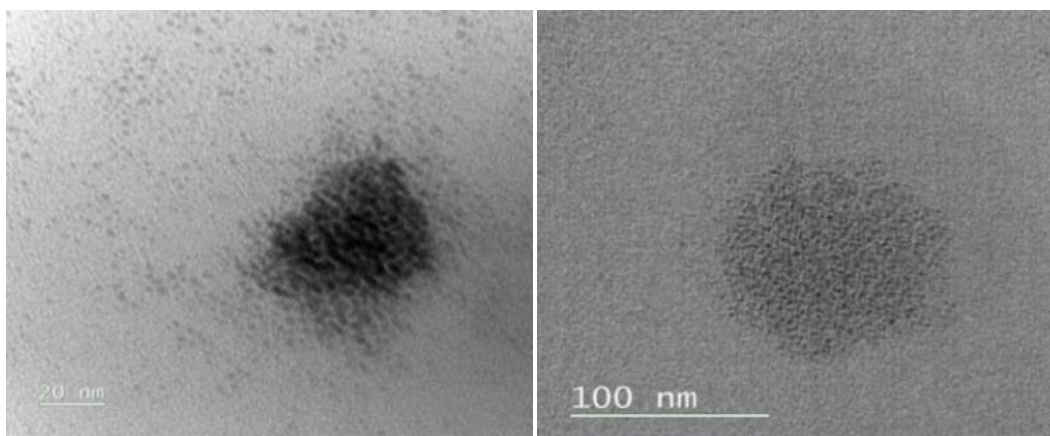


Figure 3.5 Transmission electron microscope (TEM) images of $\text{Au}_{18}(\text{SC}_2\text{H}_4\text{CO}_2\text{H})_{14}$ nanoclusters showing electron beam induced aggregation.

Figure 3.6 shows the FT-IR spectra of MPA and $\text{Au}_{18}(\text{SC}_2\text{H}_4\text{CO}_2\text{H})_{14}$. IR spectrum of MPA exhibited very broad band in the region of $2500\text{--}3500\text{ cm}^{-1}$ assigned to carboxylic O–H stretching, an intense peak at $\sim 1695\text{--}1735\text{ cm}^{-1}$ for protonated carboxylic (C=O) stretching, a peak at 654 cm^{-1} for C–S stretching, and a peak at $\sim 2572\text{ cm}^{-1}$ for S–H stretching. On the other hand, in the IR spectrum of $\text{Au}_{18}(\text{SC}_2\text{H}_4\text{CO}_2\text{H})_{14}$, the C–S stretching peak was blue-shifted to 667 cm^{-1} and the S–H vibration peak disappeared, indicating that the MPA ligand is bound to the Au cluster via S–Au bond.^[93,103] The formation of the Au–S bond is supported by XPS. (**Figure 3.7 & 3.8**)

Figure 3.6 FT-IR spectra of MPA (bottom) and $\text{Au}_{18}(\text{SC}_2\text{H}_4\text{CO}_2\text{H})_{14}$ (top) (offset for clarity). The dotted line shows the position of the (S–H) vibrational frequency peak

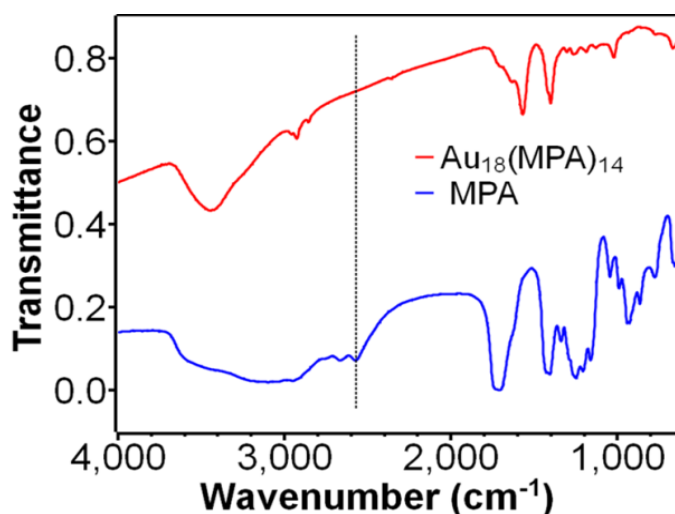


Figure 3.7 The S (sulfur) $2p$ core level X-ray photoemission spectra (XPS) of Au-MPA nanocluster sample. The spectra were fit by using Gaussian line functions for two S $2p$ doublets with the same full width at half-maximum (fwhm), the standard spin-orbit splitting of 1.2 eV, and a 2:1 ($S\ 2p_{3/2}$)/($S\ 2p_{1/2}$) area ratio

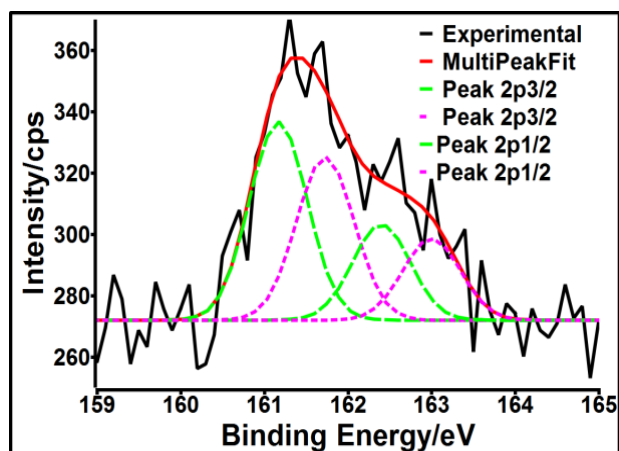


Figure 3.7 shows the XPS spectra of the sulfur $2p$ region. The spectrum can be reasonably fit by two doublets of Gaussian line shapes (with a fwhm of 0.7 eV) where each doublet has a separation of 1.2 eV with 2:1 peak-area ratio arising from a spin-orbit coupling ($2p_{3/2}$ and $2p_{1/2}$).^[104,105] The doublets with the sulfur $2p_{3/2}$ components peak at 161.2 eV and 161.8 eV. By comparison with literature, the lower energy component of the two could be assigned to either metal sulfide or atomic sulfur.^[106–108] Atomic sulfur might have formed during the X-ray irradiation as was observed by Cavalleri et al.^[107] A calculation, by using the relationship connecting the binding energy and the charge of sulfur, gives a charge of -0.39e and -0.25e on S for binding energies of 161.2 eV and 161.8 eV respectively, which suggest a covalent thiolate kind of bonds.^[106] Therefore, it is likely that these peaks arise from two different types of thiolates bound to two chemically different gold atoms in the nanocluster. Ivashenko et al. had assigned the 161.8 eV binding energy peak to the chemisorbed RS-Au species.^[109] However, researchers had reported the binding energies of S $2p_{3/2}$ in thiol compounds attached to Au nanoparticles range between 162.6 eV–162.9 eV.^[110–112] The low binding energy in the present case could be due to the formation of thiolate bonds with the low coordinated gold atoms.^[108,113,114] Castner et al. reported that the S $2p_{3/2}$ binding energy

decreased in the order: unbound thiol or disulphide > thiolate in hollow site > thiolate in low-coordination site.^[105]

Figure 3.8 The Au (gold) $4f$ core level X-ray photoemission spectra (XPS) (along with multi-peak curve fitting) of Au-MPA nanocluster sample. Three $4f$ doublets (peaks 1, 2 and 3's) with the Gaussian line functions of the same fwhm, 4:3 area ratios and splittings of 3.7 eV were fit for the major two peaks of the experimental spectrum

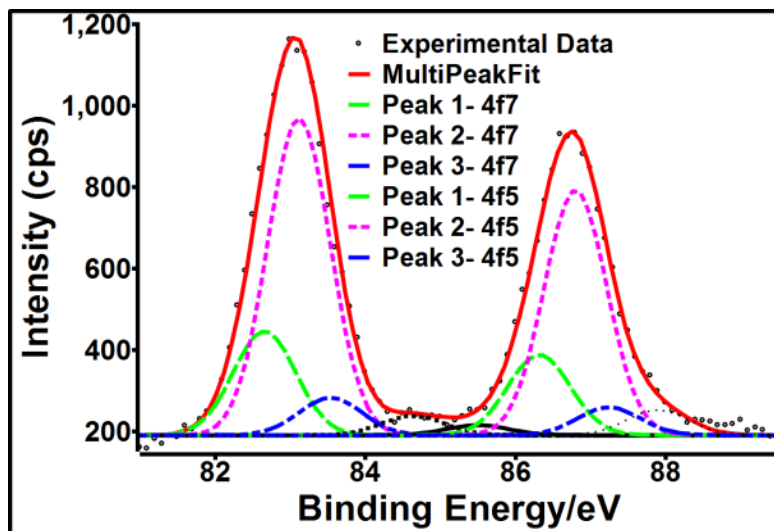


Figure 3.8 shows the representative X-ray photoelectron spectra of the Au $4f$ region. The spectrum shows Au $4f$ spin-orbit splitting with the Au $4f_{7/2}$ and $4f_{5/2}$ doublet peaks separated by 3.6 eV and a 4:3 area ratio. The binding energies of the Au $4f_{7/2}$ and Au $4f_{5/2}$ peaks centered at 83.1 eV and 86.7 eV, respectively, were slightly lower than that of the bulk metallic gold.^[115] Researchers had observed earlier similar binding energies for $4f$ regions of gold.^[116,117] Observation of such low binding energy had been attributed to the initial state effect due to $6s$ - $5d$ charge reorganization for less coordinated surface atoms of gold.^[115,118,119] A detailed shape analysis of the Au $4f$ peaks with the deconvolution profiles obtained by using Gaussian line functions reveals that the peaks are made of three doublets with binding energy separations and area ratios characteristic of the $4f$ spin-orbit splitting of gold. This suggests that gold might be present in three different oxidation states in the cluster. The Au $4f_{7/2}$ components showed peaks at 83.0, 83.3 and 83.6 eV. These binding energies could be assigned to the low coordinated surface, core and/or thiol-bound gold atoms, respectively. It has been reported earlier that the Au $4f_{7/2}$ binding energy peak shifts by +0.3 eV in the Au(I) complexes with respect to the Au(0) position. On the other hand, low coordinated surface atoms show a surface

core-level shift of 0.3 to 0.4 eV with respect to the core atoms.^[120] A similar negative shift has been reported for the presence of low-coordinated atoms that appear on the Au surface as a result of the surface restructuring.^[115] A shift of about +0.6 eV in the Au $4f_{7/2}$ binding energy has been observed with respect to that of Au⁰ due to electron donation from Au atoms in the gold nanoparticle to the surface thiolates.^[48,121] These reports qualitatively support three oxidation states of gold in the cluster.

The chemical composition of Au₁₈(SC₂H₄CO₂H)₁₄ is supported by the TGA and EDAX analysis. The TGA data showed that the weight percentages of organic materials and Au were 29.2 and 70.8 wt%, respectively (**Figure 3.9**). These experimental values agree very closely with the theoretical values for Au₁₈(SC₂H₄CO₂H)₁₄, i.e., 29.5 and 70.5 wt%, respectively. The atomic ratio of Au:S was determined to be 1:0.75 by the EDAX analysis which agrees well with the calculated value (1:0.78) for Au₁₈(SC₂H₄CO₂H)₁₄ (**Figure 3.10**).

Figure 3.9 TGA graph of Au₁₈(MPA)₁₄ nanocluster

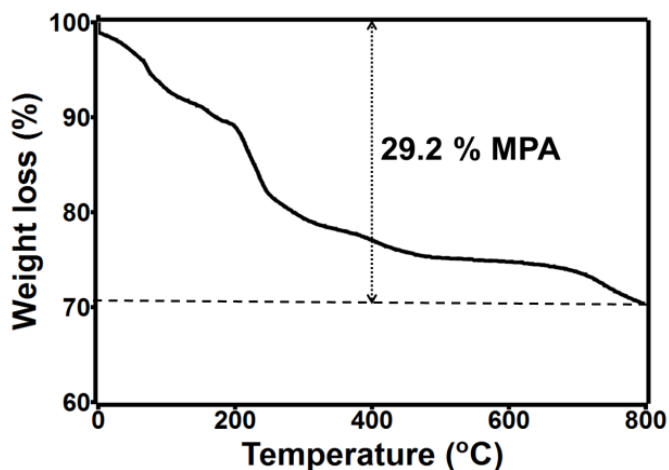
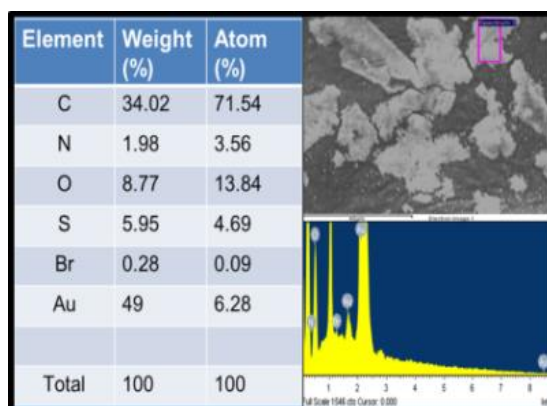


Figure 3.10 A representative SEM-EDAX spectrum of Au₁₈(MPA)₁₄ nanocluster



3.3.1 MALDI-MS analysis

Matrix-assisted laser desorption/ionization mass analysis technique has been often used for the determination of the molecular composition of the nanoclusters synthesized. We employed the matrix-assisted laser desorption ionization time of flight spectrometry (MALDI TOF-MS) in order to determine the actual composition of the synthesized nanocluster. **Figure 3.11** shows the MALDI-TOF MS of the gold nanoclusters. Here, the peak at m/z 4911.996 can be assigned as $[(Au_{18}(SC_2H_4CO_2H)_{14})-(HSC_2H_4CO_2H)]$, a fragmentation peak of the $Au_{18}(SC_2H_4CO_2H)_{14}$ nanocluster. Researchers had observed that water-soluble nanoclusters protected by hydrophilic ligands undergo extensive fragmentation upon laser illumination during MALDI-MS analysis and it is therefore not straightforward to find the parent molecular ion in the MALDI-TOF MS.^[38,122] A number of peaks in MALDI-MS appeared due to the loss of MPA ligand ($\sim m/z$ 105 gap), Au-MPA (with a gap of $m/z \sim 302 = Au^{197} + MPA^{105}$), Au atoms (m/z 197), and/or sulfur atom (m/z 32). Some of the other mass spectral peaks at lower and higher m/z regions can be attributed either to the gas phase aggregation of the clusters and clustering of clusters arising from van der Waals attractive forces among clusters.^[38,101]

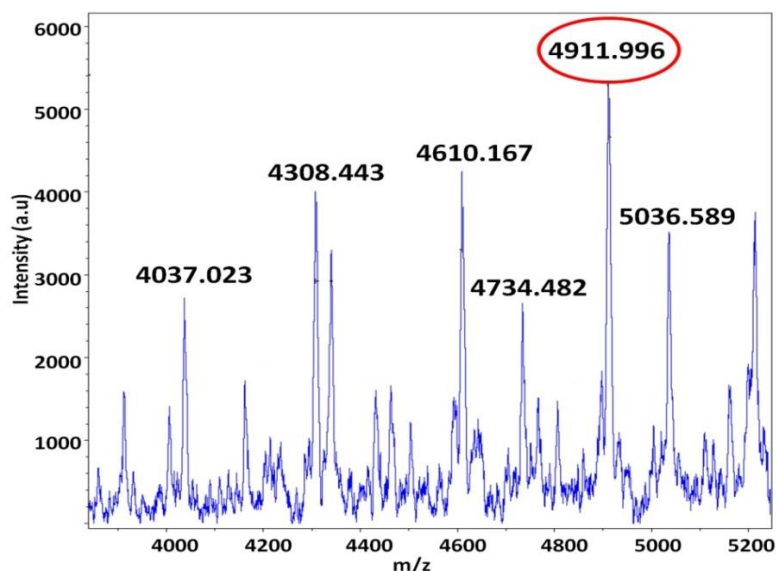


Figure 3.11 MALDI-TOF MS of $Au_{18}(SC_2H_4CO_2H)_{14}$ nanocluster sample

3.4 Conclusions

We have developed an efficient, single-step method for the preparation of pure $\text{Au}_{18}(\text{MPA})_{14}$ nanoclusters in an aqueous medium at room temperature by using a conventional reducing agent, NaBH_4 , and a hydrophilic, short carbon chain ligand, MPA. The relative quantities of the gold precursor, MPA, and NaBH_4 play the key roles in obtaining size-focused, atomically precise Au_{18} clusters in high yield. The method is straightforward and does not require any special reaction conditions such as pH or temperature control, reagent purity, etc. The synthesized ultra-small nanoclusters can be transferred into an organic phase and obtained in solid form. Techniques such as UV-Vis, fluorescence, and FT-IR spectroscopies, gel electrophoresis (PAGE), TEM, EDAX, TGA, and MALDI-MS were employed for the characterization and determination of the composition and purity of the cluster.

Synthesis of Ubiquitous Nanocluster, Au₂₅(MPA)₁₈, in Aqueous Media

4.1 Introduction

We have mentioned in the previous chapter that atomically precise, ultra-small metal nanoclusters protected with various capping ligands such as thiol, selenolate, phosphines received great attention due to their widespread applications in various sectors,^[7,123–126] for examples, catalysis, biosensing, fluorescent labeling, cellular imaging, heavy metal ion detection, and so on.^[2,3,127] Small size, less toxicity, the absence of photo-bleaching and possible manipulation of fluorescent properties of gold nanoclusters make them suitable as alternative biological labels.^[84,85,89] Among various size-selected gold nanoclusters, Au₂₅L₁₈ is one of the most extensively studied cluster systems because of its extraordinarily high stability compared to other Au NCs.

Single crystal X-ray structural studies revealed that Au₂₅L₁₈ prefer to exist in two crystallographic forms such as Au₂₅ icosahedral (ico-Au₂₅) and Au₂₅ bi-icosahedral (bi-Au₂₅). Because of two different crystal structures; ico-Au₂₅ and bi-Au₂₅, Au₂₅ NCs show distinct electrochemical HOMO-LUMO bandgaps such as ~1.65 V and ~1.54 V respectively. HOMO-LUMO band gaps of the cluster can be significantly modulated by changing the solvents and counterions in the nanocluster systems.^[128] We have discussed earlier that the gold nanoclusters have been prepared by using a number of synthesis methods, a majority of them involve two or more steps.^[10] In the early stages of cluster research, gold nanoclusters of a given size were obtained by isolating them from the polydispersed cluster mixture by employing post-synthetic separation techniques such as PAGE (polyacrylamide gel electrophoresis) and various chromatographic techniques.^[44,46,129] Such separation techniques not only offer low yields but are time-consuming and expensive also. In recent years, several procedural improvements have made in order to make the synthesis relatively easy and high

yielding. Several ligand etching (thiol etching) and thermal etching based size focusing methods have been developed to prepare the Au₂₅ clusters by using different protecting ligands. Size focusing methodology has led to the synthesis of series of atomically precise gold NCs with different core sizes including Au₂₅(SR)₁₈, Au₃₈(SR)₂₄, Au₁₄₄(SR)₆₀, and the largest ever Au₃₃₃(SR)₇₉.^[52,55–57] In addition to the size focusing methods, ligand exchange induced “size-conversion” methods have also been successfully used to synthesize the Au₂₅ clusters with different capping ligands.^[13,32,130–133]

There has been notable progress in the synthesis, isolation, and characterization of organic soluble gold nanoclusters. However, relatively little progress has been witnessed in the cases of water-soluble gold nanoclusters. Groups of Whetten^[86] and Tsukuda^[48,134] initiated the synthesis of water-soluble gold nanoclusters by using glutathione capping ligand and NaBH₄ as the reducing agent. It has been observed that it is difficult to prepare the size selected nanoclusters by employing strong reducing agents alone in the reactions. A strong reducing agent such as NaBH₄ is unable to control the reaction kinetics thereby often leading to the formation of mixed sized clusters via rapid nucleation of clusters. Weak reducing agents provide the slow reduction environment and facilitate the formation of size-selected Au nanoclusters. However, researchers used NaBH₄ with systematic pH regulation to create a weak reduction environment because the reducing capability of NaBH₄ depends strongly on the pH of the reaction medium. In recent years, Xie’s group has reported the synthesis of various mono- and bi thiolate-protected Au₂₅ NCs by using a number of hydrophilic protecting ligands and the pH-controlled NaBH₄ reduction method.^[40] The same group reported the synthesis of water-soluble Au₂₅ and other clusters such as Au₁₈, Au₁₅, and Au₁₀₋₁₂, NCs by using carbon monoxide (CO) as a weak reducing agent.^[99] Pradeep and coworkers reported the synthesis of Au₁₈(GSH)₁₈ cluster by using sodium cyanoborohydride (NaBH₃CN) which is a weak reducing agent.^[38]

In this chapter, we report a simple, one-pot synthesis of atomically precise Au₂₅(MPA)₁₈ nanoclusters in an aqueous medium at room temperature by using the strong reducing agent, sodium borohydride (NaBH₄) and a small capping ligand, mercaptopropionic acid (MPA). Atomically precise Au₂₅(MPA)₁₈ NCs were synthesized without maintaining the pH of the

reaction. It is to be noted that earlier reports of size-selected cluster synthesis focused mainly on the strength of the reducing agent and type of capping ligands. In this study, we demonstrated that, in addition to these two factors, the [Thiol]:[Au] ratio as well as [NaBH₄]:[Au] ratio play pivotal roles in controlling the metal cluster size. The clusters can be produced in relatively large quantities and can be transferred into an organic solvent and obtained in a dry state which can be redispersed in water or methanol for further studies. The nanoclusters were characterized by using polyacrylamide gel electrophoresis (PAGE), UV-Visible and FTIR spectroscopies, transmission electron microscopy (TEM), energy dispersive X-ray analysis (EDAX), thermogravimetric analysis (TGA), X-ray photoelectron spectroscopy (XPS).

4.2 Materials and Methods

4.2.1 Materials

Hydrogen tetrachloroaurate (III) hydrate (HAuCl₄·3H₂O), 3-mercaptopropionic acid (MPA), sodium borohydride (NaBH₄) were purchased from Sigma-Aldrich. Toluene, methanol, sodium hydroxide (NaOH), and tetraoctylammonium bromide (TOAB) were received from SRL Chemicals Pvt. Ltd., India. The chemicals were used as received without any further purification. Aqua-regia was used to clean the glassware throughout the reaction. Millipore water with 18.2 MΩ·cm specific resistance was used in the experiment.

4.2.2 Synthesis

In a typical synthesis, 80 mL of Millipore water was taken in a 250 mL round-bottomed flask. Then an aqueous solution of MPA (5 mM, 12 mL) was added to it and mixed. The solution was mixed by using a magnetic stirrer (~1000 rpm) at room temperature. The stirring continued through the reaction till one hour after the addition of the last portion of NaBH₄. The molar ratio of [MPA]:[Au] was 2.4. After the addition of MPA, an aqueous solution of HAuCl₄·3H₂O (10 mM, 2.5 mL) was added to the reaction solution. Ice-cold NaBH₄ (0.1 M) was added to the Au(I)-MPA complex solution in three steps. The final molar ratio of [NaBH₄]:[Au] was 22. In the first step, 2.5 mL of NaBH₄ were added 5 min after the addition of MPA. Then 2 mL of NaBH₄ were

added after 1 hr. Similarly, 1 mL of NaBH_4 were added after another 1 hr. The stirring continued for 1 more hr, then the color of the reaction solution turned into dark brown, which is the indication of the formation of atomically precise Au_{25} clusters.

4.2.3 Polyacrylamide gel electrophoresis (PAGE)

PAGE separation was carried out by using GeNei-Vertical mini Dual Gel System with a 1 mm spacer., We have chosen 3% (acrylamide/Bis, 94:6) and 25% (acrylamide/Bis, 93:7) acrylamide monomers for the stacking and separation gels, respectively. The eluting buffer consisted of 192 mM glycine and 25 mM tris(hydroxymethylamine). The solid $\text{Au}_{25}(\text{MPA})_{18}$ clusters were dissolved in 10% (v/v) glycerol-water solution at a concentration of 20 mg/mL. The sample solution was loaded in 1 mm gel lanes and was run for 1.5 hrs continuously at a constant voltage of 120 V. After the run, the band portion of the gel was cut, crushed and added to ultrapure water and stored in the refrigerator overnight. The isolated cluster solutions were centrifuged multiple times to remove the extra gel lumps. The purified clusters were used for further studies.

4.2.4 Other Characterizations

UV-Visible spectra were recorded on a PerkinElmer Lambda 35 UV-Visible spectrometer. The cluster stability under various pH conditions was studied with the help of UV-Visible spectroscopy. The pH of the as-synthesized cluster solution was increased by the addition of NaOH and was decreased by the addition of acetic acid or HCl solutions. FT-IR spectra were measured by using Bruker Tensor 27 instrument in transmittance mode. X-ray photoelectron spectroscopy (XPS) measurements of the clusters were performed by using Kratos Axis Ultra DLD spectrometer with an X-ray source for monochromatic Al $K\alpha$ radiation. The binding energy of carbon (C_{1s}) peak (284.8 eV) was used as a reference. Thermogravimetric analysis (TGA) was done by using Shimadzu differential thermal analyzer (DTG-60H, Japan). The temperature was varied from 25° to 800 °C under nitrogen flow with 20 °C/min heating rate. SEM-EDAX studies were done using HITACHI SU-1500 variable pressure scanning electron microscope (VP-SEM).

Transmission electron microscope (TEM) images were obtained on FEI-Tecnai 20G2 microscope. The differential pulse voltammetry (DPV) studies were carried out with electrochemical analyzer CHI instruments model no. CHI440B.

4.3 Results and Discussion

Various kinetic and thermodynamic controls have been employed to achieve the size focusing on nanoclusters.^[133,135–137] Similarly, researchers varied various reaction parameters such as the strength of the reducing agent, pH of the reaction medium, and the nature of the protecting ligands to achieve size focusing. In the present study, we have employed 3-mercaptopropionic acid (MPA) as binding ligand and NaBH₄ as reducing agent without any pH control. We have observed that in addition to the nature of the capping ligand and reducing agent, appropriate selection of [thiol]:[Au] and [reducing agent]:[gold] ratios also play decisive roles in the formation of atomically precise clusters.^[138] We have employed **[thiol]:[Au] ratio = 2.4** and **[NaBH₄]:[Au] = 22:1** for the synthesis of Au₂₅ nanocluster. NaBH₄ was added in a stepwise manner instead of single step addition. Stepwise addition favors the formation of size-selected nanoclusters. On the other hand, single step addition of NaBH₄ produced polydispersed gold nanoclusters, showing a featureless UV-Visible spectrum (**Figure 4.1**).

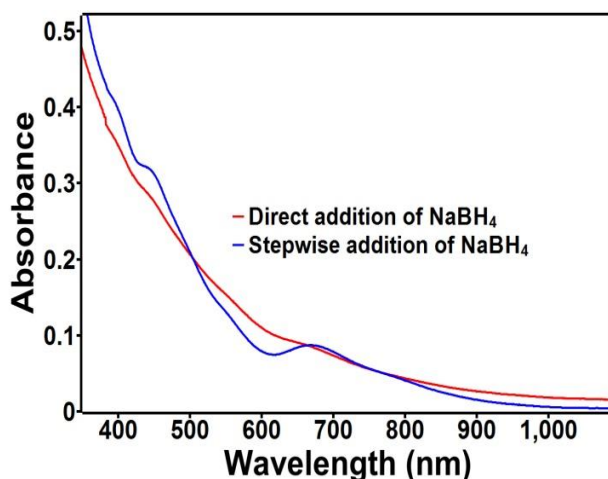


Figure 4.1 UV-Visible spectra of the cluster: direct reduction vs. stepwise reduction

UV-Visible spectroscopy was used to study the reduction kinetics of the Au₂₅ cluster formation (**Figure 4.2**). After the 2 hours, the reaction solution started showing the distinguishable Au₂₅ cluster features in UV-Visible spectra. Around 3 hours of reaction time, the color of the reaction solution turned into deep brown color, showing distinct absorption peaks at 390, 440, 670 and 760 nm in the UV-vis spectra, which are the characteristic UV-Visible absorption peaks for the Au₂₅ clusters as reported earlier in the literature reported by various research groups.^[78,99,134,139–141] The different absorption peaks (humps) observed in UV-Visible spectra arise due to the different kinds of HOMO-LUMO transitions in the cluster. The absorption peak at 672 nm (1.55 eV) corresponds to the intraband (sp-sp) transitions. The absorption features appearing in the lower wavelength region corresponding to the interband transition (sp – d).^[48]

Stepwise addition of the strong reducing agent provides possibly a slow reduction kinetics. However, even though borohydride addition steps result in the clusters of mixed sizes, the presence of excess thiol ligands could favor size focusing via ligand-mediated etching of the metastable/unstable cluster species, ultimately converting them to the single sized ubiquitous Au₂₅ clusters. The temporal evolution of the UV-vis spectra supports this proposition. Our synthesis possibly follows a combined kinetic and thermodynamic mechanism for the size-selective synthesis.

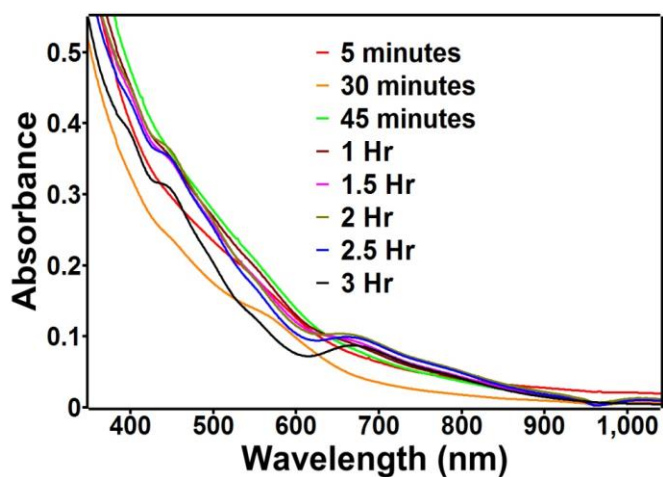


Figure 4.2 Temporal evolution of UV-Vis spectra during the formation of Au₂₅(MPA)₁₈ cluster in aqueous solution.

The synthesized Au₂₅ clusters were transferred into organic phase (Toluene) by using tetraoctylammonium bromide (TOABr) as phase transfer reagent.^[142] After phase transfer, clusters can be obtained in a dry state which can be redispersed in water or methanol for further studies. Polyacrylamide gel electrophoresis (PAGE) separation of the cluster gives a single band, which confirmed the formation of a single cluster.^[36]

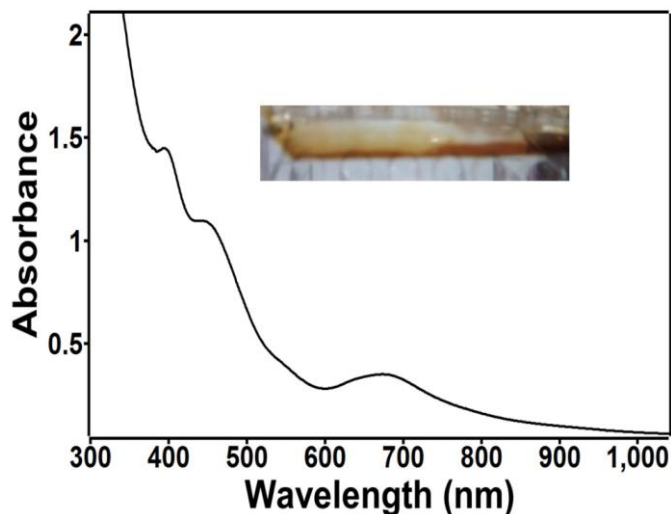


Figure 4.3 UV-Vis spectra of PAGE separated Au₂₅(MPA)₁₈ NCs (inset: PAGE band image)

Figure 4.3 shows the UV-Visible absorption spectra of the PAGE separated Au₂₅ cluster, which matches perfectly with the original Au₂₅ cluster. TEM images (**Figure 4.4**) suggest that synthesized clusters were monodispersed with an average size of ~1.5 nm. No electron beam induced aggregation was noticed during the TEM analysis.

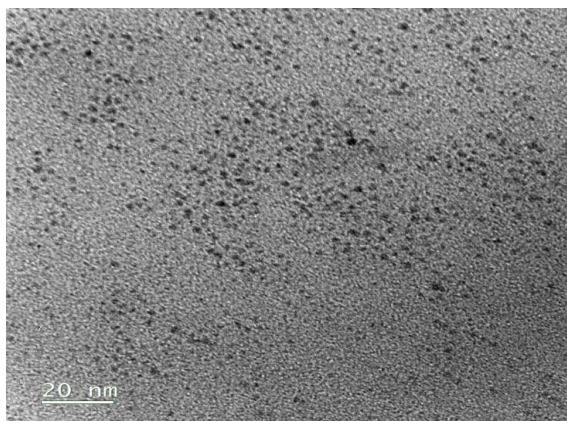


Figure 4.4 Representative TEM image of Au₂₅ NCs

The chemical composition of the $\text{Au}_{25}(\text{MPA})_{18}$ is supported by EDAX and TGA analysis. The Au:S atomic ratio in the as-synthesized cluster was determined to be 1:0.72 by using the EDAX study (**Figure 4.5**) which is in good agreement with the Au:S atomic ratio of $\text{Au}_{25}(\text{MPA})_{18}$ cluster.

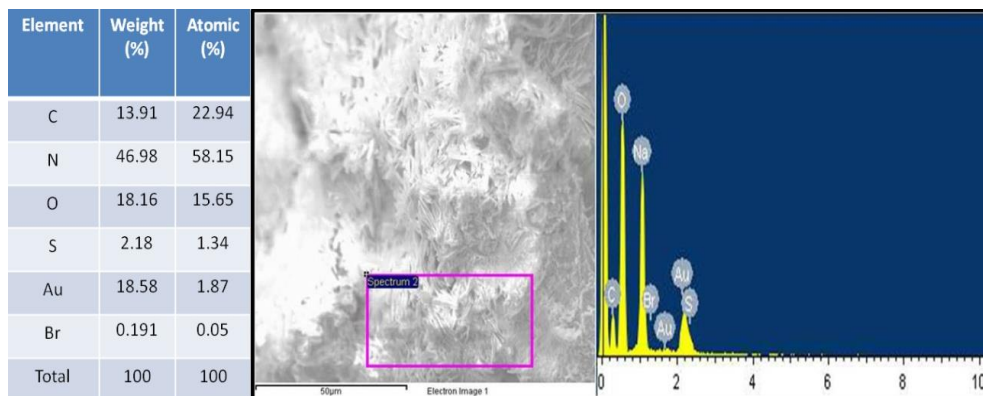


Figure 4.5 A typical SEM-EDAX data of $\text{Au}_{25}(\text{MPA})_{18}$ cluster sample

The TGA data (**Figure 4.6**) showed the weight percentages of organic material and gold were ~ 28 at % and ~ 72 wt%, these experimental values match very closely with the theoretical organic and gold contents of the $\text{Au}_{25}(\text{MPA})_{18}$ nanocluster.

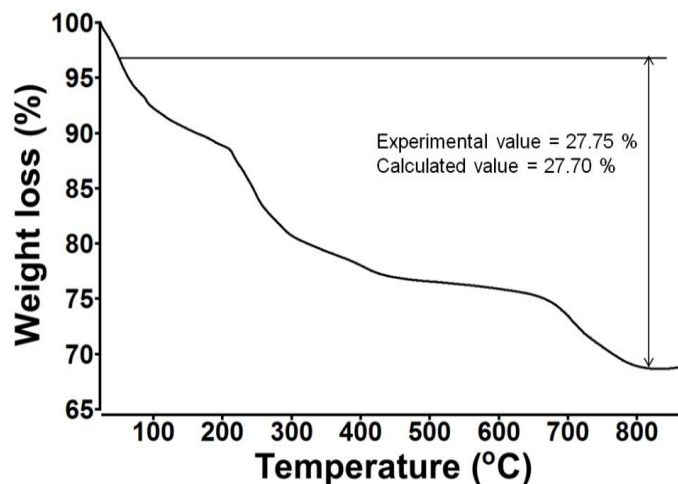


Figure 4.6 The TGA graph of $\text{Au}_{25}(\text{MPA})_{18}$ nanocluster sample

We attempted to obtain the exact mass of the synthesized clusters by using matrix-assisted laser desorption ionization time of flight spectrometer (MALDI TOF-MS). We did not get any $\text{Au}_{25}(\text{MPA})_{18}$ molecular ion peaks in MALDI because of the severe fragmentation problem in water-soluble clusters.^[139,140]

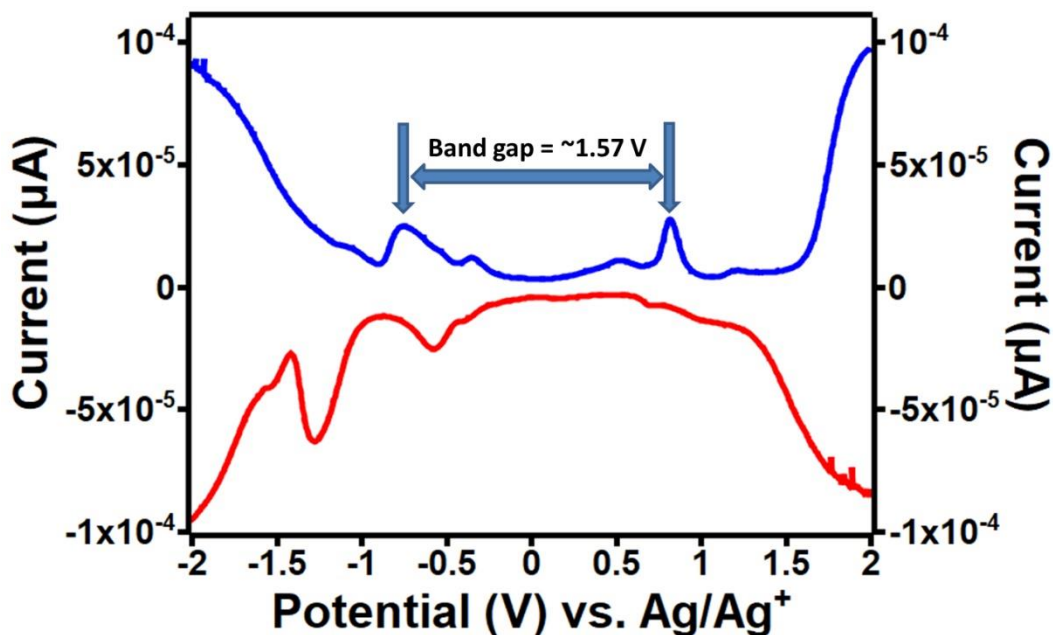


Figure 4.7 Differential Pulse Voltammetry (DPV) plot of $\text{Au}_{25}(\text{MPA})_{18}$ in 0.1M KCl solution showing the HOMO-LUMO band gap of the cluster

Atomically precise Au NCs show characteristic HOMO-LUMO band gaps which are highly dependent on cluster size and geometry.^[128] Lee and co-workers have studied the electrochemical HOMO-LUMO energy gaps of 3-mercaptopropylsulfonate (3-MPS) protected Au_{25} clusters in aqueous and organic phase. They reported that the HOMO-LUMO energy gap of the Au_{25} cluster varies from 1.39 to 1.66 V depending on solvent polarity. Band gaps obtained from electrochemical measurements (differential pulse voltammetry (DPV) or square wave voltammetry (SWV)) show good agreement with the optical band gaps obtained by the UV-Vis-DRS (Ultraviolet-Visible Diffuse reflectance spectroscopy). Electrochemical methods were widely employed to investigate the HOMO-LUMO band gaps for the organic soluble clusters by

using organic electrolytes such as tetrabutylammonium hexafluorophosphate (Bu_4NPF_6), unlike the water-soluble clusters. Electrochemical HOMO-LUMO band gaps of the $\text{Au}_{25}(\text{MPA})_{18}$ cluster was determined by differential pulse voltammetry (DPV) studies. The cluster showed ~ 1.57 eV band gap which was characteristic of the Au_{25} cluster system.^[128,141]

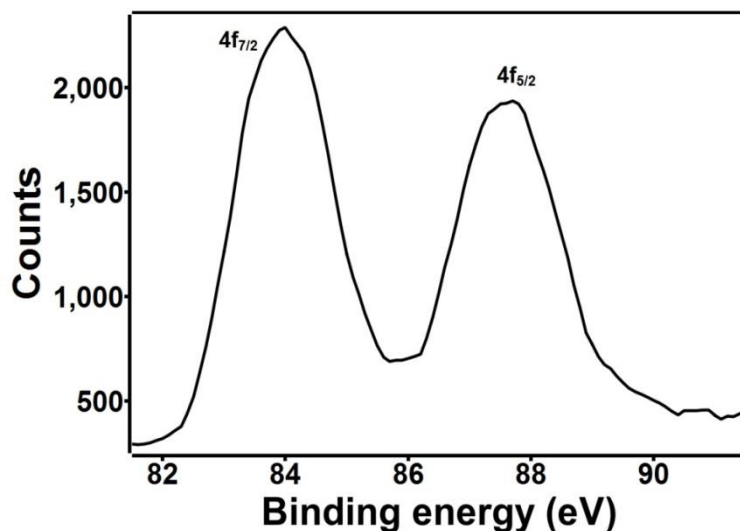


Figure 4.8 The Au 4f core level x-ray photoemission spectra (XPS) of $\text{Au}_{25}(\text{MPA})_{18}$ sample

The X-ray photoelectron spectroscopy (XPS) study showed that the binding energies of the Au $4f_{7/2}$ and Au $4f_{5/2}$ peaks centered at ~ 84.0 and 87.6 eV respectively, which were very close to the reported binding energies of Au_{25} clusters.^[99]

4.4 Conclusions

This chapter reports the stepwise reduction method for the selective synthesis of highly stable water-soluble $\text{Au}_{25}(\text{MPA})_{18}$ clusters by using NaBH_4 as reducing agent. Our method of the Au NCs synthesis is much simpler than the most of the reported strategies. The method of synthesis does not require maintenance of any special reaction conditions, such as pH, reagent purity, high or low temperature, etc. The stepwise addition of NaBH_4 into the reaction solution possibly provides milder reduction environment and/or ligand-induced etching-mediated size focusing. The nanoclusters were characterized by using a number of techniques. This study

shows an alternative straightforward route of size-selected cluster synthesis in an aqueous medium. We note that the MPA ligand can be functionalized with desired molecules via its carboxylic or thiol groups. Features like water solubility, functionality, and tailorable non-bleaching photoluminescence make Au NCs as ideal alternative fluorescent probes for many biological applications.

Tailoring the Stability and Photoluminescence Properties of Nanoclusters in Aqueous Media

5.1 Introduction

Metal nanoclusters constitute to be a prolific area of research due to their novel properties and applications. Metal nanoclusters have shown huge potentials for applications in bio-sensing, fluorescent labeling, cellular imaging, catalysis, heavy metal ion detection, and so on. Synthesis of nanoclusters of desired properties and the ability to tune the properties of the nanoclusters are two major goals of the research in this field. Properties such as water solubility, tunable stability, and photoluminescence make nanoclusters as promising candidates for various applications. Water-soluble gold clusters hold great potential for biological labeling, bio-catalysis, and nano-bioconjugates. Due to the small size, less toxicity, and non-bleaching photoluminescence properties, gold nanoclusters are considered as alternative labels for biological applications. Possible manipulation of photoluminescence properties provides an additional arm for such applications.

The stability of the nanoclusters is an important factor in various studies and applications. Highly stable NCs are required in the study of size-dependent properties and exploration of their applications. Cluster stability is strongly influenced by the nature of the capping ligand employed in the cluster synthesis. Capping ligands with long carbon chains and bulky ligands (sterically hindered) offer efficient protection compared to the other small chain capping ligands.^[22,24,143] The effects of surface charge on the stability of NCs have also been explored earlier. AbdulHalim et al. reported the synthesis of highly stable $\text{Ag}_{44}(\text{SR})_{30}$ nanoclusters by using the 5-mercapto-2-nitrobenzoic acid as capping ligand and pH-mediated surface modification strategies for enhanced stability of the silver clusters.^[35,144] Yuan et al. demonstrated various ligand-shell engineering strategies to improve the stability of Au_{25}

clusters in aqueous media.^[95] Recently, Nataraju et al. reported the phase transfer induced stability of silver nanoclusters where sterically hindered tetraoctylammonium (TOA⁺) counter ions effectively enhanced the stability of silver clusters in toluene phase.^[142] Kumar et al. synthesized thermally highly stable, water-soluble Au₂₅ nanocluster by using the captopril as capping ligand (Captopril= (2S)-1-[(2S)-2-methyl-3-sulfanylpropanoyl] pyrrolidine-2-carboxylic acid). Au₂₅(Captopril)₁₈ clusters showed higher thermal stability over the Au₂₅(Glutathione)₁₈ clusters in a water medium.^[34] Similarly, Negishi and co-workers observed the enhanced stability of selenolate protected Au-25 nanoclusters over the thiolate protected ones against thermal dissolution and laser fragmentation.^[145] Jin and co-workers reported the effects of ligand chain length on the photoluminescence of Au₂₅ NCs.^[146] Therefore, in addition to the cluster size, the surrounding or encapsulating ligands have significant impacts on various properties (such as optical, catalytic, luminescence, biological and so on) of the Au NCs. Thus, the selection of suitable capping ligand is essential in order to impart the desired properties such as enhanced stability and photoluminescence of the cluster system.^[147–149]

Despite the substantial progress made in the field of nanocluster, we are far away from establishing any essential general principles required for the rational design of size-selective synthesis as well as tuning the properties of the nanoclusters. In this chapter, we explore how the stability and photoluminescence of Au₁₈(MPA)₁₄, Au₂₅(MPA)₁₈ types of clusters can be tuned in aqueous solutions. Since the MPA ligand has two dissociable functional groups, –SH and –COOH, we have employed the pH variation strategy in order to tune the stability and photoluminescence of Au₁₈(MPA)₁₄ and Au₂₅(MPA)₁₈ clusters in aqueous media.

5.2 Methods and Characterizations

The cluster stability under various pH conditions was studied with the help of UV-Visible spectroscopy. The pH of the reaction solution after the cluster synthesis was ~8.6. The pH of the cluster solution was increased from 8.6 to 11.0 by the addition of NaOH and was decreased from 8.6 to 5.0 by the addition of acetic acid or HCl solutions. FT-IR spectra were measured by using Bruker Tensor 27 instrument in transmittance mode. Photoluminescence study was

carried out with the Horiba Jobin Yvon Model FL3-22 Fluorolog spectrofluorimeter. The quantum yields were calculated at room temperature by using rhodamine 6G (R6G) as the reference.

5.3 Results and Discussion

5.3.1 Stability of the $Au_{18}(MPA)_{14}$ Clusters

We have used MPA ($HSC_2H_4CO_2H$) which is a water-soluble bifunctional ligand. Both the functional groups are responsive towards the change in the pH of the solution. Thus, we used pH variation as a simple tool for the tailoring the cluster stability and properties like photoluminescence. The stability of the clusters under acidic and basic pH was monitored with the help of their time-dependent UV-vis absorption spectra. Time-dependent UV-vis absorption studies showed that the absorption intensity of $Au_{18}(SC_2H_4CO_2H)_{14}$ cluster began to decrease after ~ 24 hr. This suggests that the as-synthesized cluster at pH ~ 8.6 was stable for ~ 24 hr (Figure 5.1).

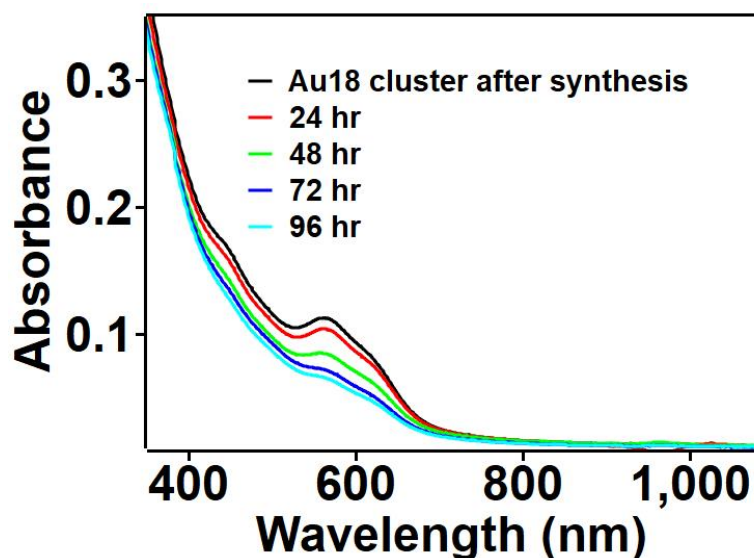


Figure 5.1 Time-dependent UV-visible absorption spectra of the $Au_{18}(MPA)_{14}$ cluster solution (pH ~ 8.6)

Figure 5.2 shows the time-dependent UV-Visible spectra of $\text{Au}_{18}(\text{MPA})_{14}$ cluster in toluene medium. In addition to the capping ligand, the solvent also plays a prime role in rendering stability to the cluster. Stability of the Au-18 cluster is gradually decreasing with time after transferring into toluene medium.

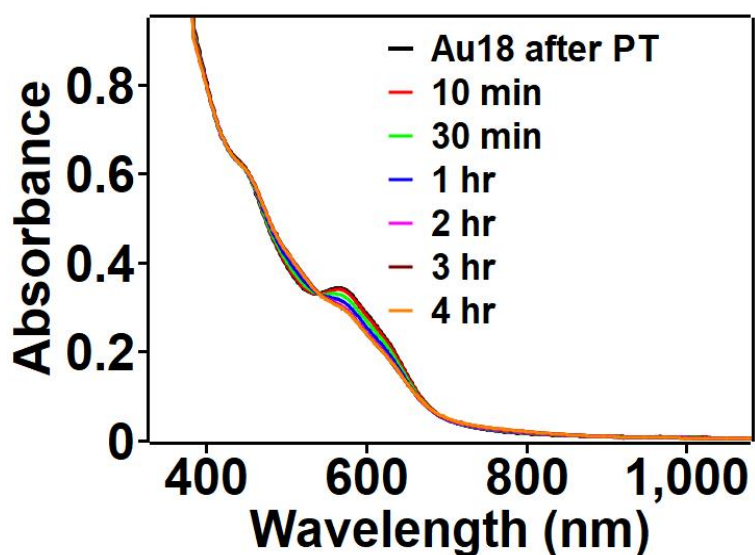


Figure 5.2 Time-dependent UV-Visible absorption spectra of the $\text{Au}_{18}(\text{MPA})_{14}$ cluster in toluene solvent medium

Figure 5.3 shows the UV-Visible spectra of the aqueous dispersions of $\text{Au}_{18}(\text{SC}_2\text{H}_4\text{CO}_2\text{H})_{14}$ under different pH conditions. The pH value of the reaction solution after the formation of $\text{Au}_{18}(\text{SC}_2\text{H}_4\text{CO}_2\text{H})_{14}$ was ~ 8.6 . It was observed that the UV-Visible spectra retained the characteristic features of the aqueous solutions of $\text{Au}_{18}(\text{SC}_2\text{H}_4\text{CO}_2\text{H})_{14}$ in the pH range $\sim 8-10$ whereas those at $\text{pH} < 7$ exhibited a spectral profile significantly different from that of $\text{Au}_{18}(\text{SC}_2\text{H}_4\text{CO}_2\text{H})_{14}$ with an isosbestic point at ~ 535 nm. Drastically different spectral feature along with the presence of the isosbestic point under acidic conditions suggests a transformation of $\text{Au}_{18}(\text{SC}_2\text{H}_4\text{CO}_2\text{H})_{14}$ to a specific species, which is corroborated by our fluorescence studies. The spectra taken after 24 hr under acidic conditions showed

characteristic features for the Au(III)-complex, which could arise from the oxidative degradation of $\text{Au}_{18}(\text{SC}_2\text{H}_4\text{CO}_2\text{H})_{14}$ cluster.

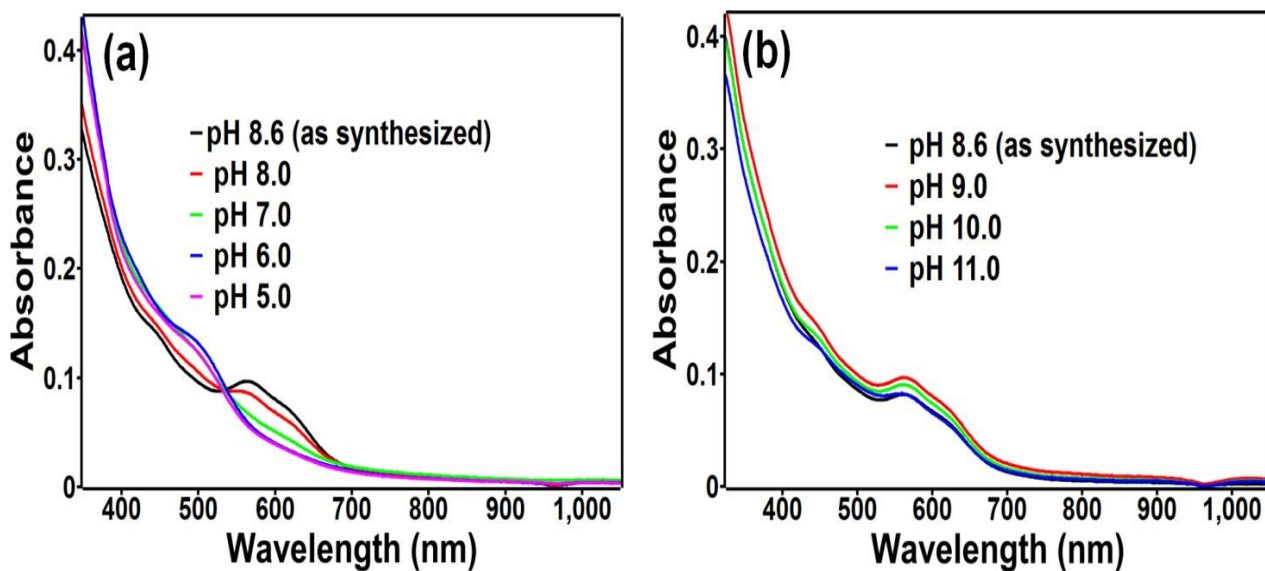


Figure 5.3 UV-Vis spectra of the aqueous solutions of $\text{Au}_{18}(\text{MPA})_{14}$ under different pH values: (a) decreasing and (b) increasing pH

5.3.2 Stability of $\text{Au}_{25}(\text{MPA})_{18}$ clusters

The pH of the original $\text{Au}_{25}(\text{MPA})_{18}$ cluster solution after the synthesis was observed to be ~ 9.40 . Time-dependent UV-vis absorption studies of the Au_{25} cluster showed that the UV-vis spectral features of the as-synthesized original $\text{Au}_{25}(\text{MPA})_{18}$ cluster began to deviate after ~ 8 hours of preparation. However, the time-dependent UV-vis absorption studies under basic pH showed that the cluster stability improved with increasing pH (from pH 9.4 to 12). (**Figure 5.4**) It was observed that the Au_{25} cluster at pH 12 showed the maximum stability of about 9 days. On the other hand, the stability of the cluster decreased significantly under acidic pH (**Figure 5.5**). The clusters either undergo aggregation or transform into mixed sized clusters under acidic conditions. It is interesting to note that the as-synthesized Au_{18} clusters were more

stable than the as-synthesized Au₂₅ clusters. However, the stability of Au₂₅ clusters enhanced drastically at pH 12.

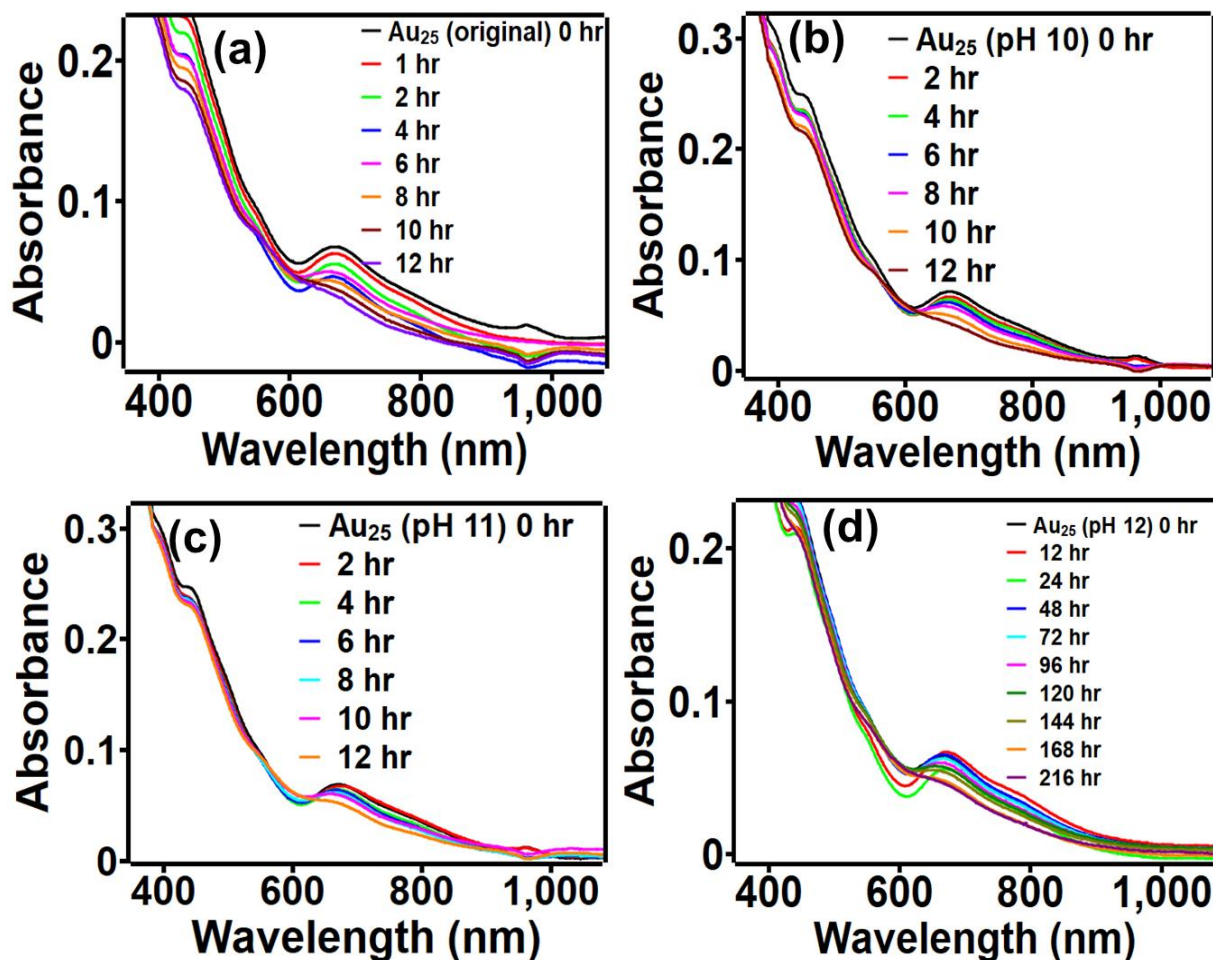


Figure 5.4 UV-Vis spectra showing the stability of Au₂₅(MPA)₁₈ clusters in basic pH: Au₂₅ original cluster (pH 9.4) (a), Au₂₅ pH 10 (b), Au₂₅ pH 11 (c), and Au₂₅ pH 12 (d)

Under basic conditions at higher pH, the majority of the carboxylic groups of the ligands on the cluster surface undergoes deprotonation forming $-\text{COO}^-$ (pK_a of MPA: ~ 4.3), which enhances the electrostatic repulsion among the clusters. These strong electrostatic repulsions among the clusters offer enhanced stability to the clusters.

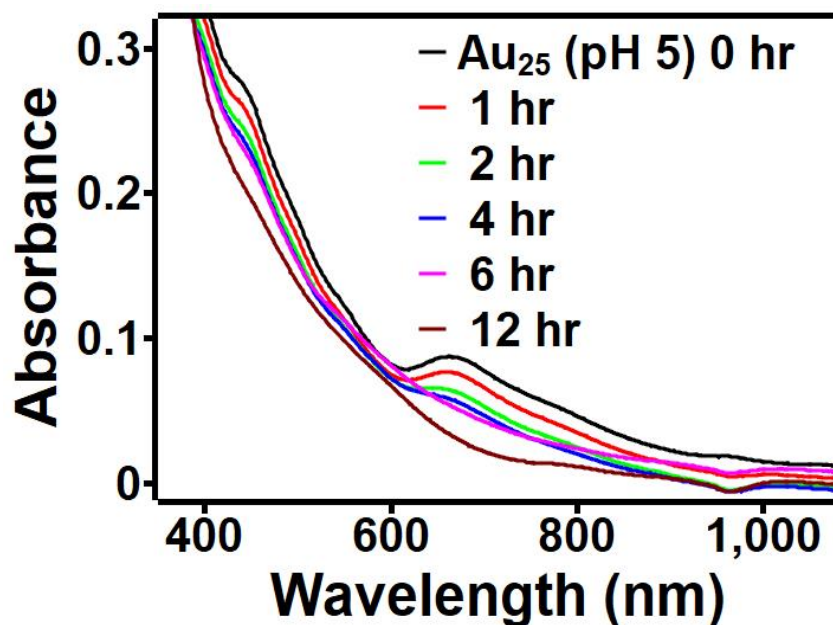


Figure 5.5 UV-Vis spectra showing the stability of $\text{Au}_{25}(\text{MPA})_{18}$ cluster in acidic pH (at pH 5)

At pH 12 clusters showed maximum stability. Recently, Yuan et al. reported how the various parameters such as ligand chain length, mixed ligands, mixed ligands with opposite charges contribute towards the stability enhancement of the Au_{25} cluster. The authors observed that the cluster stability can be significantly enhanced (up to 144 hours) by using two oppositely charged mixed thiolate capping ligands. It is worth noting that we have used a short chain capping ligand such as mercaptopropionic acid (MPA), not a long chain or oppositely charged mixed thiolate ligand system here.

5.3.3 Photoluminescence of $\text{Au}_{18}(\text{MPA})_{14}$

Small clusters show molecule-like photoluminescence (PL) properties. $\text{Au}_{18}(\text{SC}_2\text{H}_4\text{CO}_2\text{H})_{14}$ clusters showed PL properties comparable to those of $\text{Au}_{18}(\text{SG})_{14}$ ($\lambda_{\text{em}} \sim 800$ nm, QY $\sim 0.4\%$),^[48] $\text{Au}_{18}(\text{SC}_6\text{H}_{11})_{14}$ ($\lambda_{\text{em}} = 735$ nm, QY $\sim 0.05\%$),^[100] and ($\lambda_{\text{em}} = 706$ nm, QY $\sim 0.1\%$).^[101] Aqueous $\text{Au}_{18}(\text{SC}_2\text{H}_4\text{CO}_2\text{H})_{14}$ clusters in basic pH (>8.5) showed a weak PL at $\lambda_{\text{em}} = \sim 800$ nm when excited at $\lambda_{\text{ex}} = 560$ nm (**Figure 5.5a**). The intensity of the PL peak at $\lambda_{\text{em}} = \sim 800$

nm gradually increased with the increase in pH up to 10.0 (QY \sim 0.02 %). At pH \sim 6.0, we observed two PL peaks at $\lambda_{em} = \sim$ 570 nm (QY \sim 0.1%) excited at $\lambda_{ex} = 350$ nm and $\lambda_{em} = \sim$ 690 nm (QY 0.03%) excited at $\lambda_{ex} = 560$ nm (**Figures 5.6a and b**). It should be noted that the Au-MPA precursor complex at pH \sim 5.0 – 6.0 showed a similar emission at $\lambda_{em} \sim$ 575 nm (QY \sim 0.35%) when excited at $\lambda_{ex} = 350$ nm (**Figure 5.7**). However, in this case, the emission showed no drastic change in the peak position upon changing the pH, unlike the nanocluster system.

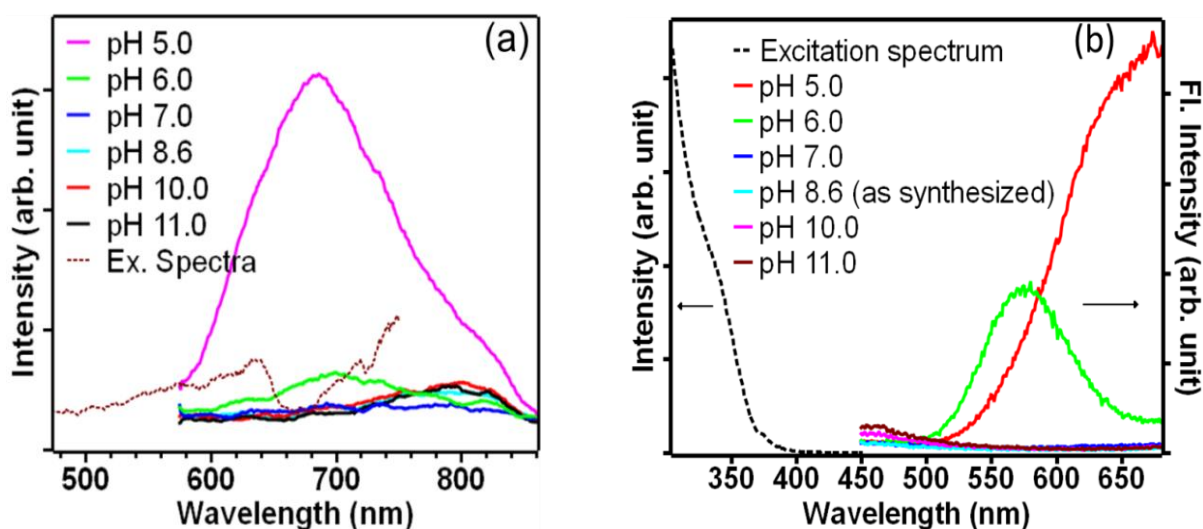


Figure 5.6 pH-Dependent photoluminescence spectra of $Au_{18}(SC_2H_4CO_2H)_{14}$ at $\lambda_{ex} = 560$ (a) and 350 (b) nm

A striking difference in the PL properties of the Au-MPA complex and the cluster was observed when the solutions were excited with $\lambda_{ex} = 560$ nm. The complex solutions did not show any significant emissions. This indicates that the \sim 570 nm emission peak could arise from Au(I)-MPA complex formed by the oxidative decomposition of the cluster in acidic condition. The former shorter wavelength PL peak of the cluster disappeared at pH \sim 5.0, whereas the latter peak at $\lambda_{em} = \sim$ 690 nm (QY \sim 0.12%) became very dominant (**Figure 5.6b**). This could be due to the conversion of $Au_{18}(SC_2H_4CO_2H)_{14}$ cluster to an unknown highly photoemissive species(**Figure 5.6b**).

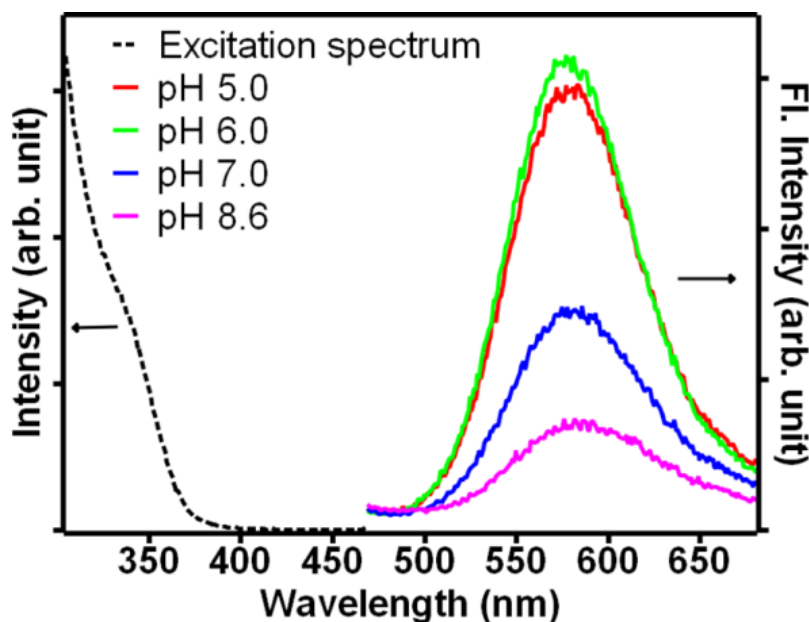


Figure 5.7 pH-Dependent photoluminescence spectra of Au-MPA complex at $\lambda_{\text{ex}}=350$ nm

The QY of the PL of $\text{Au}_{18}(\text{SC}_2\text{H}_4\text{CO}_2\text{H})_{14}$ could be enhanced by the phase transfer into organic phase (toluene) by using a phase transfer reagent such as tetraoctylammonium bromide (TOAB). The $\text{Au}_{18}(\text{SC}_2\text{H}_4\text{CO}_2\text{H})_{14}$ cluster was transferred from aqueous to toluene phase within 3–5 min after mixing the aqueous dispersion of $\text{Au}_{18}(\text{SC}_2\text{H}_4\text{CO}_2\text{H})_{14}$ and the toluene solution of TOAB. No significant difference was observed in the UV-vis absorption spectra before and after the phase transfer (**Figure 5.8a**). This indicates that the phase transfer process hardly affects the structure of $\text{Au}_{18}(\text{SC}_2\text{H}_4\text{CO}_2\text{H})_{14}$. The clusters extracted into toluene showed PL at $\lambda_{\text{em}} = \sim 800$ nm with QY $\sim 0.15\%$, which is much higher than that in water (**Figure 5.8b**). Similar enhancement of PL QY was observed in the phase transfer of Au_{12} clusters protected by mercaptosuccinic acid and could be ascribed to the suppression of the collisional quenching by a thicker protecting layer.^[82]

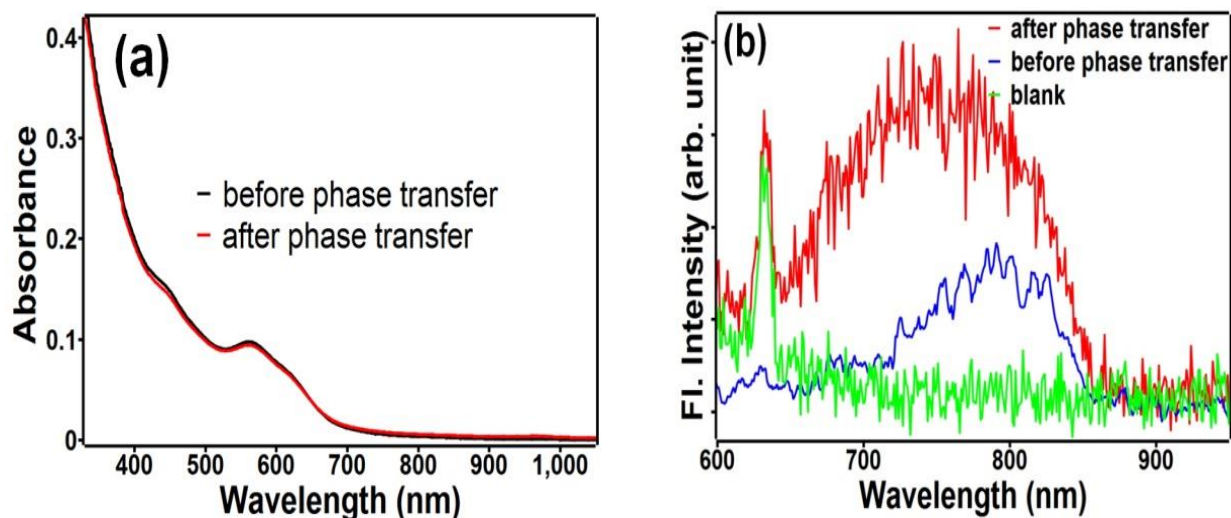


Figure 5.8 (a) UV-vis absorption and (b) PL spectra of $\text{Au}_{18}(\text{SC}_2\text{H}_4\text{CO}_2\text{H})_{14}$ before and after the water to organic phase transfer

5.3.4 Photoluminescence of $\text{Au}_{25}(\text{MPA})_{18}$

The synthesized $\text{Au}_{25}(\text{MPA})_{18}$ clusters showed red fluorescence in an aqueous medium. The small capping ligand protected $\text{Au}_{25}(\text{MPA})_{18}$ clusters showed relatively weak fluorescence compared to the previously reported Au_{25} clusters protected by bulky capping ligands. The clusters showed the emission peak at 740 nm with 470 nm excitation wavelength. Like the Au_{18} clusters, the photoluminescence intensity of Au_{25} clusters gradually increased with decreasing pH (acidic medium) (**Figure 5.9**). The calculated quantum yield (QY) of the Au_{25} original cluster was 0.001%. QYs of Au_{25} clusters were as high as 0.007% at pH 5 whereas 0.0003% at pH 11. The reported QY are comparable with the PL of $\text{Au}_{25}(\text{SG})_{18}$ (SG= Glutathione) reported by Pradeep and coworkers.^[32,150] Similar red luminescence had been observed earlier in the cases of Au_{18} and Au_{25} clusters.^[38,146] However, the peak position and the fluorescence intensity not only depend on the core but on the nature of capping also.

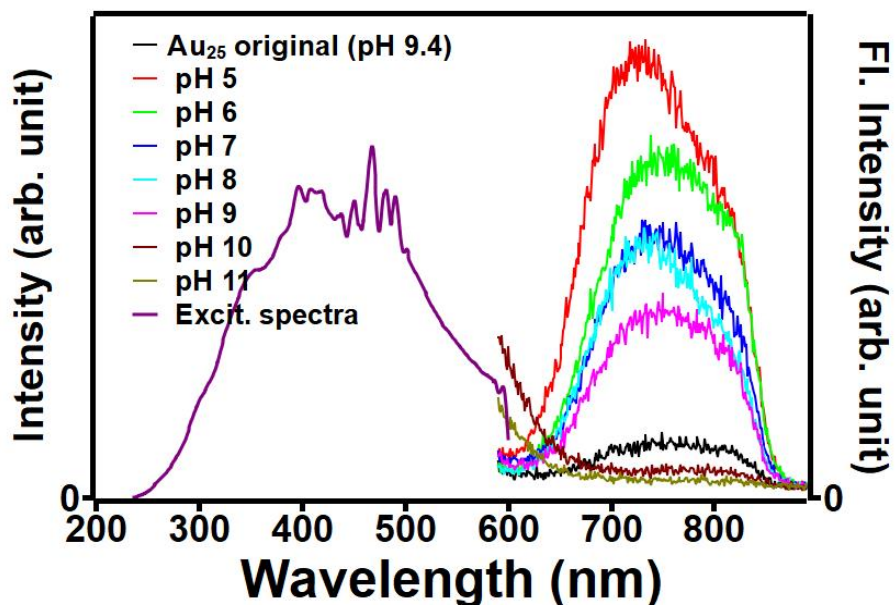


Figure 5.9 The excitation and photoluminescence spectra of $\text{Au}_{25}(\text{MPA})_{18}$ clusters in acidic and basic media

Ultra-small metal nanoclusters show photoluminescence because of their molecular like electronic states. The ultra-small size of clusters causes the strong quantum confinement of free electrons in the particles. Thus, the continuous density of states metals breaks up into discrete energy levels. This leads to the size-dependent photoluminescence and other attractive molecule-like properties. In addition to the core, the surface ligands and cluster charge play important roles in determining the photoluminescence properties of the Au NCs.^[146] The surface ligands had been proposed to influence the photoluminescence in two ways: (i) the charge transfer from the ligands to the metal NC core through the Au-S bonds and (ii) the direct donation of delocalized electrons of electron-rich atoms or groups of the ligands to the metal core.

Our nanocluster solutions showed complex pH dependent photoluminescence property. Although the exact details of the origin of such photoluminescence are not clear at this moment, the pH-dependent PL behavior is possibly associated with the degree of MPA-

mediated aggregation of the Au-MPA complex as well as the clusters. Researchers had earlier reported solvent- and ion-mediated aggregation-induced emissions for ligand-protected gold and copper clusters.^[151] At low pH, most of the –COOH groups (pK_a 4.3; but the apparent surface pK_a may be different, ~ 6.4) and almost all thiol groups ($pK_a \sim 10$) remain protonated. As a result, both the precursor complex molecules and $Au_{18}(MPA)_{14}$ clusters can form aggregates via hydrogen bonding between –COOH groups; thus showing pH-dependent aggregation-induced emission. When the pH value increases, the carboxylic (and, maybe, –SH) groups are dissociated forming negatively charged carboxylate (and thiolate) species. The deprotonation and the electrostatic repulsive force suppress the aggregation process. This explains the decrease in emission intensity at two shorter wavelengths with the increase in pH of the medium. However, the weak emission at $\lambda_{em} = \sim 800$ nm that increases in intensity with the pH increase could be ascribed to the free cluster fluorescence.

5.4 Conclusions

We have demonstrated that a simple factor such as pH of the cluster solution can be used to tailor the properties of clusters by a judicious choice of the capping ligands. The $Au_{18}(MPA)_{14}$ and $Au_{25}(MPA)_{18}$ NCs exhibit interesting pH-tunable stability and photoluminescence (both wavelength and quantum yield). The selection of the bi-functional binding ligand such as 3-mercaptopropionic acid provides simple tools for the tuning of the properties of the cluster in an aqueous medium. Our results clearly demonstrate that the stability of the cluster can be systematically improved by increasing the pH of the cluster media. The strong electrostatic repulsive forces acting between cluster species in basic medium play a crucial role in enhancing the stability of the cluster in basic medium. The tunable photoluminescence arises from the pH-mediated assemblage and disassemblage phenomena of the bi-functional ligand, MPA. Quantum yield of Au_{18} cluster photoluminescence at ~ 800 nm increased with the increase in pH value (0.02% at $pH \sim 10$) and further increased to 0.1% after phase transfer by tetraoctylammonium ions into toluene medium.

Catalytic Properties of $\text{Au}_{18}(\text{MPA})_{14}$ and $\text{Au}_{25}(\text{MPA})_{18}$ Nanoclusters: Reductions of Ortho- and Para-Nitroanilines by NaBH_4 in Water

6.1 Introduction

Finely divided metals are highly desirable as catalysts in many chemical transformations. Although bulk gold is relatively inert, in the late 1980s, Haruta and coworkers discovered the exceptional catalytic behavior of supported gold nanoparticles towards the CO oxidation at sub-ambient temperatures (200 K).^[152] Since then researchers had employed finely divided gold, particularly nanoscale gold particles, of different sizes and morphologies as catalysts in various kinds of reactions. Nanoparticles show excellent catalytic properties, which are highly dependent on the size and shape of the particles. In last two decades, gold nanoparticles became irreplaceable catalysts for a wide range of chemical reactions.^[153–155]

Nanoscale systems constitute of broadly two regimes, namely, nanoclusters and nanoparticles. Nanoparticles provide plenty of active sites for enhanced catalysis owing to their structural features like corners, edges, steps, crystal facets, and defects and the large surface-to-volume ratio. On the other hand, nanoclusters consist of a small number of atoms like molecular entities. Thus, the nanoclusters could act as individual active sites and could show strong catalytic activity. Further, it is worth noting that, from a given quantity of materials, the number of ultra-small clusters that can be prepared is very large compared to that of nanoparticles. Thus, the cluster catalysis requires a very small quantity of materials, which is an important factor in the cases of precious metals. These interesting sets of properties make nanoclusters very promising as catalysts. However, often solid-supported nanoclusters have been used in catalysis.

In recent years, ligand-protected gold nanoclusters have attracted tremendous attention because of their ultra-small size (~1-2nm) and novel physicochemical properties.^[74] Au NCs can act as efficient catalysts for different chemical transformations because of ultra-small size and tunable surface chemistry.^[53,153,156] Ultra-small Au NCs protected by thiolate capping ligands have been used as catalysts for various oxidation and reduction chemical reactions. Ligand protected gold nanoclusters deposited on various solid supports such as metal oxides (e.g., SiO₂, TiO₂, Al₂O₃, etc.), CNTs, graphene oxide, and activated carbon (AC) act as promising catalysts for chemical transformations like oxidations of carbon monoxide (CO), alcohols, alkenes, etc. and reductions of nitro derivative, carbonyls, etc.^[157] In the cases of supported metal nanocluster catalysts, metal-support interactions play a critical role in influencing the catalytic activities of Au NCs. In addition, solid support protects the nanocluster from aggregation during catalysis process. Hence, selection of suitable solid support is crucial in enhancing the catalytic activity of clusters. Recently Fang et al. demonstrated the role of solid support in tuning the catalytic activity of Au₂₅ NCs.^[158]

The oxidation of carbon monoxide has been extensively studied by using various supported Au NC catalysts.^[159] Several computational studies on the oxidation of carbon monoxide by using supported Au NCs were also reported.^[160] Jin et al. and Chen et al. have successfully employed the TiO₂-supported Au₂₅(SR)₁₈ and Au₁₀₂(SPh)₄₄ catalysts for the selective oxidation of various organic sulfide derivatives into sulfoxides by using idosylbenzene (PhIO) oxidant.^[137,161] Supported Au₂₅(SR)₁₈ and Au₁₀₂(SPh)₄₄/TiO₂ catalysts have shown excellent catalytic activity under mild reaction conditions. Recently, Wan et al. have reported the catalytic activity of Au₃₈/TiO₂ supported catalysts for the semi-hydrogenation of alkynes also demonstrated the effects of the capping ligand in tuning the catalytic activity of Au₃₈ NCs.

In addition to the heterogeneous catalysis, free-standing atomically precise Au NCs also have been used as efficient catalysts in homogeneous catalysis. It is relatively easy to modulate the accessibility, activity, and selectivity of the catalysts in homogeneous catalysis. Xie and coworkers demonstrated various ligand shell engineering strategies to improve the catalytic activity of Au₂₅ NCs in aqueous media. It was observed that the clusters with small capping

ligands showed enhanced the catalytic activity by facilitating the better accessibility of the reactant molecules onto the catalyst surface.^[162] Thiol-stabilized Au₂₅L₁₈ clusters were employed as homogeneous catalysts for the reduction of 4-nitrophenol. They observed that Au₂₅ clusters could retain their structural integrity during the catalysis because of their high stability.^[163]

It is evident that the capping ligands play important roles in the catalytic activities of Au NCs. Bulkier ligands offer more steric hindrance and restrict the cluster-reactant interactions during catalysis which could decrease the catalytic efficiency of Au NCs. Therefore, it is highly desirable to choose the suitable surface capping ligand in order to achieve a higher catalytic activity of Au NCs. Further, recent studies revealed that capping ligands could modulate the reaction pathway also. Xie and co-workers reported that Au₂₅(p-MBA)₁₈ catalyst modulate the reaction pathway of 4-nitrophenol hydrogenation.^[164] In this chapter, we describe a study on the catalytic properties of mercaptopropionic acid (MPA) protected aqueous Au₁₈ and Au₂₅ NCs towards the reduction of nitroanilines by a NaBH₄ reducing agent in water solvent without using any solid support. Water solubility and small surface capping ligand, MPA make Au clusters as promising candidates for catalytic applications.

The reduction of nitroaromatic compounds to amino derivatives is a frequently studied model reaction. This reaction can be easily monitored spectrophotometrically due to the color change that occurs during the reaction. Ortho and para nitroanilines are very important nitro compounds, which can be readily used as the starting materials for the synthesis of phenylenediamines (diaminobenzenes). Ortho- and para-phenylenediamines can act as attractive intermediates in the preparation of many organic dyes, pigments, and polymers.^[165] Further, ortho- and para-nitroanilines are very toxic to the humans as well as aquatic organisms. Nitroanilines are considered as nonbiodegradable or slowly degradable which are highly hazardous to the environment if released as a pollutant.^[166,167] Therefore, it is important to design suitable catalysts for the efficient reduction of ortho- and para-nitroanilines under ambient conditions. We demonstrate that our nanoclusters at ppm level concentrations show superior catalytic activity in comparison with spherical Au nanoparticles.

6.2 Materials and Methods

6.2.1 Materials

Hydrogen tetrachloroaurate (III) hydrate ($\text{HAuCl}_4 \cdot 3\text{H}_2\text{O}$), 3-mercaptopropionic acid (MPA), sodium borohydride (NaBH_4) were purchased from Sigma-Aldrich. Toluene, methanol, sodium hydroxide (NaOH), and tetraoctylammonium bromide (TOAB) were received from SRL Chemicals Pvt. Ltd., India. The chemicals were used as received. Aqua-regia was used to clean the glassware throughout the reaction. Millipore water with 18.2 $\text{M}\Omega\cdot\text{cm}$ specific resistance was used throughout the experiment.

6.2.2 Characterizations

UV-Visible spectra were recorded on a PerkinElmer Lambda 35 UV-Visible spectrometer. The pH of the reaction solution after the cluster synthesis was ~ 8.6 . FT-IR spectra were measured by using Bruker Tensor 27 instrument in transmittance mode.

6.2.3 Reduction of Nitroanilines

Reduction of nitroaniline to diaminobenzene by using NaBH_4 was carried out at room temperature ($25\text{ }^\circ\text{C}$). In a typical reaction, 50 μL of Au NCs (0.0025 mg) was added to the NA solution. $3 \times 10^{-4}\text{ M}$ and $1.125 \times 10^{-4}\text{ M}$ solutions of 2-NA and 4-NA, respectively, were used. After mixing, 300 μL of NaBH_4 (0.1M) was added to initiate the reaction. The pH of the reaction solution was ~ 5.8 before the addition of NaBH_4 which changed to 9.45 after the addition of NaBH_4 . The progress of the reduction was monitored by using a UV-vis spectrophotometer as nitroaniline absorbs in the UV-vis range of electromagnetic spectrum. The reaction was performed in a quartz cuvette.

6.3 Results and Discussion

It has been demonstrated that various supported and non-supported thiol protected Au NCs nanoclusters act as potential catalysts for the reduction of nitro compounds including nitrobenzene, nitroanilines, nitrophenols and their derivatives.^[162,163] In most of the reports, ultra-small Au NCs on different solid supports were employed for the efficient and selective

reduction (hydrogenation) of nitro compounds.^[156] Capping agents play important roles in the catalyzed reactions. We employed water-soluble MPA-capped Au₁₈ and Au₂₅ NCs as model catalysts for the reduction of 2-nitroaniline and 4-nitroaniline by NaBH₄ at room temperature. As synthesized MPA protected Au₁₈ and Au₂₅ clusters act as efficient catalysts for the reduction of ortho- and para-nitroaniline (2-NA and 4-NA respectively) to respective diaminobenzenes. Au₂₅ cluster retains its structural integrity in catalysis reactions (which allows the cluster recyclability) because of its remarkable stability and stable crystal structure. However, Au₁₈ clusters undergo degradation during catalysis.^[168]

Aqueous nitroanilines show yellow color. 2-NA shows its characteristic UV-vis absorption bands peaking at ~280 and 410nm whereas 4-NA shows at ~220 and 370nm in water (**Figures 6.1**). Therefore, Au NCs catalyzed reduction kinetics was monitored by using UV-vis spectroscopy. **Figures 6.1** shows the time-dependent UV-vis absorption spectral change during the Au NCs catalyzed reductions of nitroanilines by sodium borohydride at room temperature.

The disappearance of yellow color indicates the progress of the reduction reaction, i.e., the conversion of a nitro group into amine group. We followed the reduction kinetics by following the decrease in the absorbance of 420 nm and 370 nm peaks in the case of 2-NA and 4-NA respectively. The absorbances of the Au NCs do not affect the absorbance of nitroanilines at these two wavelengths because the quantities of the Au NCs used as catalysts were negligible. The new absorption bands that appeared indicate the formation of diaminobenzenes. 4-NA showed greater induction period (~3 minutes). On the other hand, no significant induction period was observed for 2-NA during the catalyzed reaction. **Figure 6.1** shows that the absorbance decreases almost linearly with time after the induction period of 10 seconds.

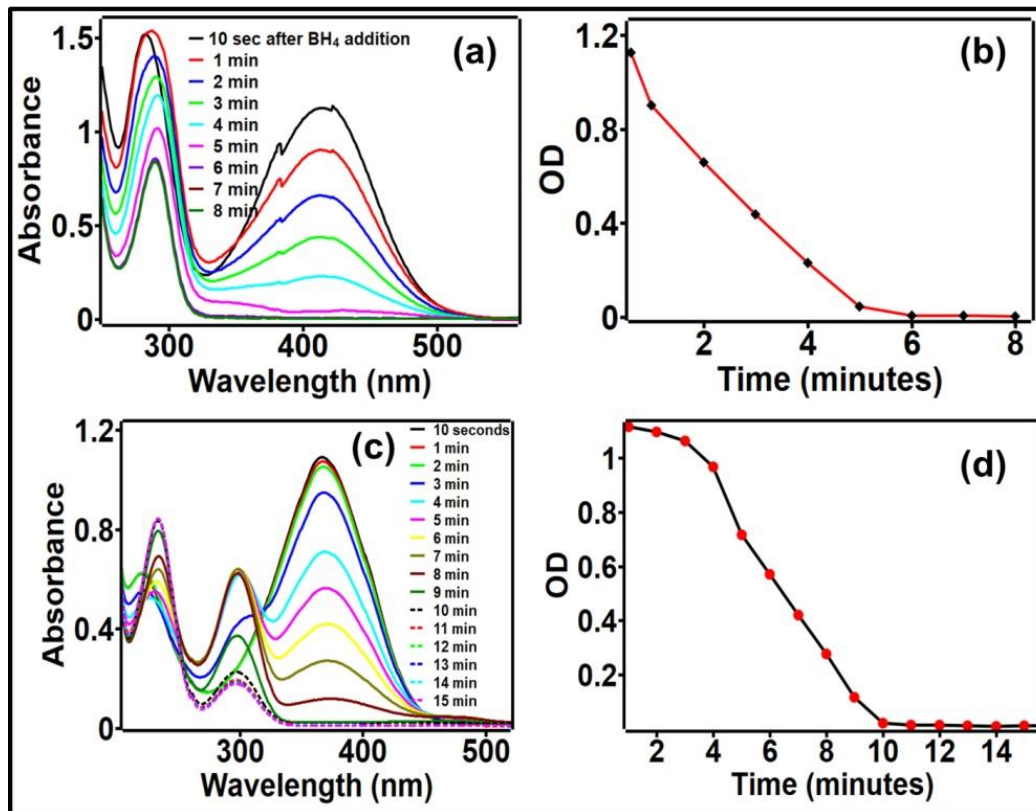


Figure 6.1 UV-Vis spectra and absorbance vs. time plot showing the Au₂₅ catalyzed reduction of ortho-nitroaniline (a,b) and para-nitroaniline (c,d) by using NaBH₄ as the reducing agent in water solvent

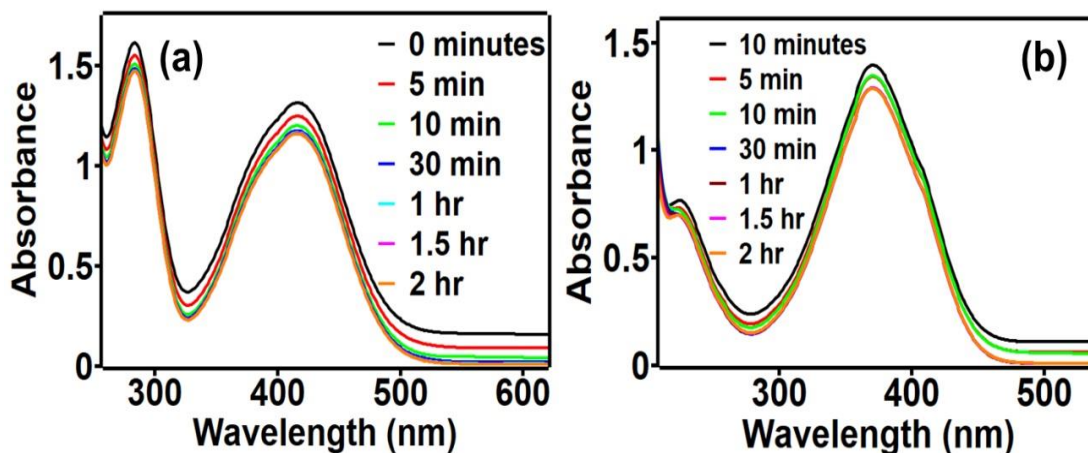


Figure 6.2 Control experiments: UV-Vis spectra showing the reduction of 2-NA (a) and 4-NA (b) by NaBH₄ in the absence of Au NC catalyst

In the absence of Au NCs as catalysts, hardly any reduction occurs. The control experiments show that the reduction reactions are extremely slow in the absence of Au NCs.

Figure 6.1 shows that the absorbance vs. time plot is linear up to ~80 to 90% of the reaction. It suggests that Au NCs catalyzed nitroaniline reductions follow zero order reaction kinetics according to equation (1).

$$A_t - A_0 = - kt \quad \dots\dots\dots(1)$$

Where A_t and A_0 are the absorbance values at times, t and 0 respectively, of the reaction and k is the zero order rate constant or specific reaction rate. The magnitude of k can be a measure of the catalytic efficiency. The rate constant, k , can be calculated from the slope of the straight line obtained by plotting A_t vs. t graph as shown in **Figure 6.1**. The rate constants (k 's) were determined to be $0.22 \text{ M}\cdot\text{min}^{-1}$ and $0.16 \text{ M}\cdot\text{min}^{-1}$ for 2-NA and 4-NA respectively for $50\mu\text{L}$ of Au NCs. We have used up to $200\mu\text{L}$ of Au NCs; however, the rate constants hardly changed in this change range. The zero order reaction suggests that the catalyst is possibly saturated with the reactants and the reaction might be a surface catalyzed reaction. It is not clear at present why there is a longer induction period present and why the Au NCs catalyzed the reduction of 4-NA has a smaller rate constant compared to that of 2-NA. These could be due to their structural difference leading to different interactions with the Au NCs. The almost similar catalytic property was observed in the case of Au_{18} NCs. It is interesting to note that a comparison of k values revealed that the Au NCs showed superior catalytic activity compared to many gold nanoparticle counterparts of 10 to 20 nm sizes.^[169–172]

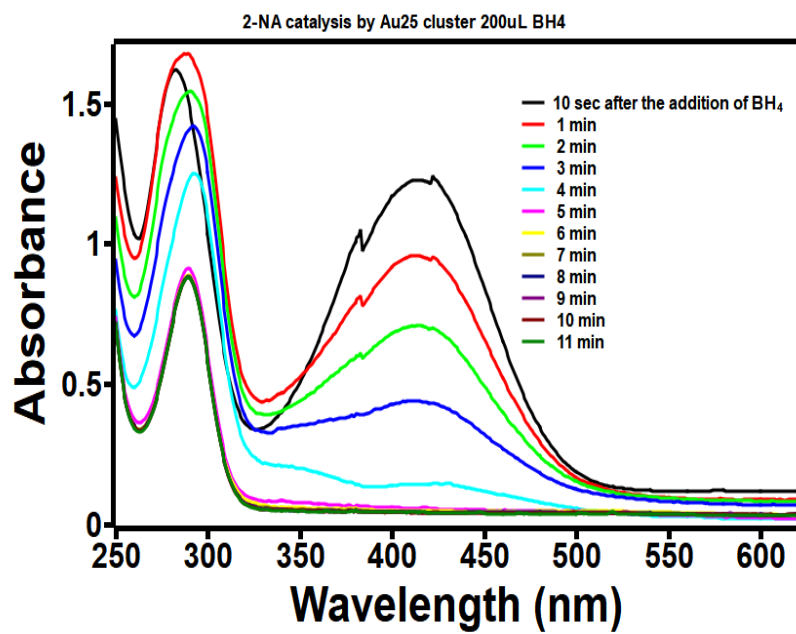
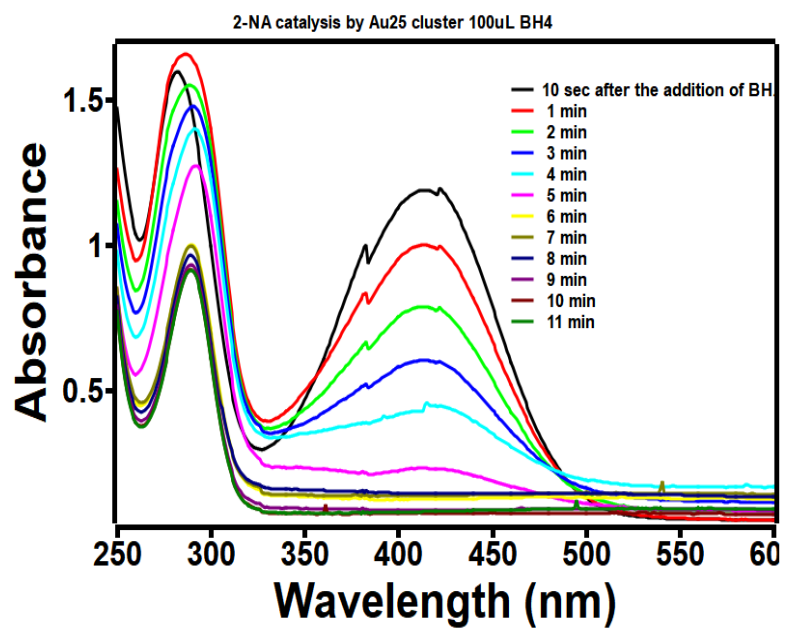


Figure 6.3 UV-Vis spectra showing the 2-NA catalysis with 100 and 200 μ L Au NCs

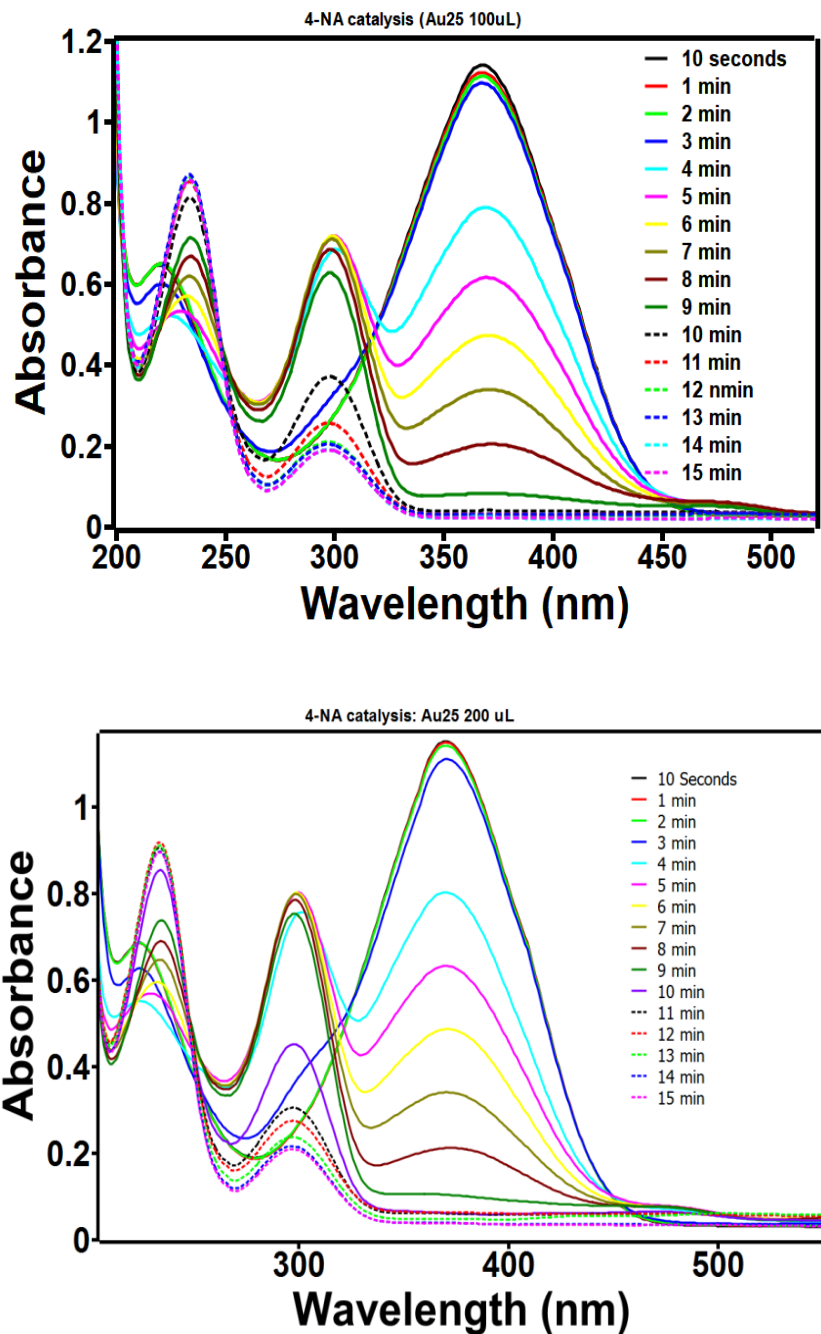


Figure 6.4 UV-Vis spectra showing the 4-NA catalysis with 100 and 200 uL Au NC

We know that finely divided particles and nanoparticles offer large surface-to-volume ratio as well as many corners, edges, steps, crystal facets, defects, etc. which provide plenty of active sites for enhanced chemical reactivity and/or catalysis. However, nanoclusters consist of only a

small number of atoms like molecular entities. NCs have defined frontier orbitals, HOMO, and LUMO, which can interact with other molecules. Thus, the small nanoclusters can act as individual active sites and can exhibit huge catalytic activity owing to the presence of huge numbers of ultra-small clusters-cum-active sites.

6.4 Conclusions

In this chapter, we described the catalytic properties of water-soluble clusters, $\text{Au}_{18}(\text{MPA})_{14}$ and $\text{Au}_{25}(\text{MPA})_{18}$, in the reduction of nitroanilines by using NaBH_4 as reducing agent in water solvent media. Gold nanoclusters with hydrophilic binding ligands act as water-soluble homogeneous catalysts. The as-synthesized $\text{Au}_{18}(\text{MPA})_{14}$ and $\text{Au}_{25}(\text{MPA})_{18}$ nanoclusters showed superior catalytic effects compared to that of gold nanoparticles of 10-20 nm sizes.

Au₁₈(MPA)₁₄ and Au₂₅(MPA)₁₈ Nanoclusters as Raman Substrates: pH-Mediated Tuning of Raman Scattering Properties of MPA

7.1 Introduction

Surface-enhanced Raman scattering (SERS) is a well-established and highly sensitive analytical technique which can provide valuable information about the molecular structure, conformation and molecular interactions.^[173-178] In recent years, surface-enhanced Raman scattering spectroscopy (SERS) has gained tremendous attention because of its widespread applications in various analytical techniques.^[179-183] Noble metal nanoparticles (particularly gold and silver nanoparticles) of different sizes and shapes already being used as an excellent Raman supporting materials for SERS because of their unique localized electromagnetic field enhancement.^[184,185] Significant progress has been made in the synthesis of metal nanoparticle systems of desired size, shape and composition in order to achieve the effective SERS signals of the analyte molecules.^[186]

Recent reports have demonstrated that, in addition to the nanoparticle systems, nanoclusters of silver and gold also act as efficient substrates for Raman signal enhancements.^[187,188] Several theoretical and computational studies involving gold and silver nanoclusters predicted moderate to high Raman signal enhancements of analyte molecules.^[75,189] Chakraborty et al. used Ag₁₅₂ cluster for the Raman enhancement of Rhodamine 6G (R6G), crystal violet (CV), and adenine. The cluster showed strong enhancement of the order of 10⁹.^[190]

G.C. Schatz and co-workers reported detailed time-dependent density functional theory (TDDFT) studies on Raman enhancement of Pyridine and Pyrazine molecules by using Ag₂₀ nanoclusters.^[191,192] The same group systematically applied the time-dependent density functional theory (TDDFT) in order to understand the^[193] size dependence of Raman

enhancement of pyridine molecule adsorbed on silver clusters, Ag_n ($n = 2-8, 20$). There have been several other TDDFT studies on the Raman enhancement of pyrazine and pyridine molecules on different silver and gold nanoclusters.^[193,194] Most of the previous theoretical studies (DFT, TDDFT) were focused on the SERS of silver nanoclusters, very limited reports were available on SERS of gold nanoclusters. Aikens et al. studied the absorption and surface-enhanced Raman scattering of pyridine molecule by using Au_{20} nanocluster system and reported nearly 10^2 - 10^4 fold Raman enhancement.^[195] Researchers reported that gold caged clusters such as M@Au_{12} ($\text{M} = \text{V}^-, \text{Nb}^-, \text{Ta}^-, \text{Cr}, \text{Mo}, \text{W}, \text{Mn}^+, \text{Tc}^+, \text{and Re}^+$) and bimetallic gold nanoclusters such as Au_5Ag_5 , Au-Ag also act as efficient Raman substrates for various probe molecules.^[189,196-198] Tlahuice et al. have calculated the IR and Raman spectra of thiolate-protected gold clusters with 4,12,18,19,25 Au atoms by using DFT calculations.^[199] Varnholt et al. systematically studied the Raman spectra of gold nanoclusters with different sizes and capping ligands to understand the effect of cluster size and capping ligand on the binding of Au-S bond.^[200] In this Chapter, we demonstrate how the Raman scattering property of the capping ligand, MPA, of $\text{Au}_{18}(\text{MPA})_{14}$ and $\text{Au}_{25}(\text{MPA})_{18}$ nanoclusters can be tailored by varying the pH of the cluster solutions.

7.2 Materials and Methods

$\text{Au}_{18}(\text{MPA})_{14}$ and $\text{Au}_{25}(\text{MPA})_{18}$ cluster solutions, 1M NaOH (aq. Solution), 0.1M HCl solution and Millipore water (18.2 Mega Ohm resistance) were used. Synthesis of $\text{Au}_{18}(\text{MPA})_{14}$, $\text{Au}_{25}(\text{MPA})_{18}$ clusters are given in Chapters 2 and 3. The pH of $\text{Au}_{18}(\text{MPA})_{14}$ and $\text{Au}_{25}(\text{MPA})_{18}$ cluster solutions after the synthesis was 8.6 and 9.40 respectively. The pH of the cluster solutions was modulated by using 1M NaOH and 1M HCl solutions.

EZ Raman-N EM Wave Optronics spectrometer was used to study the Raman enhancements, the UV-Visible spectrophotometer was employed to monitor absorption spectra of clusters at different pH conditions.

7.3 Results and Discussion

We have taken the $\text{Au}_{25}(\text{MPA})_{18}$ and $\text{Au}_{18}(\text{MPA})_{14}$ nanoclusters (NCs) as model systems in order to study the Raman enhancement of MPA capping ligand by using Au NCs as Raman substrates. **Figure 7.1** shows that the characteristic Raman signal intensity of the MPA ligand in $\text{Au}_{25}(\text{MPA})_{18}$ original cluster is very small. MPA ligand interacts with the gold core through sulfur atom (Au–S) which was evidenced by the FT-IR studies. Thiol group (–SH) of MPA molecule gives its characteristic vibrational peak at 2575 cm^{-1} , which was absent in Au-MPA clusters. The disappearance of –S–H vibrational peak (at $\sim 2575\text{ cm}^{-1}$) confirms the formation of Au–S bond.^[201]

Upon the pH variation of the cluster solution, it was observed that the Raman spectra of the cluster bound MPA are highly sensitive to the pH of the cluster medium. For example, comparison of the Raman spectra of the free MPA and MPA bound to Au_{25} clusters (**Figure 7.1**) shows that there is a significant increase in the Raman intensities of certain vibrational modes of MPA molecule with the decrease in the pH of the medium. The detailed Raman peak assignment and their intensity enhancements are given in **Table 7.1**. The vibrational peaks for the MPA molecule were assigned mainly based on the literature values.^[201] We focused on a few important vibrational modes such as Au–S–C stretching mode ($\sim 220\text{ cm}^{-1}$), Au–S breathing mode ($\sim 270\text{ cm}^{-1}$), in-plane bending C–S–H ($\sim 890\text{ cm}^{-1}$), C–S stretching mode ($\sim 760\text{ cm}^{-1}$), O–C–O rocking mode ($\sim 476\text{ cm}^{-1}$), –CH₂ wagging modes ($\sim 1250\text{ cm}^{-1}$, $\sim 1320\text{ cm}^{-1}$), in-plane bending of –CH₂ ($\sim 1430\text{ cm}^{-1}$), and C=O stretching mode ($\sim 1710\text{ cm}^{-1}$).

The Au–S breathing ($\sim 270\text{ cm}^{-1}$) and Au–S–C stretching ($\sim 220\text{ cm}^{-1}$) modes were significantly enhanced when the pH of the medium decreased to 5. The appearance of the 220 and 270 cm^{-1} vibrational peaks suggest that the MPA ligand binds to the cluster through sulfur (Au–S bonding). This was corroborated by our FT-IR and XPS studies. In acidic medium, symmetric stretching of C–S ($\sim 760\text{ cm}^{-1}$) and in-plane bending of C–S–H ($\sim 890\text{ cm}^{-1}$) vibrations were enhanced up to ~ 50 and ~ 90 times respectively with respect to that of the original cluster solution. Nearly 35 and 25 folds of enhancements were observed for the CH₂ wagging and

bending modes respectively. The carbonyl stretching (CO) peak of MPA has enhanced ~130 folds at pH 5.

Table 7.1 SERS peak and corresponding Raman intensity of MPA bound $\text{Au}_{25}(\text{MPA})_{18}$ clusters at different pH values

| Vibrational modes | Wavenumbers (cm ⁻¹) | MPA | Original $\text{Au}_{25}(\text{MPA})_{18}$ cluster(pH 9.40) | pH-5 | pH-6 | pH-7 | pH-8 | pH-12 |
|---------------------|---------------------------------|--------|---|------|------|------|------|-------|
| Au-S breathing | ~ 220 cm ⁻¹ | - | 42 | 140 | 112 | 63 | 33 | 12 |
| Au-S-C bending | ~ 270 cm ⁻¹ | - | 22 | 192 | 128 | 75 | 30 | 2 |
| CS stretching (sym) | ~ 760 cm ⁻¹ | 35 | 51 | 580 | 465 | 140 | 135 | 23 |
| -SH inplane bending | ~ 890cm ⁻¹ | 72 | 94 | 2090 | 1470 | 540 | 335 | 31 |
| CO stretching | ~ 1710 cm ⁻¹ | 14 | 120 | 1860 | 1400 | 520 | 330 | 145 |
| CH2 wagging | ~ 1250, 1320 cm ⁻¹ | 25, 35 | 120 | 2400 | 1400 | 660 | 380 | 79 |
| CH2 inplane bending | ~ 1430 cm ⁻¹ | 14 | 55 | 1250 | 865 | 363 | 202 | 47 |
| OCO rocking | ~ 476 cm ⁻¹ | 40 | 75 | 645 | 410 | 168 | 130 | 45 |

We have observed the similar Raman enhancements in the case of $\text{Au}_{18}(\text{MPA})_{14}$ cluster also. However, in spite of the same MPA concentration, higher Raman enhancement was observed in the case of Au_{25} clusters under the same pH conditions.

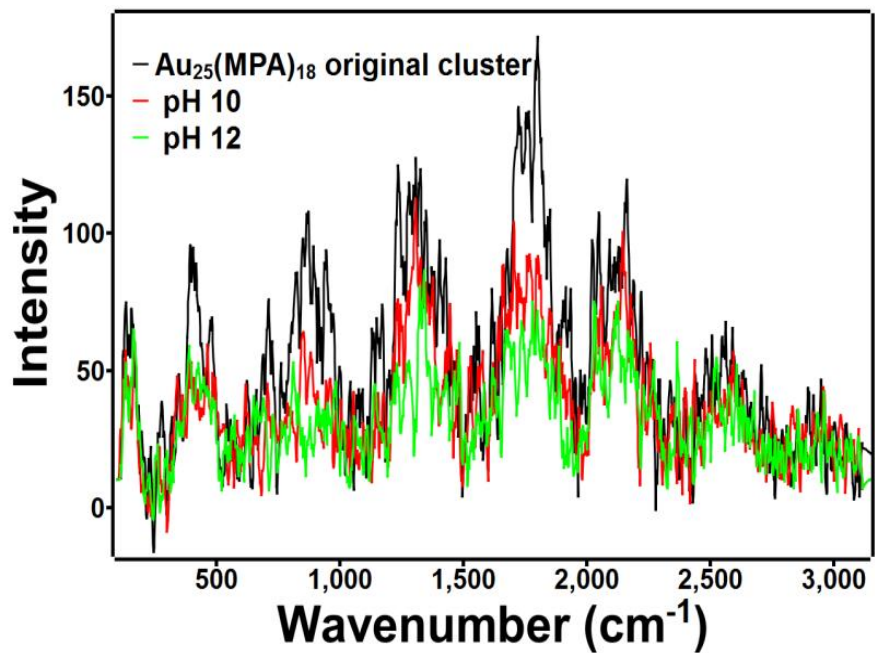


Figure 7.1 SERS spectra of $\text{Au}_{25}(\text{MPA})_{18}$ nanocluster in basic media

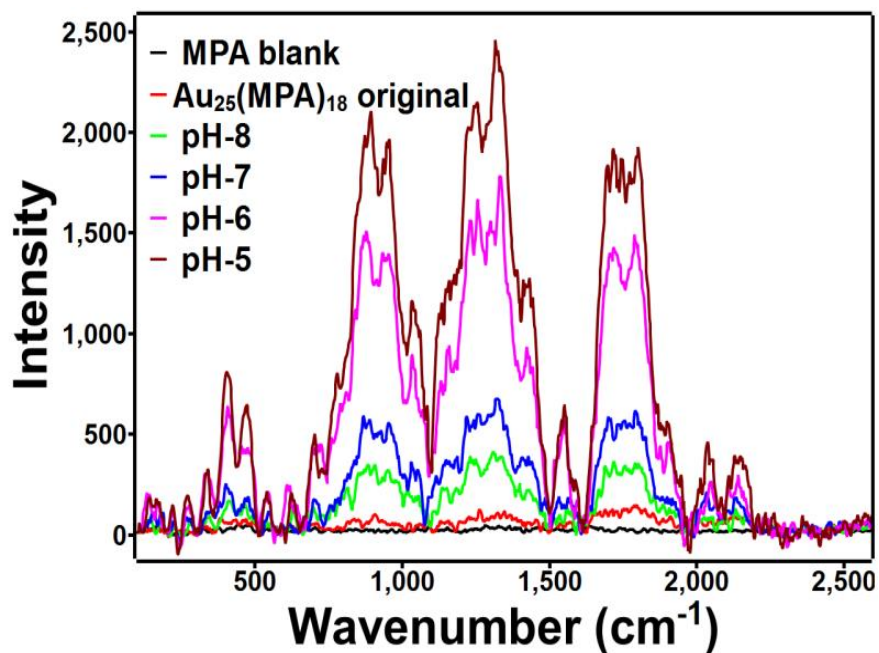


Figure 7.2 SERS spectra of $\text{Au}_{25}(\text{MPA})_{18}$ NCs in acidic media

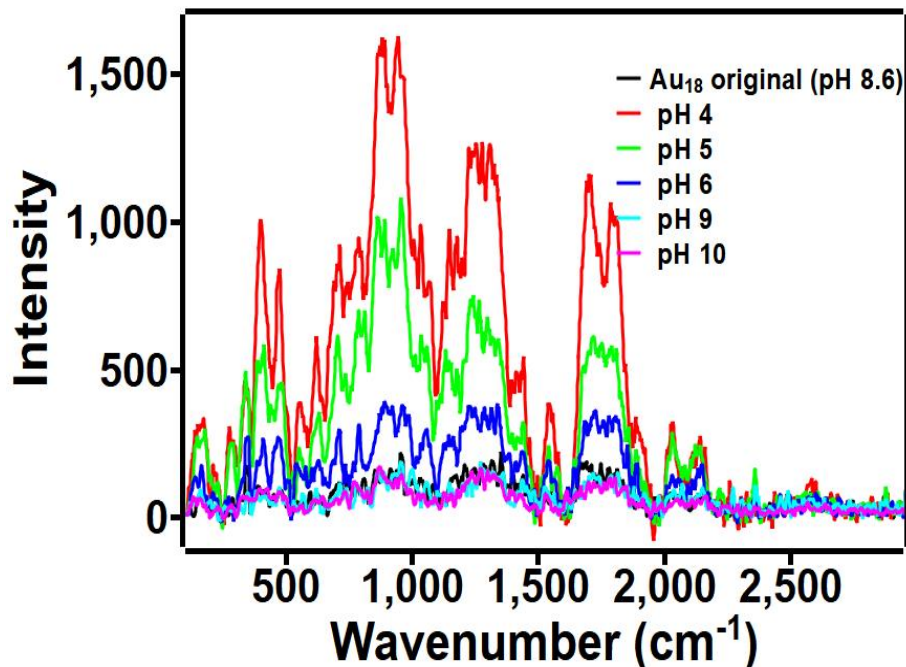


Figure 7.3 Raman spectra of $\text{Au}_{18}(\text{MPA})_{14}$ under acidic and basic pH conditions

It's generally believed that SERS signals are enhanced by two mechanisms: chemical and electromagnetic enhancement mechanisms. Chemical enhancement is attributed to the change in the polarizability owing to the charge-transfer (CT) between the substrate cluster and probe molecule. On the other hand, the electromagnetic enhancement (EM) owes its origin to the enhanced local electromagnetic field caused by the intra-metallic excitation.^[198] The clusters are too small to exhibit the plasmon effect such as local field enhancement. Moreover, no plasmonic particle features were observed in the UV-vis spectra in acidic pH which ruled out the formation of nanoparticles. Therefore, we believe that the Raman enhancement in the cases of such ultra-small clusters occurred via the chemical enhancement mechanism. However, the total change in the polarizability of the system depends on various factors such as molecule-cluster interactions, the charge transfer from the molecule to the metal cluster, and the orientation of the molecule with respect to the substrate.^[75]

In our cases, the Raman enhancement depends on the pH of the medium. We speculate that pH-dependent aggregation of the clusters in acidic medium might bring two or more clusters closer to each other thereby enhancing the Raman signal as was predicted by a theoretical study by Schatz and coworkers.^[191] Theoretical calculations showed that a pyrazine molecule bridging two Ag₂₀ clusters showed very high Raman enhancement (nearly 10⁵ folds). However, the relative orientation of the ligand molecule, interactions between the ligand molecules as well as the ligand and the cluster have also been reported to strongly influence the Raman signal intensities of the ligand molecules.

In order to better understand these factors, we collaborated on a Density Functional Theory (DFT) based study on the pH-dependent Raman spectra of Au₃ clusters capped with MPA. The interaction energy (E_{int}) calculated based on zero point corrected electronic energy (E_z) of dimer Au₃-MPA-Con1 and dimer Au₃-MPA-Con2 (Con1, con2 are conformations 1 and 2 respectively) were -29.9 and -18.5 kcal/mol respectively (**Figure 7.4**). In terms of free energy, the Con1 is lower by 6.1 kcal/mol compared to Con2. This indicates that a dimer system bridged by the interaction of MPA carbonyl oxygen of one cluster with the neighboring gold cluster is more stable compared to the dimer formed by the ligand to ligand interaction through carboxylic groups. Both the conformations show similar trends in acidic and basic conditions (**Figures 7.5 and 7.6**). While the interaction energies of con1 and 2 of the acidic dimer are -46.5 and -3.8 kcal/mol respectively, the energies for con1 and con2 of basic dimers are -120.9 and -60.4 kcal/mol. Further discussion is carried out only on conformations 1 of acidic and basic dimers.

Optimized dimer geometries of neutral, acidic and basic conditions **shown in Figures 7.4 to 7.6** are C₂ symmetric. Compared to the basic structure, the gold clusters aggregated largely in an acidic environment (**Figures 7.5 and 7.6**). This agrees with experimental observation. The Au-S bond length in acidic and basic structures was 2.6 Å and 2.4 Å respectively. The larger Au-S bond lengths in acidic structure compared to that of basic geometry indicates that possibility of gold cluster aggregation in the realistic acidic environment.

The calculated static polarizability of neutral, acidic and basic dimers of Au₃-MPA (all are Con1) were 381.95, 418.72 and 371.52 a.u. respectively. The larger polarizability of acidic structure compared to its counterparts indicates that change in charge distribution of acidic dimer when it interacts with the external electric field is greater than that of other two dimers. The larger change in the distribution of charge leads to a greater induced moment. We ponder over the vibrational modes that cause for larger molecular polarization of the acidic structure in the following discussion.

The interaction of light (or external electric field) with the molecule may lead to either non-resonance (normal) or resonance Raman scattering. In normal condition, the molecular vibration that leads to induced dipole moment is characterized as totally symmetric and non-totally symmetric based on depolarization ratio (ρ). Comparison of Raman spectra along with depolarization ratio on acidic and basic structures for all the modes of vibrations is shown in **Figure 7.7** and data of a few modes are shown in **Table 7.2**. From **Figure 7.7**, we notice that the number of modes of depolarization ratio greater than 0.7 is more in acidic dimer compared to that of basic dimer except in the frequency range 500-1000 cm⁻¹. In the range, 1500 - 2500 cm⁻¹, only the acidic structure shows intense spectral line at 2500 cm⁻¹ with Raman intensity of 173.9 a.u. The spectral peak is assigned to S-H stretching, which is absent in basic structure.

Experimentally observed enhanced Raman intensity of acidic structure compared to the basic structure is agreed with theoretical Raman spectra for a few modes of vibrations, namely ν_1 and ν_2 , in the frequency range of 500-1000 cm⁻¹ (**Table 7.2**). This is due to smaller depolarization ratios of the modes in acidic structure ($\rho = 0.3706$, and 0.2791) compared to that in basic structure ($\rho = 0.7446$). The mode, ν_3 is absent in basic structure. The modes ν_4 and ν_4' are not comparable between the structures as the former couples SH rocking with CCC symmetric stretching whereas the latter is only CCC symmetric stretching. The Raman intensity of modes ν_5 and ν_6 are greater in basic structure as their depolarization ratios are smaller than that of an acidic structure. The mode ν_7 is specific to the basic structure. Other modes ν_8 - ν_{10} can be seen only in acidic medium. Even though the depolarization ratio of mode, ν_{10} , is above 0.7, it shows large Raman intensity due to the electronic coupling of OH group with the gold

cluster. The coupling leads to charge transfer and can be considered as chemical enhancement of the mode. Out of all the 10 modes shown in the **Table 7.2** only 4 modes are common ν_1 , ν_2 , ν_5 , ν_6 to both the structures. While the first two are intense spectral lines in acidic structure, the last two are intense in basic structure. Five modes, ν_3 , ν_4 , ν_8 - ν_{10} are specific to acidic structure and show significant peaks in the spectra. The ν_7 is seen only in basic structure. Overall, data indicates greater polarizability of acidic structure compared to that of its basic counterpart is due to significant Raman activity of S-H and O-H stretchings, which are absent in basic structure. The theoretical study indicates that the acidic and basic structures of Au₃-MPA are different and number of modes that show intense Raman activity increases as medium changes from basic to acidic nature. This may be the reason why the intensity of Raman spectral lines increased in the acidic medium compared to that observed in basic medium.

Table 7.2 Modes of vibrations, wavenumbers, Raman intensities and depolarization ratios of dimer Au₃-MPA, con1 optimized at B3LYP/6-31++G U LANL2DZ level of theory in the gas phase. Here, ω : wavenumber, R.I.: Raman Intensity, ρ : Depolarization ratio.

| Symbol | Mode of vibration | Dimer Au ₃ -MPA, con1 | | | | | |
|--------|---|----------------------------------|----------------------------|------------------|---|-------------|--------|
| | | Acidic | | | Basic | | |
| | | ω cm ⁻¹ | R.I. (a.u.) | ρ | ω cm ⁻¹ | R.I. (a.u.) | P |
| v1 | C-C-C-O torsion | 540.9 571.5 | 41.1 45.8 | 0.3706 0.2791 | 546.8 | 9.2 | 0.7446 |
| v2 | C-S stretching | 599.1 597.6 | 21.1 17.5 | 0.1818 0.2405 | 640.7 641.5 | 14.8 0.0 | 0.3137 |
| v3 | O-H & S-H rocking | 789.6 827.6 | 57.3 52.5 | 0.3541 0.3715 | - | - | - |
| v4 | S-H rocking + C-C-C sym. Stretching | 840.8 843.6 | 12.7 7.6 | 0.2313 0.4687 | 847.4 (v4': C-C-C sym. Stretching | 29.4 | 0.1700 |
| v5 | C-C-C out of plane bending | 956.1 | 7.1 | 0.5812 | 942.9 | 38.9 | 0.3935 |
| v6 | H-C-H in plane bending | 1495.7 1511.5 | 24.8 17.3 | 0.6136 0.6352 | 1505.4 | 27.5 | 0.5749 |
| v7 | O=C=O ⁻ symmetric stretching | - | - | - | 1542.1 | 78.3 | 0.4345 |
| v8 | C=O stretching | 1658.8 1638.0 | 41.6 32.1 | 0.1558 0.3041 | - | - | - |
| v9 | S-H stretching | 2500.2 2497.4 | 173.9 145.2 | 0.2130 0.1597 | - | - | - |
| v10 | O-H Stretching | 2954.53 | 548.6 | 0.7189 | - | - | - |

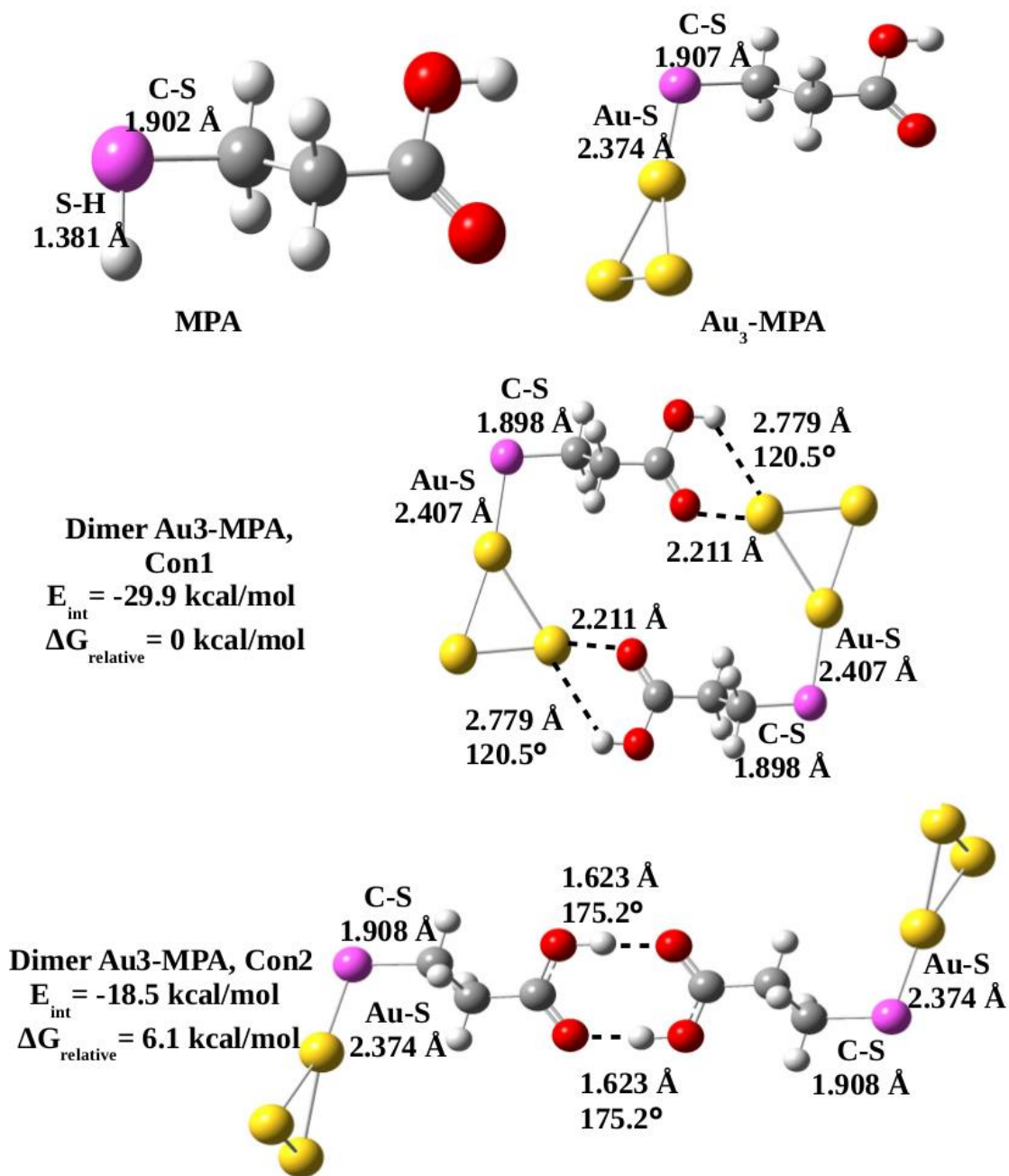


Figure 7.4 Geometries of mercaptopropionic acid (MPA), Au₃ tagged MPA (Au₃-MPA), and dimers of Au₃-MPA (Dimer Au₃-MPA) optimized at B3LYP/6-31++G U LANL2DZ level of theory in the gas phase. Here, Con1 and con2 stand for conformation 1 and conformation 2 respectively. (Color labels: yellow = Au, pink = S, red = Oxygen, grey = Carbon and white = Hydrogen)

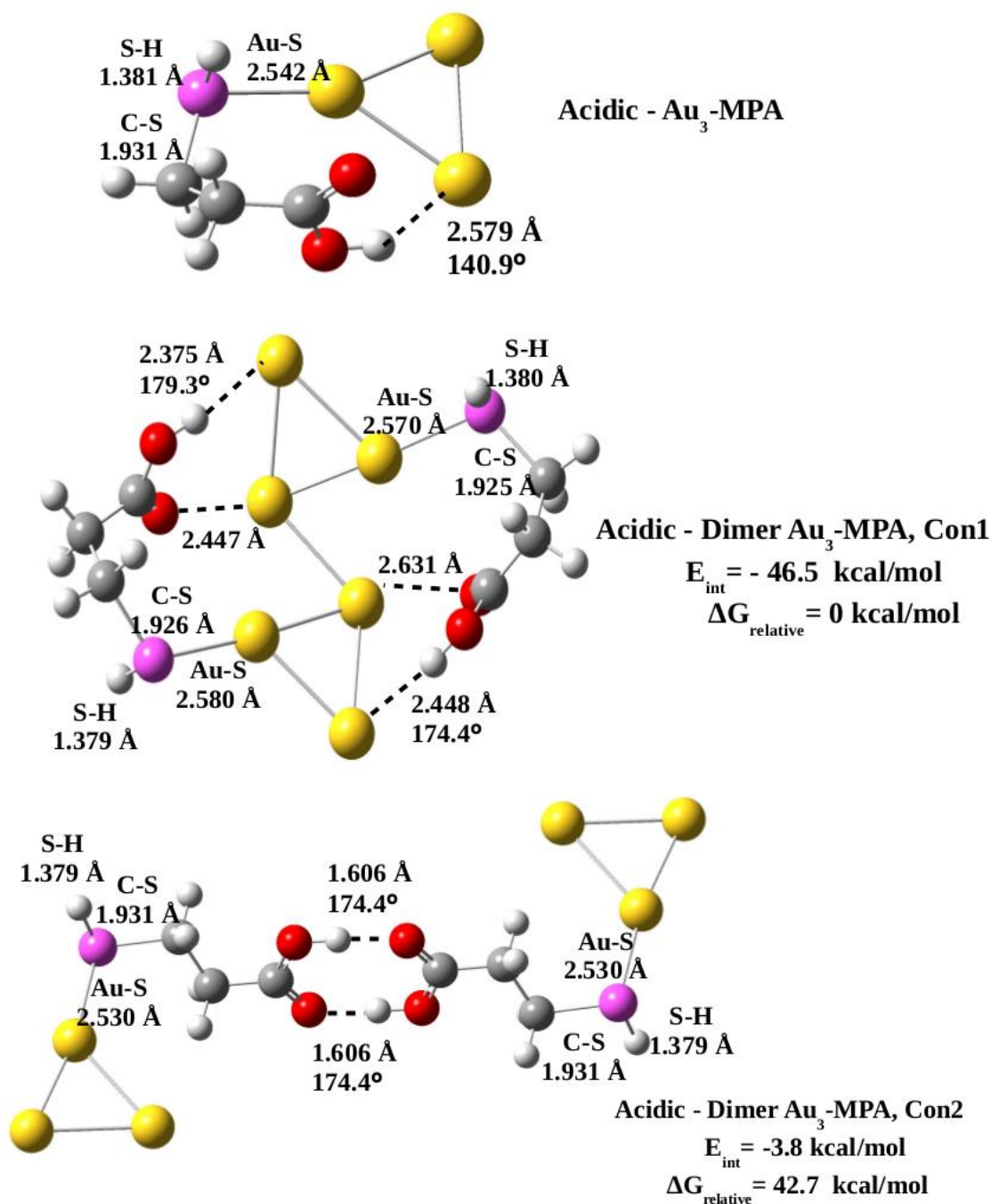


Figure 7.5 Geometries of Au₃ tagged MPA (acidic-Au₃-MPA), and dimers of Au₃-MPA (Acidic - Dimer Au₃-MPA) optimized at B3LYP/6-31++G U LANL2DZ level of theory in the gas phase. Here, Con1 and con2 stand for conformation 1 and conformation 2 respectively. (Color labels: yellow = Au, pink = S, red = Oxygen, grey = Carbon and white = Hydrogen)

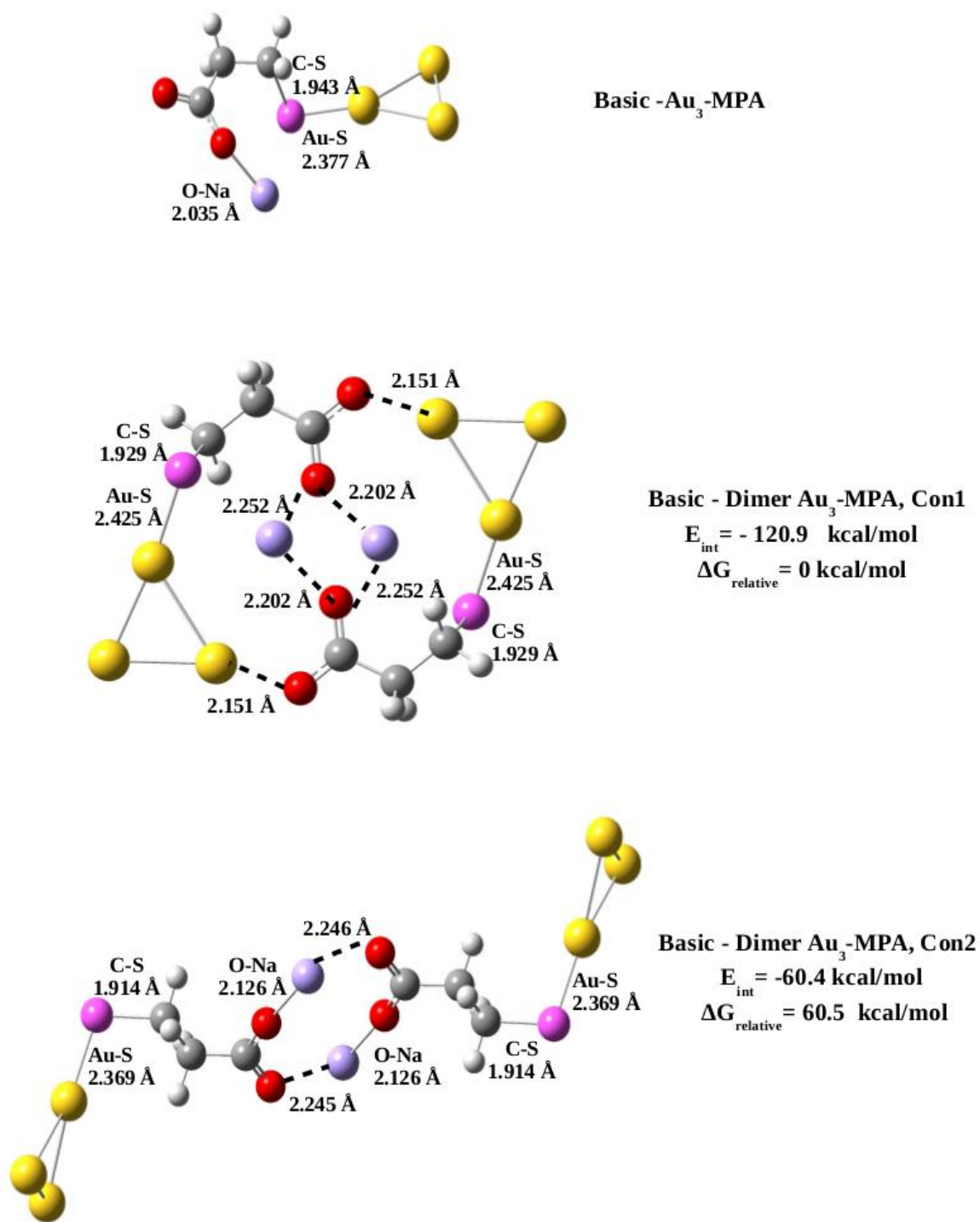


Figure 7.6 Geometries of Au₃ tagged MPA (basic-Au₃-MPA), and dimers of Au₃-MPA (Basic - Dimer Au₃-MPA) optimized at B3LYP/6-31++G U LANL2DZ level of theory in the gas phase. Here, Con1 and con2 stand for conformation 1 and conformation 2 respectively. (Color labels: yellow = Au, pink = S, red = Oxygen, grey = Carbon and white = Hydrogen)

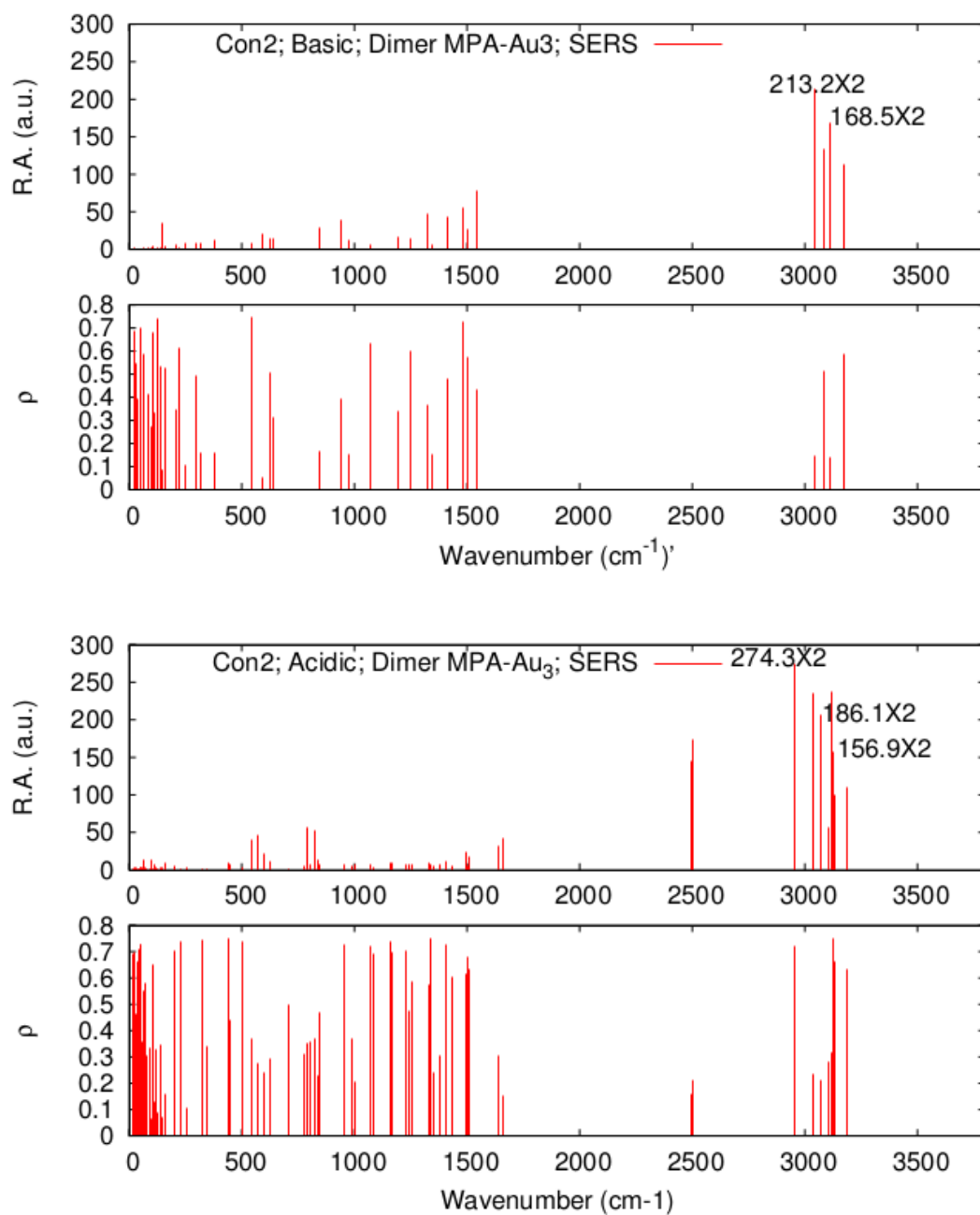


Figure 7.7 Depolarization ratios and corresponding Raman spectrum of acidic (below) and basic (above) dimers of Au₃-MPA

7.4 Conclusions

We have chosen $\text{Au}_{18}(\text{MPA})_{14}$ and $\text{Au}_{25}(\text{MPA})_{18}$ cluster systems as the Raman substrates. We demonstrated that as-synthesized clusters were poor Raman substrates. The Au NCs become excellent Raman substrates under acidic pH conditions. This demonstrates that the pH of the medium could be an important factor in modulating the Raman intensity of the Raman probes. The Raman enhancements are attributed to the chemical interactions and/or charge transfer between the MPA ligand and Au cluster core. The work shows also how the thiol interactions with the clusters change with varying pH of the media.

We attempted to provide a theoretical justification to the experimentally seen enhanced Raman spectra. Raman spectra of both structures are studied for a few modes of vibrations along with their depolarization ratios. At lower frequency end, particularly in 500-1000 cm^{-1} region, a few spectral lines, ν_1 and ν_2 show larger intensity in acidic structure compared to its basic counterpart, which is a partial agreement with experimental observation. Five modes, ν_3 , ν_4 , and ν_8 - ν_{10} , are specific to acidic structure and show significant peaks in the spectra. The theoretical study indicates that a number of modes that show intense Raman activity increases as medium changes from basic to acidic nature. This may be the reason why the intensity of Raman spectral lines increased in the acidic medium compared to that observed in basic medium.

Summary and General Conclusions

Ultra-small, metal nanoclusters considered to be a prolific area of research due to their unique physical and chemical properties. Properties of the nanoclusters depend on their size, geometry, and capping ligands. Synthesis of atomically precise nanoclusters is therefore of paramount importance in order to explore their properties and applications. The synthesis, characterization, and molecular formula determination of metal nanoclusters continue to be a challenging task and there are no well-established guiding principles available to prepare the nanoclusters of definite size/molecular formula.

Developing a toolbox that will help in the rational design of size-selective synthesis as well as tuning of the properties of the nanoclusters will be of immense importance. Among all other synthetic routes, “size focusing” route is the well demonstrated and relatively easier for the synthesis of definitely sized nanoclusters. Size focusing methodology works in two steps. In the first step, the formation of polydispersed nanoclusters takes place and the second step involves with the conversion of poly-dispersed clusters into monodispersed clusters by using thermal or ligand etching processes. Thermal and ligand etching based size focusing methods require high temperatures and excess thiols with prolonged reaction times. Hence, it is necessary to explore the alternate synthesis protocols which can produce the atomically precise metal nanoclusters in high yields under ambient conditions. The dissertation work focused on the synthesis of water-soluble atomically precise gold nanoclusters such as $\text{Au}_{18}(\text{MPA})_{14}$ and $\text{Au}_{25}(\text{MPA})_{18}$ by using hydrophilic binding ligand, MPA, and a strong and conventional reducing agent NaBH_4 under ambient conditions. The methods of synthesis were straightforward and do not require any special reaction conditions such as pH, temperature control or prolonged reaction times. The reported synthesis methods are effective, highly convenient, easy to handle and economically viable prepare the atomically precise gold nanoclusters in high yields under ambient conditions.

We demonstrated that the relative quantities of capping agent to the gold precursor ([thiol/Au] ratio) and the gold precursor to reducing agent ([Au]/[NaBH₄] ratio) played decisive roles in obtaining size-focused atomically precise gold nanoclusters. It was observed that the systematic tuning of these ratios may result in different atomically precise gold nanoclusters. The formation, composition, and purity of the product clusters were confirmed by using polyacrylamide gel electrophoresis (PAGE), UV-visible and FTIR spectroscopies, transmission electron microscopy (TEM), energy dispersive X-ray analysis (EDAX), thermogravimetric analysis (TGA), X-ray photoelectron spectroscopy (XPS) and matrix-assisted laser desorption ionization-time of flight mass spectrometry (MALDI-TOF MS).

Surface capping ligands play a decisive role in the size determination and tuning of the properties of definitely sized gold nanoclusters. Capping ligands also play dominant roles in determining the stability, photoluminescence and catalytic properties of NCs. We have chosen a bifunctional capping ligand, MPA, in our synthesis. This allowed us to tune/tailor the nanocluster stability as well as the properties such as photoluminescence, Raman scattering, and catalytic activity over a wide range in aqueous media simply via the variation of the pH of the media. It was demonstrated that the stability of the clusters can be systematically improved by increasing the pH of the cluster media. When the pH value increases, the carboxylic (–COOH) groups on the cluster surface are dissociated forming negatively charged carboxylate anion species. The strong electrostatic repulsive forces exerted between the cluster species in basic medium play a crucial role in enhancing the stability of the clusters in basic medium. On the other hand, the stability of the cluster gradually decreases in acidic pH.

We observed that the photoluminescence property of the clusters could be modulated by changing the pH of the cluster. Fluorescence intensity of the cluster systems significantly increased with decreasing the pH of the media. At lower pH, the majority of the –COOH groups and almost all thiol groups remain protonated. As a result, the neutral species both the precursor complex molecules and Au₁₈(MPA)₁₄ clusters can form aggregates and show pH-dependent aggregation-induced emission. When the pH value increases, the carboxylic (and, maybe, –SH) groups are dissociated forming negatively charged carboxylate (and thiolate)

species. The deprotonation and the electrostatic repulsive force suppress the aggregation process. This explains the decrease in emission intensity at two shorter wavelengths with the increase in pH of the medium. However, the weak emission at $\lambda_{em} = \sim 800$ nm that increases in intensity with the pH increase could be ascribed to the free cluster fluorescence.

Ligand plays a decisive role in influencing the catalytic activity. Clusters with small capping ligands pose less steric hindrance facilitating the better accessibility of the reactant molecules onto the catalyst surface compared to the bulky capping ligands. We explored the catalytic properties of water-soluble clusters, $Au_{18}(MPA)_{14}$ and $Au_{25}(MPA)_{18}$, by using the reduction of nitroanilines by $NaBH_4$ in aqueous media. Gold nanoclusters with hydrophilic binding ligands can act as water-soluble homogeneous catalysts. It was observed that water-soluble ultra-small gold nanoclusters, $Au_{18}(MPA)_{14}$ and $Au_{25}(MPA)_{18}$, showed superior catalytic effects compared to that of gold nanoparticles of 10-20 nm size. This could be due to the presence of a larger number of active sites in the nanocluster systems compared nanoparticles.

Metal nanoclusters with molecule-like definite compositions and structures can act as reproducible nanoscale Raman substrates. We explored the $Au_{18}(MPA)_{14}$ and $Au_{25}(MPA)_{18}$ cluster systems as the Raman substrates and demonstrated how the Raman scattering property of the capping ligand, MPA, on $Au_{18}(MPA)_{14}$ and $Au_{25}(MPA)_{18}$ nanoclusters can be tailored by varying the pH of the cluster solutions. It was observed that the Raman spectra of the cluster bound MPA are highly sensitive to the pH of the cluster medium. A comparison of the Raman spectra of the free MPA with MPA bound to Au-25 clusters shows that there is a significant increase in the Raman intensities of certain vibrational modes of MPA molecule with the decrease in the pH of the medium (from pH 9.4 to 5.0). On the other hand, the Raman intensity of most of these vibrational modes of MPA decreased when pH of the cluster was increased to the basic region. The aggregation of the clusters in the acidic medium could give rise to the Raman signal enhancement of some of the vibrational modes of MPA. The Raman enhancements could be attributed to the chemical interactions and/or charge transfer between the MPA ligand and Au cluster core. A computational work involving a simple system MPA

protected Au₃ cluster system supported the aggregation-mediated polarizability change and Raman signal enhancements.

References

- [1] E. Roduner, *Chem. Soc. Rev.* **2006**, *35*, 583.
- [2] H. Tsunoyama, H. Sakurai, Y. Negishi, T. Tsukuda, *J. Am. Chem. Soc.* **2005**, *127*, 9374.
- [3] J. Xie, Y. Zheng, J. Y. Ying, *J. Am. Chem. Soc.* **2009**, *131*, 888.
- [4] H. Tsunoyama, Y. Liu, T. Akita, N. Ichikuni, H. Sakurai, S. Xie, T. Tsukuda, *Catal Surv Asia* **2011**, *15*, 230.
- [5] A. Mathew, T. Pradeep, *Part. Part. Syst. Charact.* **2014**, *31*, 1017.
- [6] L.-Y. Chen, C.-W. Wang, Z. Yuan, H.-T. Chang, *Anal. Chem.* **2015**, *87*, 216.
- [7] C. Y. Tay, Y. Yu, M. I. Setyawati, J. Xie, D. T. Leong, *Nano Research* **2014**, *7*, 805.
- [8] K. Zheng, M. I. Setyawati, T.-P. Lim, D. T. Leong, J. Xie, *ACS Nano* **2016**, *10*, 7934.
- [9] K. Zheng, M. I. Setyawati, D. T. Leong, J. Xie, *ACS Nano* **2017**, *11*, 6904.
- [10] M. Brust, M. Walker, D. Bethell, D. J. Schiffrin, R. Whyman, *Journal of the Chemical Society, Chemical Communications* **1994**, *0*, 801.
- [11] T. Dainese, S. Antonello, J. A. Gascón, F. Pan, N. V. Perera, M. Ruzzi, A. Venzo, A. Zoleo, K. Rissanen, F. Maran, *ACS Nano* **2014**, *8*, 3904.
- [12] W. W. Weare, S. M. Reed, M. G. Warner, J. E. Hutchison, *J. Am. Chem. Soc.* **2000**, *122*, 12890.
- [13] Y. Shichibu, Y. Negishi, T. Tsukuda, T. Teranishi, *J. Am. Chem. Soc.* **2005**, *127*, 13464.
- [14] H. Tsunoyama, T. Tsukuda, *J. Am. Chem. Soc.* **2009**, *131*, 18216.
- [15] Y. Zhang, Q. Hu, M. C. Paau, S. Xie, P. Gao, W. Chan, M. M. F. Choi, *J. Phys. Chem. C* **2013**, *117*, 18697.
- [16] M. J. Hostetler, S. J. Green, J. J. Stokes, R. W. Murray, *J. Am. Chem. Soc.* **1996**, *118*, 4212.
- [17] M. J. Hostetler, J. E. Wingate, C. J. Zhong, J. E. Harris, R. W. Vachet, M. R. Clark, J. D. Londono, S. J. Green, J. J. Stokes, G. D. Wignall, G. L. Glish, M. D. Porter, N. D. Evans, R. W.

Murray, *Langmuir : the ACS journal of surfaces and colloids*, *Langmuir : the ACS journal of surfaces and colloids.*, *Langmuir®: The ACS Journal of Surfaces and Colloids* **1998**, *14*, 17.

- [18] S. Chen, R. W. Murray, *Langmuir* **1999**, *15*, 682.
- [19] C. J. Ackerson, P. D. Jadzinsky, R. D. Kornberg, *J. Am. Chem. Soc.* **2005**, *127*, 6550.
- [20] C. L. Cleveland, U. Landman, T. G. Schaaff, M. N. Shafigullin, P. W. Stephens, R. L. Whetten, *Phys. Rev. Lett.* **1997**, *79*, 1873.
- [21] T. G. Schaaff, M. N. Shafigullin, J. T. Khoury, I. Vezmar, R. L. Whetten, W. G. Cullen, P. N. First, C. Gutiérrez-Wing, J. Ascensio, M. J. Jose-Yacamán, *J. Phys. Chem. B* **1997**, *101*, 7885.
- [22] A. Dass, A. Stevenson, G. R. Dubay, J. B. Tracy, R. W. Murray, *J. Am. Chem. Soc.* **2008**, *130*, 5940.
- [23] H. Tsunoyama, P. Nickut, Y. Negishi, K. Al-Shamery, Y. Matsumoto, T. Tsukuda, *J. Phys. Chem. C* **2007**, *111*, 4153.
- [24] Q. Xu, S. Wang, Z. Liu, G. Xu, X. Meng, M. Zhu, *Nanoscale* **2013**, *5*, 1176.
- [25] E. S. Shibu, B. Radha, P. K. Verma, P. Bhyrappa, G. U. Kulkarni, S. K. Pal, T. Pradeep, *ACS Appl. Mater. Interfaces* **2009**, *1*, 2199.
- [26] O. Palacios-Álvarez, A. Tlahuice-Flores, *Phys. Chem. Chem. Phys.* **2017**, *19*, 26545.
- [27] J.-Y. Wang, J. Chen, J. Yang, H. Wang, X. Shen, Y.-M. Sun, M. Guo, X.-D. Zhang, *Int J Nanomedicine* **2016**, *11*, 3475.
- [28] N. Goswami, Q. Yao, Z. Luo, J. Li, T. Chen, J. Xie, *J. Phys. Chem. Lett.* **2016**, *7*, 962.
- [29] A. Fernando, C. M. Aikens, *J. Phys. Chem. C* **2015**, *119*, 20179.
- [30] S. Hossain, W. Kurashige, S. Wakayama, B. Kumar, L. V. Nair, Y. Niihori, Y. Negishi, *J. Phys. Chem. C* **2016**, *120*, 25861.
- [31] C. L. Heinecke, T. W. Ni, S. Malola, V. Mäkinen, O. A. Wong, H. Häkkinen, C. J. Ackerson, *J. Am. Chem. Soc.* **2012**, *134*, 13316.
- [32] A. Mathew, E. Varghese, S. Choudhury, S. K. Pal, T. Pradeep, *Nanoscale* **2015**, *7*, 14305.

- [33] T. Huang, R. W. Murray, *J. Phys. Chem. B* **2001**, *105*, 12498.
- [34] S. Kumar, R. Jin, *Nanoscale* **2012**, *4*, 4222.
- [35] L. G. AbdulHalim, S. Ashraf, K. Katsiev, A. R. Kirmani, N. Kothalawala, D. H. Anjum, S. Abbas, A. Amassian, F. Stellacci, A. Dass, I. Hussain, O. M. Bakr, *J. Mater. Chem. A* **2013**, *1*, 10148.
- [36] N. Kothalawala, J. L. W. Iv, A. Dass, *Nanoscale* **2013**, *6*, 683.
- [37] Y. Yu, X. Chen, Q. Yao, Y. Yu, N. Yan, J. Xie, *Chem. Mater.* **2013**, *25*, 946.
- [38] A. Ghosh, T. Udayabhaskararao, T. Pradeep, *J. Phys. Chem. Lett.* **2012**, *3*, 1997.
- [39] Q. Yao, Y. Yu, X. Yuan, Y. Yu, J. Xie, J. Y. Lee, *Small* **2013**, *9*, 2696.
- [40] X. Yuan, B. Zhang, Z. Luo, Q. Yao, D. T. Leong, N. Yan, J. Xie, *Angew. Chem. Int. Ed.* **2014**, *53*, 4623.
- [41] C. Zeng, R. Jin, in *Gold Clusters, Colloids and Nanoparticles I*, Springer, Cham, **2014**, pp. 87–115.
- [42] Y. Negishi, Y. Takasugi, S. Sato, H. Yao, K. Kimura, T. Tsukuda, *J. Am. Chem. Soc.* **2004**, *126*, 6518.
- [43] Y. Negishi, Y. Takasugi, S. Sato, H. Yao, K. Kimura, T. Tsukuda, *J. Phys. Chem. B* **2006**, *110*, 12218.
- [44] S. Knoppe, J. Boudon, I. Dolamic, A. Dass, T. Bürgi, *Anal. Chem.* **2011**, *83*, 5056.
- [45] Y. Negishi, C. Sakamoto, T. Ohyama, T. Tsukuda, *J. Phys. Chem. Lett.* **2012**, *3*, 1624.
- [46] A. Ghosh, J. Hassinen, P. Pulkkinen, H. Tenhu, R. H. A. Ras, T. Pradeep, *Anal. Chem.* **2014**, *86*, 12185.
- [47] A. Shivhare, L. Wang, R. W. J. Scott, *Langmuir* **2015**, *31*, 1835.
- [48] Y. Negishi, K. Nobusada, T. Tsukuda, *J. Am. Chem. Soc.* **2005**, *127*, 5261.
- [49] Y. Niihori, M. Matsuzaki, C. Uchida, Y. Negishi, *Nanoscale* **2014**, *6*, 7889.
- [50] Y. Niihori, M. Matsuzaki, T. Pradeep, Y. Negishi, *J. Am. Chem. Soc.* **2013**, *135*, 4946.

- [51] Y. Niihori, C. Uchida, W. Kurashige, Y. Negishi, *Phys. Chem. Chem. Phys.* **2016**, *18*, 4251.
- [52] R. Jin, H. Qian, Z. Wu, Y. Zhu, M. Zhu, A. Mohanty, N. Garg, *J. Phys. Chem. Lett.* **2010**, *1*, 2903.
- [53] R. Jin, C. Zeng, M. Zhou, Y. Chen, *Chem. Rev.* **2016**, *116*, 10346.
- [54] M. Zhu, E. Lanni, N. Garg, M. E. Bier, R. Jin, *J. Am. Chem. Soc.* **2008**, *130*, 1138.
- [55] H. Qian, Y. Zhu, R. Jin, *ACS Nano* **2009**, *3*, 3795.
- [56] H. Qian, R. Jin, *Nano Lett.* **2009**, *9*, 4083.
- [57] H. Qian, Y. Zhu, R. Jin, *PNAS* **2012**, *109*, 696.
- [58] Y. Shichibu, Y. Negishi, H. Tsunoyama, M. Kanehara, T. Teranishi, T. Tsukuda, *Small* **2007**, *3*, 835.
- [59] L. Dhanalakshmi, T. Udayabhaskararao, T. Pradeep, *Chem. Commun.* **2011**, *48*, 859.
- [60] T. Shimizu, T. Teranishi, S. Hasegawa, M. Miyake, *J. Phys. Chem. B* **2003**, *107*, 2719.
- [61] Y. Chen, C. Zeng, D. R. Kauffman, R. Jin, *Nano Lett.* **2015**, *15*, 3603.
- [62] M. Rambukwella, A. Dass, *Langmuir* **2017**, *33*, 10958.
- [63] Q. Xu, S. Kumar, S. Jin, H. Qian, M. Zhu, R. Jin, *Small* **2014**, *10*, 1008.
- [64] H. Qian, M. Zhu, U. N. Andersen, R. Jin, *J. Phys. Chem. A* **2009**, *113*, 4281.
- [65] H. Qian, Y. Zhu, R. Jin, *J. Am. Chem. Soc.* **2010**, *132*, 4583.
- [66] H. Qian, R. Jin, *Chem. Commun.* **2011**, *47*, 11462.
- [67] T. G. Schaaff, G. Knight, M. N. Shafigullin, R. F. Borkman, R. L. Whetten, *J. Phys. Chem. B* **1998**, *102*, 10643.
- [68] E. Gross, J. H. Liu, S. Alayoglu, M. A. Marcus, S. C. Fakra, F. D. Toste, G. A. Somorjai, *J. Am. Chem. Soc.* **2013**, *135*, 3881.
- [69] S. Chattoraj, K. Bhattacharyya, *J. Phys. Chem. C* **2014**, *118*, 22339.

- [70] L. Shang, R. M. Dörlich, S. Brandholt, R. Schneider, V. Trouillet, M. Bruns, D. Gerthsen, G. U. Nienhaus, *Nanoscale* **2011**, *3*, 2009.
- [71] M. A. Abbas, T.-Y. Kim, S. U. Lee, Y. S. Kang, J. H. Bang, *J. Am. Chem. Soc.* **2016**, *138*, 390.
- [72] H. Choi, Y.-S. Chen, K. G. Stampelcoskie, P. V. Kamat, *J. Phys. Chem. Lett.* **2015**, *6*, 217.
- [73] R. L. Donkers, D. Lee, R. W. Murray, *Langmuir* **2004**, *20*, 1945.
- [74] R. Jin, *Nanoscale* **2010**, *2*, 343.
- [75] S. Bhardwaj, S. Rai, T. K. Sau, H. Singh, *Vibrational Spectroscopy* **2015**, *76*, 38.
- [76] Y. Zhu, H. Qian, B. A. Drake, R. Jin, *Angewandte Chemie* **2010**, *122*, 1317.
- [77] S. Yamazoe, T. Yoskamtorn, S. Takano, S. Yadnum, J. Limtrakul, T. Tsukuda, *The Chemical Record* **2016**, *16*, 2338.
- [78] N. Goswami, Q. Yao, T. Chen, J. Xie, *Coordination Chemistry Reviews* **2016**, *329*, 1.
- [79] N. Goswami, Z. Luo, X. Yuan, D. T. Leong, J. Xie, *Mater. Horiz.* **2017**, DOI 10.1039/C7MH00451F.
- [80] Z. Luo, X. Yuan, Y. Yu, Q. Zhang, D. T. Leong, J. Y. Lee, J. Xie, *J. Am. Chem. Soc.* **2012**, *134*, 16662.
- [81] X. Su, J. Liu, *ACS Appl. Mater. Interfaces* **2017**, *9*, 3902.
- [82] Y. Negishi, T. Tsukuda, *Chemical Physics Letters* **2004**, *383*, 161.
- [83] H. Tsunoyama, N. Ichikuni, T. Tsukuda, *Langmuir* **2008**, *24*, 11327.
- [84] S. Choi, R. M. Dickson, J. Yu, *Chem. Soc. Rev.* **2012**, *41*, 1867.
- [85] S. Palmal, S. Basiruddin, A. R. Maity, S. C. Ray, N. R. Jana, *Chem. Eur. J.* **2013**, *19*, 943.
- [86] T. G. Schaaff, G. Knight, M. N. Shafigullin, R. F. Borkman, R. L. Whetten, *J. Phys. Chem. B* **1998**, *102*, 10643.
- [87] D. Crasto, A. Dass, *J. Phys. Chem. C* **2013**, *117*, 22094.

- [88] M. Brust, C. J. Kiely, *Colloids and Surfaces A: Physicochemical and Engineering Aspects* **2002**, *202*, 175.
- [89] M. A. H. Muhammed, P. K. Verma, S. K. Pal, R. C. A. Kumar, S. Paul, R. V. Omkumar, T. Pradeep, *Chemistry - A European Journal* **2009**, *15*, 10110.
- [90] M. A. Habeeb Muhammed, S. Ramesh, S. S. Sinha, S. K. Pal, T. Pradeep, *Nano Research* **2008**, *1*, 333.
- [91] Y. Shichibu, Y. Negishi, H. Tsunoyama, M. Kanehara, T. Teranishi, T. Tsukuda, *Small* **2007**, *3*, 835.
- [92] C. Gautier, T. Bürgi, *J. Am. Chem. Soc.* **2006**, *128*, 11079.
- [93] X. Yang, Y. Su, M. C. Paa, M. M. F. Choi, *Anal. Chem.* **2012**, *84*, 1765.
- [94] Z. Wu, J. Chen, R. Jin, *Adv. Funct. Mater.* **2011**, *21*, 177.
- [95] X. Yuan, N. Goswami, I. Mathews, Y. Yu, J. Xie, *Nano Res.* **2015**, *8*, 3488.
- [96] X. Jia, X. Yang, J. Li, D. Li, E. Wang, *Chem. Commun.* **2013**, *50*, 237.
- [97] J. M. Forward, D. Bohmann, J. P. Fackler, R. J. Staples, *Inorg. Chem.* **1995**, *34*, 6330.
- [98] S.-H. Cha, J.-U. Kim, K.-H. Kim, J.-C. Lee, *Chem. Mater.* **2007**, *19*, 6297.
- [99] Y. Yu, X. Chen, Q. Yao, Y. Yu, N. Yan, J. Xie, *Chem. Mater.* **2013**, *25*, 946.
- [100] A. Das, C. Liu, H. Y. Byun, K. Nobusada, S. Zhao, N. Rosi, R. Jin, *Angew. Chem. Int. Ed.* **2015**, *54*, 3140.
- [101] S. Chen, S. Wang, J. Zhong, Y. Song, J. Zhang, H. Sheng, Y. Pei, M. Zhu, *Angew. Chem. Int. Ed.* **2015**, *54*, 3145.
- [102] Y. Yu, Q. Yao, K. Cheng, X. Yuan, Z. Luo, J. Xie, *Part. Part. Syst. Character.* **2014**, *31*, 652.
- [103] M. Wang, W. Niu, X. Wu, L. Li, J. Yang, S. Shuang, C. Dong, *RSC Adv.* **2014**, *4*, 25183.
- [104] B. J. Lindberg, K. Hamrin, G. Johansson, U. Gelius, A. Fahlman, C. Nordling, K. Siegbahn, *Phys. Scr.* **1970**, *1*, 286.
- [105] D. G. Castner, K. Hinds, D. W. Grainger, *Langmuir* **1996**, *12*, 5083.

- [106] M.-C. Bourg, A. Badia, R. B. Lennox, *J. Phys. Chem. B* **2000**, *104*, 6562.
- [107] O. Cavalleri, G. Gonella, S. Terreni, M. Vignolo, P. Pelori, L. Floreano, A. Morgante, M. Canepa, R. Rolandi, *J. Phys.: Condens. Matter* **2004**, *16*, S2477.
- [108] D. R. Mullins, P. F. Lyman, *J. Phys. Chem.* **1993**, *97*, 12008.
- [109] O. Ivashenko, J. T. van Herpt, B. L. Feringa, W. R. Browne, P. Rudolf, *Chemical Physics Letters* **2013**, *559*, 76.
- [110] P. Gobbo, M. C. Biesinger, M. S. Workentin, *Chem. Commun.* **2013**, *49*, 2831.
- [111] P. Gobbo, S. Novoa, M. C. Biesinger, M. S. Workentin, *Chem. Commun.* **2013**, *49*, 3982.
- [112] P. Gobbo, Z. Mossman, A. Nazemi, A. Niaux, M. C. Biesinger, E. R. Gillies, M. S. Workentin, *J. Mater. Chem. B* **2014**, *2*, 1764.
- [113] D. R. Mullins, P. F. Lyman, *J. Phys. Chem.* **1993**, *97*, 9226.
- [114] T. S. Rufael, D. R. Huntley, D. R. Mullins, J. L. Gland, *J. Phys. Chem.* **1995**, *99*, 11472.
- [115] A. Y. Klyushin, T. C. R. Rocha, M. Hävecker, A. Knop-Gericke, R. Schlögl, *Phys. Chem. Chem. Phys.* **2014**, *16*, 7881.
- [116] X. Liang, Z. Wang, C. Liu, *Nanoscale Research Letters* **2009**, *5*, 124.
- [117] M. S. Islam, W. S. Choi, H.-J. Lee, Y. B. Lee, I. C. Jeon, *J. Mater. Chem.* **2012**, *22*, 8215.
- [118] S. Peters, S. Peredkov, M. Neeb, W. Eberhardt, M. Al-Hada, *Surface Science* **2013**, *608*, 129.
- [119] P. H. Citrin, G. K. Wertheim, Y. Baer, *Phys. Rev. B* **1983**, *27*, 3160.
- [120] A. Tanaka, Y. Takeda, M. Imamura, S. Sato, *Phys. Rev. B* **2003**, *68*, 195415.
- [121] V. Yong, H. T. Hahn, *Advances in Nanoparticles* **2013**, *02*, 1.
- [122] K. M. Harkness, D. E. Cliffel, J. A. McLean, *Analyst* **2010**, *135*, 868.
- [123] Y. Liu, H. Tsunoyama, T. Akita, T. Tsukuda, *Chem. Commun.* **2010**, *46*, 550.
- [124] A. Leelavathi, T. U. Bhaskara Rao, T. Pradeep, *Nanoscale Research Letters* **2011**, *6*, 123.

- [125] Y. Zhu, H. Qian, B. A. Drake, R. Jin, *Angewandte Chemie International Edition* **2010**, *49*, 1295.
- [126] H. Chen, J. Yeh, L. Wang, H. Khurshid, N. Peng, A. Y. Wang, H. Mao, *Nano Res.* **2010**, *3*, 852.
- [127] A. Mathew, T. Pradeep, *Part. Part. Syst. Charact.* **2014**, *31*, 1017.
- [128] K. Kwak, D. Lee, *J. Phys. Chem. Lett.* **2012**, *3*, 2476.
- [129] K. Kimura, N. Sugimoto, S. Sato, H. Yao, Y. Negishi, T. Tsukuda, *J. Phys. Chem. C* **2009**, *113*, 14076.
- [130] E. S. Shibu, M. A. H. Muhammed, T. Tsukuda, T. Pradeep, *J. Phys. Chem. C* **2008**, *112*, 12168.
- [131] X. Meng, Q. Xu, S. Wang, M. Zhu, *Nanoscale* **2012**, *4*, 4161.
- [132] T. W. Ni, M. A. Tofanelli, B. D. Phillips, C. J. Ackerson, *Inorg. Chem.* **2014**, *53*, 6500.
- [133] C. Zeng, Y. Chen, A. Das, R. Jin, *J. Phys. Chem. Lett.* **2015**, *6*, 2976.
- [134] Y. Negishi, Y. Takasugi, S. Sato, H. Yao, K. Kimura, T. Tsukuda, *J. Am. Chem. Soc.* **2004**, *126*, 6518.
- [135] M. Zhu, H. Qian, R. Jin, *J. Phys. Chem. Lett.* **2010**, *1*, 1003.
- [136] Z. Wu, M. A. MacDonald, J. Chen, P. Zhang, R. Jin, *J. Am. Chem. Soc.* **2011**, *133*, 9670.
- [137] Y. Chen, J. Wang, C. Liu, Z. Li, G. Li, *Nanoscale* **2016**, *8*, 10059.
- [138] S. Jin, S. Jin, X. Meng, X. Meng, S. Jin, S. Jin, M. Zhu, M. Zhu, *Journal of Nanoscience and Nanotechnology* **2013**, *13*, 1282.
- [139] M. Zhu, C. M. Aikens, F. J. Hollander, G. C. Schatz, R. Jin, *J. Am. Chem. Soc.* **2008**, *130*, 5883.
- [140] M. A. Habeeb Muhammed, T. Pradeep, *Journal of Cluster Science* **2009**, *20*, 365.
- [141] I. Chakraborty, T. Pradeep, *Chem. Rev.* **2017**, *117*, 8208.

- [142] B. Nataraju, E. Kalenius, T. Udayabhaskararao, T. Pradeep, H. Siegenthaler, T. Wandlowski, *Journal of Cluster Science* **2017**, DOI 10.1007/s10876-017-1299-5.
- [143] A. C. Templeton, M. J. Hostetler, C. T. Kraft, R. W. Murray, *J. Am. Chem. Soc.* **1998**, *120*, 1906.
- [144] L. G. AbdulHalim, Z. Hooshmand, M. R. Parida, S. M. Aly, D. Le, X. Zhang, T. S. Rahman, M. Pelton, Y. Losovyj, P. A. Dowben, O. M. Bakr, O. F. Mohammed, K. Katsiev, *Inorg. Chem.* **2016**, *55*, 11522.
- [145] W. Kurashige, M. Yamaguchi, K. Nobusada, Y. Negishi, *J. Phys. Chem. Lett.* **2012**, *3*, 2649.
- [146] Z. Wu, R. Jin, *Nano Lett.* **2010**, *10*, 2568.
- [147] H.-Y. Chang, H.-T. Chang, Y.-L. Hung, T.-M. Hsiung, Y.-W. Lin, C.-C. Huang, *RSC Adv.* **2013**, *3*, 4588.
- [148] Y.-T. Tseng, Z. Yuan, Y.-Y. Yang, C.-C. Huang, H.-T. Chang, *RSC Adv.* **2014**, *4*, 33629.
- [149] W.-Y. Chen, C.-C. Huang, L.-Y. Chen, H.-T. Chang, *Nanoscale* **2014**, *6*, 11078.
- [150] M. A. H. Muhammed, A. K. Shaw, S. K. Pal, T. Pradeep, *J. Phys. Chem. C* **2008**, *112*, 14324.
- [151] X. Gao, Y. Lu, M. Liu, S. He, W. Chen, *J. Mater. Chem. C* **2015**, *3*, 4050.
- [152] M. Haruta, T. Kobayashi, H. Sano, N. Yamada, *Chem. Lett.* **1987**, *16*, 405.
- [153] M. S. Ide, R. J. Davis, *Acc. Chem. Res.* **2014**, *47*, 825.
- [154] S. Panigrahi, S. Basu, S. Praharaj, S. Pande, S. Jana, A. Pal, S. K. Ghosh, T. Pal, *J. Phys. Chem. C* **2007**, *111*, 4596.
- [155] M. Stratakis, H. Garcia, *Chem. Rev.* **2012**, *112*, 4469.
- [156] J. Fang, B. Zhang, Q. Yao, Y. Yang, J. Xie, N. Yan, *Coord. Chem. Rev.* **2016**, *322*, 1.
- [157] G. Li, R. Jin, *Acc. Chem. Res.* **2013**, *46*, 1749.
- [158] J. Fang, J. Li, B. Zhang, X. Yuan, H. Asakura, T. Tanaka, K. Teramura, J. Xie, N. Yan, *Nanoscale* **2015**, *7*, 6325.

- [159] M. Haruta, S. Tsubota, T. Kobayashi, H. Kageyama, M. J. Genet, B. Delmon, *Journal of Catalysis* **1993**, *144*, 175.
- [160] Y. Gao, N. Shao, Y. Pei, Z. Chen, X. C. Zeng, *ACS Nano* **2011**, *5*, 7818.
- [161] G. Li, H. Qian, R. Jin, *Nanoscale* **2012**, *4*, 6714.
- [162] J. Li, R. R. Nasaruddin, Y. Feng, J. Yang, N. Yan, J. Xie, *Chem. Eur. J.* **2016**, *22*, 14816.
- [163] A. Shivhare, S. J. Ambrose, H. Zhang, R. W. Purves, R. W. J. Scott, *Chem. Commun.* **2012**, *49*, 276.
- [164] J. Xie, R. R. Nasaruddin, T. Chen, J. Li, N. Goswami, J. Zhang, N. Yan, *ChemCatChem* **n.d.**, n/a.
- [165] W. Wu, L. Wen, L. Shen, R. Liang, R. Yuan, L. Wu, *Appl. Catal. B: Environmental* **2013**, *130–131*, 163.
- [166] A. Öztürk, M. I. Abdullah, *Science of The Total Environment* **2006**, *358*, 137.
- [167] L. G. Devi, N. Kottam, S. G. Kumar, *J. Phys. Chem. C* **2009**, *113*, 15593.
- [168] G. Li, D. Jiang, S. Kumar, Y. Chen, R. Jin, *ACS Catal.* **2014**, *4*, 2463.
- [169] J. J. Kim, W. B. Ko, *Elastomers and Composites* **2015**, *50*, 274.
- [170] C.-Y. Chiu, P.-J. Chung, K.-U. Lao, C.-W. Liao, M. H. Huang, *J. Phys. Chem. C* **2012**, *116*, 23757.
- [171] X. Bai, Y. Gao, H. Liu, L. Zheng, *J. Phys. Chem. C* **2009**, *113*, 17730.
- [172] T. N. J. I. Edison, M. G. Sethuraman, Y. R. Lee, *Res Chem Intermed* **2016**, *42*, 713.
- [173] H. Yamamoto, H. Yano, H. Kouchi, Y. Obora, R. Arakawa, H. Kawasaki, *Nanoscale* **2012**, *4*, 4148.
- [174] K. Sharma, V. Bhalla, M. Kumar, *RSC Adv.* **2014**, *4*, 53795.
- [175] null Nie, null Emory, *Science* **1997**, *275*, 1102.
- [176] H. Ko, S. Singamaneni, V. V. Tsukruk, *Small* **2008**, *4*, 1576.

- [177] C. Shen, C. Hui, T. Yang, C. Xiao, J. Tian, L. Bao, S. Chen, H. Ding, H. Gao, *Chem. Mater.* **2008**, *20*, 6939.
- [178] P. L. Stiles, J. A. Dieringer, N. C. Shah, R. P. V. Duyne, *Annual Review of Analytical Chemistry* **2008**, *1*, 601.
- [179] S. Abalde-Cela, P. Aldeanueva-Potel, C. Mateo-Mateo, L. Rodríguez-Lorenzo, R. A. Alvarez-Puebla, L. M. Liz-Marzán, *Journal of The Royal Society Interface* **2010**, rsif20100125.
- [180] A. J. Chung, Y. S. Huh, D. Erickson, *Nanoscale* **2011**, *3*, 2903.
- [181] J. B. Jackson, N. J. Halas, *PNAS* **2004**, *101*, 17930.
- [182] W. E. Doering, S. Nie, *J. Phys. Chem. B* **2002**, *106*, 311.
- [183] L. Rodríguez-Lorenzo, R. A. Álvarez-Puebla, I. Pastoriza-Santos, S. Mazzucco, O. Stéphan, M. Kociak, L. M. Liz-Marzán, F. J. García de Abajo, *J. Am. Chem. Soc.* **2009**, *131*, 4616.
- [184] J. F. Li, Y. F. Huang, Y. Ding, Z. L. Yang, S. B. Li, X. S. Zhou, F. R. Fan, W. Zhang, Z. Y. Zhou, D. Y. Wu, B. Ren, Z. L. Wang, Z. Q. Tian, *Nature* **2010**, *464*, 392.
- [185] G. Doria, J. Conde, B. Veigas, L. Giestas, C. Almeida, M. Assunção, J. Rosa, P. V. Baptista, *Sensors* **2012**, *12*, 1657.
- [186] T. K. Sau, A. L. Rogach, F. Jäckel, T. A. Klar, J. Feldmann, *Adv. Mater.* **2010**, *22*, 1805.
- [187] J.-F. Li, Y.-J. Zhang, S.-Y. Ding, R. Panneerselvam, Z.-Q. Tian, *Chem. Rev.* **2017**, *117*, 5002.
- [188] Y. Cao, D. Li, F. Jiang, Y. Yang, Z. Huang, "Engineering Metal Nanostructure for SERS Application," can be found under <https://www.hindawi.com/journals/jnm/2013/123812/>, **2013**.
- [189] B. Paramanik, A. Patra, *J. Mater. Chem. C* **2014**, *2*, 3005.
- [190] I. Chakraborty, S. Bag, U. Landman, T. Pradeep, *J. Phys. Chem. Lett.* **2013**, *4*, 2769.
- [191] L. L. Zhao, L. Jensen, G. C. Schatz, *Nano Lett.* **2006**, *6*, 1229.
- [192] Zhao, L. Jensen, G. C. Schatz, *J. Am. Chem. Soc.* **2006**, *128*, 2911.

- [193] N. Ramos-Berdullas, D. López-Carballeira, M. Mandado, I. Pérez-Juste, *Theoretical Chemistry Accounts* **2015**, *134*, DOI 10.1007/s00214-015-1661-3.
- [194] L. Jensen, L. L. Zhao, G. C. Schatz, *J. Phys. Chem. C* **2007**, *111*, 4756.
- [195] C. M. Aikens, G. C. Schatz, *J. Phys. Chem. A* **2006**, *110*, 13317.
- [196] Q. Li, Q. Ding, W. Lin, J. Wang, M. Chen, M. Sun, *RSC Adv.* **2017**, *7*, 12170.
- [197] L. Chen, Y. Gao, Y. Cheng, H. Li, Z. Wang, Z. Li, R.-Q. Zhang, *Nanoscale* **2016**, *8*, 4086.
- [198] Q. Li, M. Chen, *Nanotechnology* **2017**, *28*, 475201.
- [199] A. Tlahuice-Flores, R. L. Whetten, M. Jose-Yacamán, *J. Phys. Chem. C* **2013**, *117*, 12191.
- [200] B. Varnholt, P. Oulevey, S. Lubner, C. Kumara, A. Dass, T. Bürgi, *J. Phys. Chem. C* **2014**, *118*, 9604.
- [201] J. L. Castro, M. R. López-Ramírez, J. F. Arenas, J. C. Otero, *J. Raman Spectrosc.* **2004**, *35*, 997.